UNIVERSITY OF TRENTO

PhD Program in Biomolecular Sciences

Department of Cellular, Computational and Integrative Biology – CIBIO

35th Cycle

"The role of Parkin R274W in genetic forms of Parkinson's disease"

Tutor

Prof. Giovanni PICCOLI

University of Trento

Ph.D. Thesis of

Martina SEVEGNANI

Academic Year 2021-2022

DECLARATION OF ORIGINAL AUTHORSHIP

Declaration:
I Martina Sevegnani confirm that this is my own work and the use of all material from other sources has been properly and fully acknowledged.

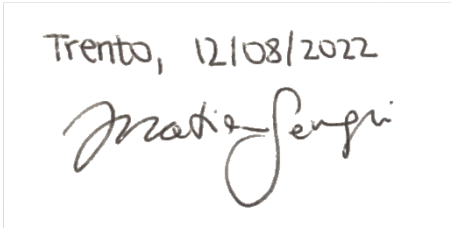

INDEX

GRAPHICAL ABSTRACT

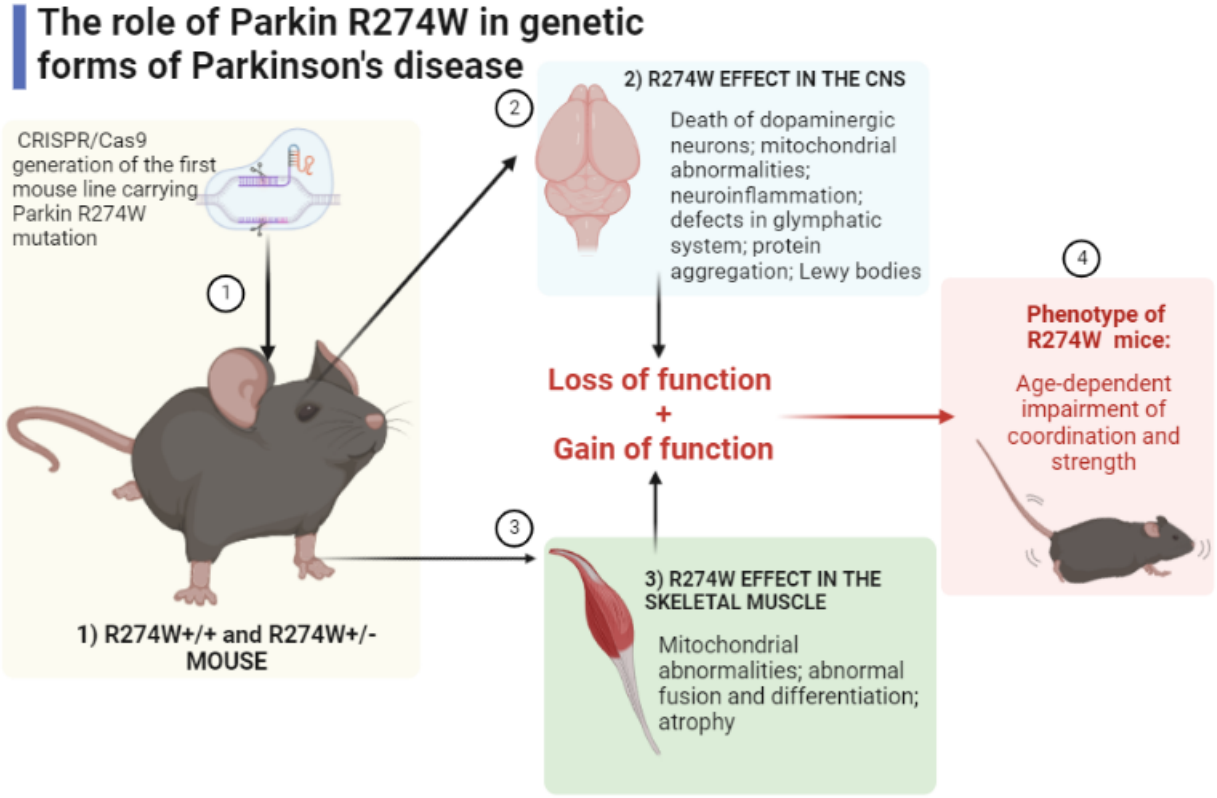

ABSTRACT

Parkinson's disease (PD) is a neurodegenerative disorder characterized by the progressive loss of nigral dopaminergic (DA) neurons and the formation of Lewy bodies. Despite most cases being idiopathic, mutations in several genes have been implicated in familial forms of PD.

In particular, recessive mutations in Parkin gene (PARK2) are the most common cause of young-onset inherited parkinsonism. Parkin is an E3 ubiquitin ligase involved both in the control of mitochondrial turnover and in the proteasome-dependent degradation of proteins, two pathways that have been causally linked to PD development. Although initially described as a recessive disorder, experimental evidence suggests that heterozygous Parkin mutations can exert dominant toxic effects causing neurodegeneration. In accordance with this idea, in 2012 Ruffmann and colleagues identified the first pure heterozygous R275W Parkin patient with clinical features of typical late-onset PD and a diffuse Lewy body pathology.

To assess the impact of R275W Parkin, we generated the first mouse line carrying Parkin R274W mutation, which corresponds to the human R275W substitution.

Unlike Parkin deficient mouse models, both homo- and heterozygous R274W mice show an age-related motor impairment, degeneration of dopaminergic neurons and neuroinflammation. We detected structural and functional mitochondrial abnormalities related to PARIS-PGC-1α axis impairment in R274W+/+ mice brain and skeletal muscle. Strikingly, we noticed signs of protein aggregation in both R274W+/- and +/+ mice, while we identified *bona fide* Lewy bodies only in the midbrain of heterozygous mice.

Additionally, in the brains of R274W mice we discovered overt abnormalities of the glymphatic system, the main route for brain waste clearance. Our preliminary observations suggest that Parkin influences aquaporin-4 (AQP4) localization.

Altogether, our data suggest that R274W Parkin substitution behaves both as a loss of- and a gain of toxic function, highlighting a link between Parkin dominant toxicity and age-dependent motor impairment, neuroinflammation, DA neurons loss, glymphatic system dysfunctions and α-synuclein aggregation *in vivo*.

Hence, our study provides a new robust mouse model to explore PD pathogenesis and glymphatic dysfunctions, offering the possibility to test novel therapeutic strategies with great predictivity.

INTRODUCTION

1 Parkinson's disease (PD)

Parkinson's disease is the most common movement disorder and the second most frequent neurodegenerative condition after Alzheimer's disease (AD), affecting 2-3% of the worldwide population over the age of 65 (Tysnes et al., 2017). The prevalence of PD changes by sex, age, and ethnicity. In the western hemisphere, it ranges from 130 to 200 per 100000 in community-based studies, but it increases exponentially in the ageing population, reaching 2000 per 100000 in people over the age of 80 (Mehanna et al., 2019). This trend highlights the global burden of Parkinson's disease: indeed, with an ageing population and the increase in worldwide life expectancy, people affected by PD are expected to increase by more than 50% in the next ten years (Dorsey et al., 2007; Simon et al., 2020). Gender differences pertaining to the incidence of Parkinson's disease are reflected in a 3:2 ratio of males to females (Miller et al., 2010), making gender an established risk factor for the disorder.

The first description of PD was elaborated in 1817 by James Parkinson, who described the disease as a "shaking palsy" presenting with bradykinesia, muscular rigidity, tremor, and mental alterations (Parkinson, 1817). Despite the heterogeneity of PD motor features, the motor manifestations described in 1817 represent the prominent components of the disease and are still used for diagnosis and classification (Goetz, 2011).

The motor symptoms of Parkinson's disease are consequence of the loss of dopaminergic (DA) neurons in the substantia nigra pars compacta (SN pc) (Antony et al., 2013; Kalia et al., 2015), although alterations in other neurotransmitters pathways have been observed as well. Dopamine reduction and eventually depletion within the extrapyramidal system leads to decreased excitation of the motor cortex, with the net result of progressively inhibiting motor activity (Andersen et al., 1990; Hornykiewicz et al., 2008) [Figure 1].

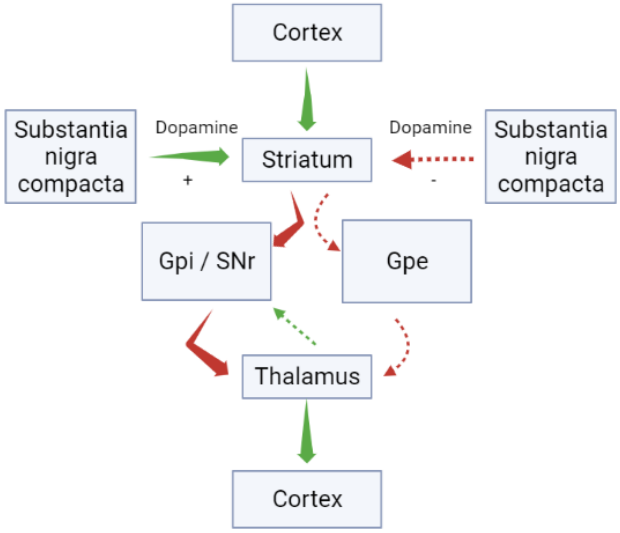

Figure 1: Direct and indirect pathway of the extrapyramidal system. Dopamine produced in the substantia nigra acts differentially in the modulation of two subsets of striatal neurons. The net effect of dopamine in the direct pathway (bold arrows) is the potentiation of striatal inhibition on Globus pallidus internal (Gpi), blocking its inhibitory function on the thalamus and finally enabling excitation of the cerebral motor cortex. In the indirect pathway (dashed arrows), dopamine diminishes striatal inhibition on Globus pallidus external (Gpe), which can subsequently inhibit the thalamus. The net result of this is the activation of Gpi inhibitory outputs, leading to a decrease in motor cortical activity. Green lines indicate excitatory connections, red the inhibitory ones. Created with BioRender.com.

1.1 Treatments for motor symptoms

Current treatments only allow to cope with the symptoms of the disorder and aim at replacing/restoring dopamine levels in the patient's brain. Still, the management of PD is complex and faceted, so it requires a tailored pharmacological and non-pharmacological approach for every patient.

Levodopa (L-3,4-dihydroxyphenylalanine; L-DOPA) is the most used drug and is especially effective in the early stages of PD. L-DOPA is a pro-drug able to cross the blood-brain barrier (BBB), reach the brain, and be converted to dopamine in neurons expressing DOPA decarboxylase. Administration in combination with inhibitors of peripheral DOPA decarboxylase like Carbidopa (Morgan et al., 2016) allows the avoidance of peripheral conversion of Levodopa to dopamine. Despite being the most effective drug to deal with PD motor symptoms, L-DOPA has been shown to become less efficient with time, probably as the result of progressive neurodegeneration that affects also non-dopaminergic brain areas (Olanow et al., 2011). Additionally, after long-term usage, there is an emergence of complications and side effects that include dyskinesia, motor fluctuations, and psychosis.

For these reasons, other pharmacological agents can be used before or in combination with L-DOPA. Examples are drugs that mimic dopamine, like DA agonists, and drugs that inhibit dopamine breakdown, like monoamine oxidase B (MAO-B) inhibitors and catechol-o-methyltransferase (COMT) inhibitors.

Gene therapy, stem cell therapy, surgical intervention, and deep brain stimulation are also options that can be taken into consideration to temporarily halt the symptoms of Parkinson's disease; however, no definitive disease-modifying cure has been proposed yet.

1.2 Non-motor symptoms

Along with typical motor symptoms, PD also presents itself with a set of non-motor disturbances. Among the most common we find olfactory alterations (hyposmia), cognitive impairment, psychiatric symptoms (especially depression and anxiety), sleep

disorders (excessive daytime sleeping and rapid eye movement sleep behaviour disorder), autonomic dysfunction, pain, fatigue, and constipation. While motor impairment appears after 50-80% loss of DA neurons (Hawkes et al., 2009), non-motor symptoms are observed in the early phase of PD and often precede the onset of classical motor symptoms. Such pre-motor phase is referred to as the prodromal phase and can last for a long time: indeed, the average latency between constipation, sleep disorders, and motor symptoms is 15 years [Figure 2]. This suggests that the pathogenic processes that cause PD are ongoing during the pre-motor phase, which can be used as a temporal window to administer disease-modifying drugs to prevent or at least delay the symptomatic phase (Antony et al., 2013).

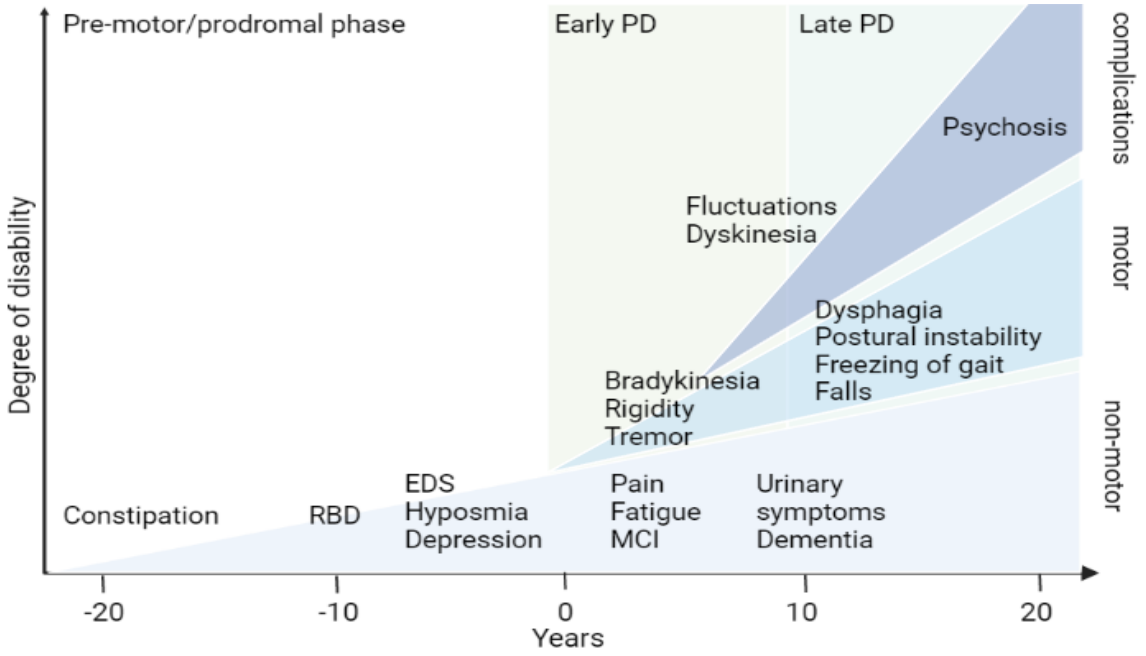

Figure 2: Non-motor and motor clinical manifestations of Parkinson's disease. The prodromal phase can precede the onset and diagnosis of motor symptoms (0 years) of more than 20 years. Non-motor symptoms characterize also later phases of the disease. RBD: REM sleep behaviour disorder; EDS: excessive daytime sleep; MCI: mild cognitive impairment. Created with BioRender.com.

1.3 Lewy pathology is a histological hallmark of PD

In the last few decades, the presence of misfolded proteins arranged in intra- and extracellular aggregates has been identified as a common feature of many neurodegenerative disorders, including AD and PD. Indeed, together with the loss of DA neurons within the SN pc, another hallmark of Parkinson's disease is the presence of Lewy bodies (LBs) in many brain areas including the brainstem and cortical regions. LBs were first observed in 1912 by Dr. Friedrich Lewy, who described them as "abnormal protein deposits that disrupt the brain's normal functioning" (Lewy, 1912).

LBs are eosinophilic inclusions of 5-25 µm diameter composed of a dense core of filamentous and granular material surrounded by radially oriented fibres. LBs are found within the cytoplasm of neurons, while the inclusions found in neuronal processes are defined as Lewy neurites (Spillantini et al., 1998) [Figure 3]. Lewy pathology is not observed only in the brain but can also be present in the spinal cord and peripheral nervous system (Beach et al., 2010). To date, more than 70 different proteins have been found to localize in Lewy bodies and neurites, the most common being tau, ubiquitin, and α-synuclein, which has eventually been identified as the major component of LBs.

The mechanism leading to the formation of Lewy bodies and neurites and their role in neurodegeneration still remain elusive. Clearly, LBs are not necessary nor sufficient to induce cell death, given that many cases of PD without Lewy pathology have been reported (Wakabayashi et al., 2007).

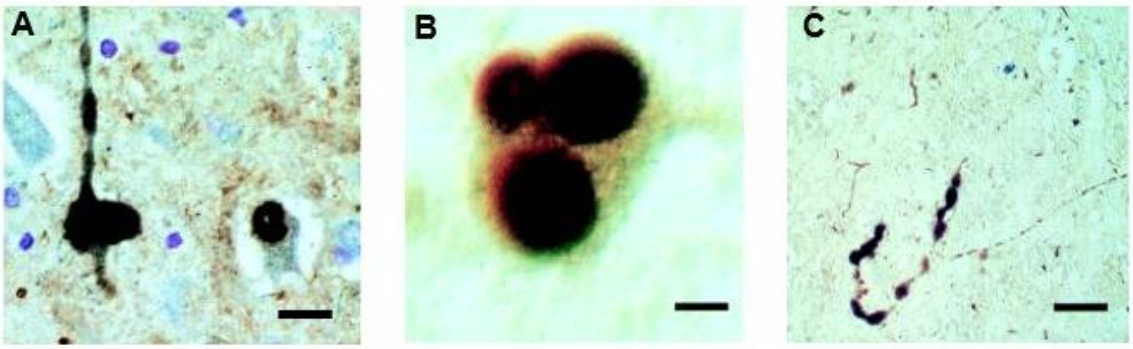

Figure 3: Lewy bodies and neurites in patients' brains with PD or Lewy body dementia. α-synuclein immunostaining (brown) reveals the presence of Lewy bodies and Lewy neurites (A, B) in the substantia nigra of patients with PD. (C) shows intraneural Lewy bodies and neurites in the cingulate cortex of a patient with LB dementia. Ubiquitin is stained in blue. Scale bar (A) = 10 µm; (B) = 90 µm; (C) = 18 µm. Adapted from Spillantini et al., 2018.

2 Pathogenesis of Parkinson's disease

The pathogenic mechanisms leading to the loss of DA neurons remain unclear. Indeed, the aetiology of Parkinson's disease is complex and depends on several factors, both environmental and hereditary.

2.1 The role of α-synuclein in neuronal death

After its identification as the major component of LBs, α-synuclein and its aggregation have emerged as a central element for several diseases classified as synucleinopathies such as PD, multiple system atrophy (MSA) and Lewy bodies dementia (LBD) (Lee et al., 2016).

α-synuclein is a phosphoprotein abundantly expressed in the presynaptic sites in an unstructured state. Although the physiological role of the protein is still mostly

unknown, it may be involved in intracellular trafficking in the endoplasmic reticulum (ER) and Golgi. Several studies have reported that overexpression of α-synuclein in different cell and animal models induces cell death, with the catecholaminergic neurons being especially sensitive to this phenomenon (Krueger et al., 1998; Cooper et al., 2006; Van Ham et al., 2008).

To date, the more accredited hypothesis is that the aggregation of α-synuclein triggers cell death. Indeed, it has been shown that α-synuclein exists in a variety of structures such as oligomers, protofibrils, fibrils, and filaments. The most toxic forms are thought to be protofibrils and fibrils, which can become insoluble under specific conditions and accumulate into Lewy bodies and neurites. Potential triggers for the aggregation can be protein load, alterations in protein structure, proteasomal dysfunctions, autophagy alterations, mitochondrial damage, and oxidative stress (Xu et al., 2002). Additionally, α-synuclein itself seems to promote these processes, in a putative self-amplifying loop (Fuchs et al., 2008).

There are two main pathological mechanisms underlying α-synuclein-driven cellular death. First, α-synuclein protofibrils could permeabilize neuronal membranes forming pore-like structures (Volles et al., 2002). On the other hand, aggregated α-synuclein may interfere with microtubule-based subcellular transport, causing synaptic dysfunctions and perturbations to neuronal homeostasis (Sheng et al., 2012).

2.2 The role of protein aggregation in neuronal death

2.2.1 The ubiquitin-proteasome system (UPS)

Protein aggregation is emerging as a central motif common to different neurodegenerative disorders. The discovery that a various number of proteins are present in Lewy bodies points towards a prominent role for protein aggregation in the pathology of Parkinson's disease. However, the causative mechanism is still unknown.

The proteasome is a protein complex that degrades damaged or misfolded proteins through a process called proteolysis, in which peptide bonds are broken. A series of evidence suggest a link between the ubiquitin-proteasome system (UPS), protein aggregation, and the development of Parkinson's disease.

First, histological analysis of LBs revealed the presence of multiple UPS components like ubiquitin and proteasomal subunits. Additionally, post-mortem analysis of brain specimens from PD patients revealed a 40% decrease in the activity of the proteasome especially in the SN pc (McNaught et al., 2001), suggesting a link between UPS dysfunction and accumulation of proteins in affected brains.

Accordingly, the inhibition of the proteasome in cell culture and mouse striatum gives rise to ubiquitin- and α-synuclein-positive inclusions and cell death preferentially in

dopaminergic neurons (Rideout et al., 2001). Additionally, coherent with the age-related nature of PD, proteasome activity decreases with ageing (Saez et al., 2014).

2.2.2 The autophagy/lysosomal pathway (ALP)

An alternative route that can be exploited by the cells to get rid of proteins and protein aggregates is the autophagy/lysosomal pathway (ALP). Implications of autophagy in PD came from the detection of autophagic markers in the SN pc of PD patients' brains, together with the observation that mouse models deficient for Atg proteins, which are responsible for autophagosome formation, display neurodegeneration and ubiquitin-positive aggregates (Anglade et al., 1997). However, to date, it is unclear whether autophagy may actually play a role in neuronal loss. Indeed, some experimental settings have shown that ALP activation has a protective effect, while in other systems it promoted cell death (Hara et al., 2006). The current hypothesis is that autophagic pathway activation is protective in Parkinson's disease, while its dysfunctions contribute to neurodegeneration.

2.2.3 Endoplasmic reticulum (ER) stress and unfolded protein response (UPR)

Protein misfolding and aggregation could exert cytotoxicity by triggering ER stress. Indeed, recent studies have identified signs of ER stress in many of the neurodegenerative diseases characterized by protein accumulation also called "conformational diseases" (Ogen-Shtern et al., 2016; Schaffar et al., 2004).

Incorrectly folded secretory proteins are degraded by endoplasmic reticulum-associated degradation (ERAD). After an initial trimming by the ERAD system, misfolded proteins accumulate in the endoplasmic reticulum quality control compartment (ERQC), where they are poly-ubiquitinated by E3 ubiquitin ligases and then directed to the proteasome for their degradation.

ER stress arises as the consequence of a disproportionate accumulation of misfolded proteins in the ER itself, but also from ERAD and UPS inhibition or dysfunctions (Duennwald et al., 2008; Leitman et al., 2013). The cell must respond quickly to such stress in order to re-establish homeostasis, and this response is known as unfolded protein response (UPR). UPR is initiated by three different triggers: inositol requiring 1 (IRE1), double-strand RNA-activated protein kinase-like ER kinase (PERK) and activating transcription factor 6 (ATF6) (Schroeder et al., 2005; Gardner et al., 2013). The net result of such activation is the overexpression of other downstream transcription factors, such as C/EBP homologous protein (CHOP), and ER chaperons, like binding immunoglobulin protein (BiP), to eventually compensate and get rid of ER

stress. At this point, if such initial response fails to restore homeostasis and the condition of stress persists, the cell eventually undergoes apoptosis.

Interestingly, post-mortem brain samples of PD patients showed increased amounts of BiP, activated IRE1, and PERK (Hoozemans et al., 2007). High BiP levels were also observed in AD, Huntington's disease (HD), and amyotrophic lateral sclerosis (ALS) patients (Hoozemans et al., 2009; O'Connor et al., 2008; Carnemolla et al., 2009). Coherently, UPR activation was noticed in the brains of animal models of HD (Cho et al., 2009; Carnemolla et al., 2009), ALS (Prell et al., 2012; Nishitoh et al., 2008), AD (Kohler et al., 2014), and PD (Bellucci et al., 2011).

Finally, α-synuclein oligomers can be found in the endoplasmic reticulum both in PD animal models and in brain specimens from PD patients (Colla et al., 2012; Hetz et al., 2014).

Altogether, such data point toward a strong correlation between protein aggregation, ER stress, and unfolded protein response in the pathogenesis of Parkinson's disease.

2.3 The role of mitochondria and oxidative stress

The first evidence of a link between mitochondria dysfunctions and PD development came in the 1980s from the so-called "frozen addicts", drug users that developed rapid onset parkinsonism responsive to L-DOPA treatment after the assumption of a new type of synthetic heroin. Indeed, it was observed that 1-methyl-4-phenyl-1,2,5,6-tetrahydropyridine (MPTP), a side product of the synthesis process, was able to cross the BBB and enter the brain, where it was converted by MAO-B to the toxic 4-phenylpyridinium (MPP^+). MPP^+ is selectively imported by dopaminergic neurons, where it inhibits mitochondria complex I of the respiratory chain, leading to the production of reactive oxygen species (ROS), ATP depletion, and cell death. MPTP is now commonly used to generate mouse models of Parkinson's disease (Langston et al., 1983).

Other evidence of the involvement of mitochondria in PD pathology came from the study of post-mortem human brain specimens. Indeed, the brain and especially the substantia nigra of PD patients showed a substantial reduction of mitochondria complex I and, more in general, a restricted functionality of respiratory chain complexes (Schapira et al., 1990). Additionally, PD patients also displayed a higher rate of mitochondrial DNA (mtDNA) mutations compared to healthy controls (Bender et al., 2006).

Dysfunctions in respiratory chain complexes are linked to the production of ROS. Accordingly, signs of oxidative stress like lipid peroxidation, DNA damage, protein oxidation, and increased iron deposition have been observed in the SN pc of numerous

PD patients (Mann et al., 1994). However, whether such condition is a consequence of neuronal stress or can cause the neurodegeneration remains elusive. Interestingly, dopamine itself can be oxidized and react with other cellular species, thus contributing to ROS production: dopamine toxic metabolite may explain the selective susceptibility of DA neurons to neurodegeneration (Palacino et al., 2004; Blesa et al., 2015).

2.4 The role of neuroinflammation

Studies in animal models and humans support a role for neuroinflammation in PD progression. In the brain, the inflammatory response is mediated by glial (microglia and astrocytes) activation and peripheral immune cell infiltration. Reactive microglia in the SN pc of PD patients' brains was detected for the first time in 1988 (McGeer et al., 1988). In the next decades, other elements connected to inflammation have been observed in autoptic PD brain samples, such as astrogliosis and high levels of pro-inflammatory cytokines like inducible nitric oxide synthase (iNOS), cyclooxygenase 2 (COX2), tumour necrosis factor-alpha (TNF-α), interleukin-1 beta (IL-1β), and interferon-gamma (IFN-γ) (Wang et al., 2015).

Interestingly, the activation of the neuroinflammatory system can result in a positive or detrimental outcome, according to the different types of stimuli and responses of immune cells. Indeed, microglia activation due to an insult can result in M1 state, which produces pro-inflammatory cytokines, nitric oxide (NO), and ROS, or in M2 state which plays an immunosuppressive role and promotes tissue repair. Supporting a detrimental role for neuroinflammation in neurodegenerative diseases, PD animal models have shown that misfolded α-synuclein activates M1 microglia and downregulates gene markers expressed by M2 microglia (Tang et al., 2015).

Astrocytes are glial cells that play a supportive role for neurons and respond to inflammatory stimuli. Astrocyte activation (astrogliosis) has been observed both in PD patients' brains and in animal models of Parkinson's disease (Glass et al., 2010).

Overall, it seems clear that uncontrolled inflammation caused by synergic activation of glial cells may contribute to neurodegeneration. However, it remains to be investigated whether neuroinflammation plays a causal role in the pathogenesis of PD or if it is just a consequence of neuronal death.

3 The glymphatic system

The clearance of metabolic waste is fundamental for maintaining brain homeostasis, and dysfunctions in this process can lead to protein accumulation and neurodegeneration.

Consequently, it is surprising to know that the brain lacks the typical structures that drive waste clearance in the other tissues (Jessen et al., 2015).

In the periphery indeed, possibly toxic proteins and metabolic by-products are cleared through the lymphatic system: an ultrafiltrate of blood plasma percolates from the microvasculature through the tissue, collects metabolic waste, and enters the lymphatic capillaries. Once in these capillaries, it is pulled into larger vessels and lymph nodes via vessels contraction and one-way valves. Finally, the fluid returns to the venous circulatory system. Waste products are eventually delivered to the liver, where they can be degraded or reused (Liao et al., 2013).

Conversely, the brain does not display traditional lymphatic vessels (LVs) and ultrafiltration of plasma is restricted by the BBB (Johanson et al., 2008).

The idea that cerebrospinal fluid (CSF) could serve as a sort of “sink” for brain waste has been proposed in the 1980s (Rennels et al., 1985; Rennels et al., 1990; Ichimura et al., 1991), but the description of a proper system with its own structure and activity has been possible only in 2012 (Ilif et al., 2012), when studies on rodents discovered a dynamic network used for brain clearance that was named “glymphatic system” for its similarities with the peripheral lymphatic system and the involvement of glial cells.

3.1 Structure and functions of the glymphatic system

The glymphatic system is now considered the functional analogue of the lymphatic system in the central nervous system (CNS). It is a complex and highly polarized network that allows the rapid interchange of CSF and interstitial fluid (ISF) through convective fluid fluxes along tunnel-like perivascular spaces (PVSs).

PVSs are doughnut-shaped CSF-containing channels that run alongside the brain blood vessels: internally, they are layered by smooth muscle cells or pericytes, while externally they are enclosed by the astrocytes vascular endfeet. Astrocytes are fundamental to regulate both perivascular and interstitial flows by the highly polarized expression of AQP4 water channel at the vascular endfeet [Figure 4 A].

The functioning of the glymphatic system has been proposed as follows (Ilif et al., 2012):

(1) CSF is produced by the choroid plexus in the third, fourth, and lateral ventricle (Oreskovic et al., 2010) from where it continuously moves to the subarachnoid spaces surrounding the cerebral hemispheres.

(2) At this point CSF is propelled along the periarterial spaces by a combination of arterial pulsatility and CSF pressure gradients. AQP4 channels on astrocytes' endfeet facilitates fluid transport into the brain parenchyma, enabling the generation of a CSF-ISF mix that allows for waste removal.

(3) CSF-ISF mixed with metabolic waste enters with convective movements the perivenous spaces surrounding deep brain veins, from where it ultimately exits the brain and reaches the peripheric lymphatic system through cranial nerves, large vessels, and lymphatic network associated with the meninges (*dura*) (Aspelund et al., 2015) [Figure 4 B].

However, while the periarterial influx pathways have been documented in several studies using different imaging techniques, the efflux routes are less well described. Indeed, acoustic, hypoglossal, optical, olfactory, and vagal nerves have been identified as efflux pathways *in vivo* using dynamic-contrast magnetic resonance imaging (MRI) studies (Lee et al., 2015; Ilif et al., 2013), but it is still unclear whether interstitial waste metabolites travel along the nerves or inside the nerve itself. The contribution of lymphatic vessels (Ma et al., 2017) of the *dura* compared to more peripheral LVs has been debated as well.

Since its discovery in the rodent brain, the glymphatic system has been identified in other animals including cats, dogs, pigs, flies, and non-human primates (Rennels et al., 1985; van Alphen et al., 2021). To date, the existence and functionality of a proper glymphatic system in humans have substantially been accepted (Ringstad et al., 2017), even though some controversies are still being debated (Mestre et al., 2020). In the last ten years, impairment in the glymphatic system function has been linked to age-related issues and several neurodegenerative disorders like AD and PD.

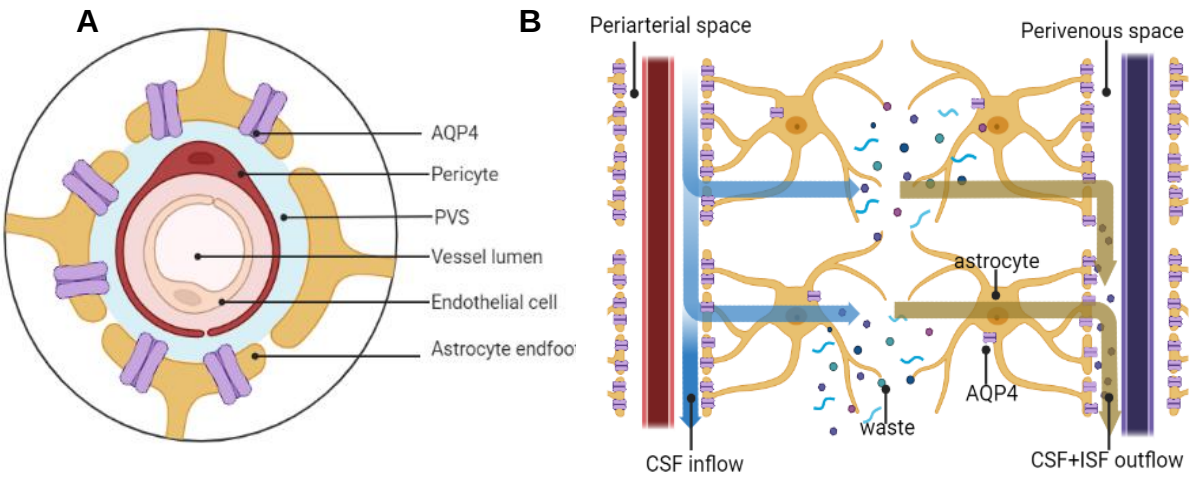

Figure 4: Basic structure and function of the glymphatic system. A) Perivascular spaces (PVSs) are doughnut-shaped structures along brain blood vessels, delimited by pericytes and astrocytes endfeet, where AQP4 is highly expressed. B) Moving through the

periarterial spaces CSF enters brain parenchyma (blue arrows) where it mixes with ISF and waste products that leave the brain through perivenous space (brown arrows) to more traditional lymphatic network. Fluid convective movements are tightly regulated by AQP4 (purple) at astrocytes' endfeet (yellow). Created with BioRender.com.

3.2 Factors that influence the glymphatic system activity

3.2.1 AQP4 water channels

AQP4 is an integral membrane protein that regulates the water flow across membranes in response to tonicity and osmolarity changes and represents a fundamental element of the basic structure of the glymphatic system.

A variety of aquaporins is expressed in the brain and spinal cord, but the most abundant forms are AQP1, AQP4, and AQP9. AQP4 is the most prevalent aquaporin channel in the CNS, where it localizes especially in the astrocyte vascular endfeet (Nielsen et al., 1997). Two distinct splice variants have been identified in the CNS: M1 and M23. While M23 AQP4 isoforms are larger and usually stably found in large square arrays in the astrocyte foot process, M1 isoforms appear to be smaller and can move freely in the cell membrane (Oklinski et al., 2016). AQP4 expression is not uniform in the brain, being lowest in the cortex, hippocampus, and inferior colliculi (Ilif et al., 2013): such differences may reflect in the regional heterogeneity of the glymphatic transport observed in the rodent brain.

Structurally, AQP4 consists of six transmembrane domains with five connecting loops that form the water channel or aqueous pore, measuring 2.8 angstroms (Halsey et al., 2018). Like other aquaporins, AQP4 is able to assemble into tetramers; in particular, both M1-M23 heterotetramers and homotetramers have been observed to be organized in orthogonal arrays of intramembranous particles (OAPs) by freeze-fracture microscopy organized (Silberstein et al., 2004) [Figure 5].

AQP4 OAPs are anchored on the membrane by several proteins, including the dystrophin-associated complex (DAC), which contains α-syntrophin (SNTA1) and dystroglycan (DAG1), α-dystrobrevin (DTN-A), and dystrophin. Knock-out (KO) animal models have demonstrated the key role of AQP4 and its interacting partners for the correct structure and activity of the glymphatic system (Rainey-Smith et al., 2018).

In particular, AQP4 KO mice revealed a reduction of around 65% in CSF flux into the brain parenchyma and a strong decrease in the clearance of waste solutes compared to controls (Teng et al., 2018).

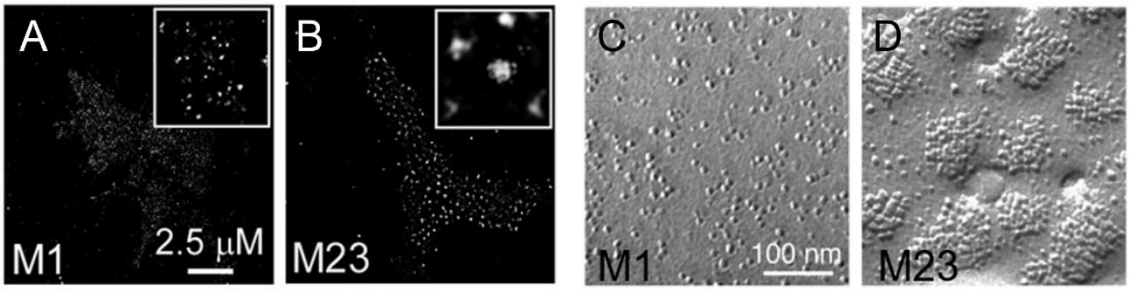

Figure 5: AQP4 M1-M23 organization reveals differences in cluster formation. A, B) PALM (photoactivation localization microscopy) of U87MG cells shows that AQP4 M23 (B) assembles in larger clusters compared to M1 (A). The scale bar of the small square is 100 nm. Adapted from Rossi et al., 2012. C, D) Freeze-fracture electron micrographs of COS-7 cells plasma membrane transfected with AQP4-M1 (C) or M23 (D). Adapted from Crane et al., 2008.

3.2.2 Sleep

Sleep is a fundamental function conserved through all the known organisms, and sleep deprivation has proven to be detrimental in all species (Irwin et al., 2017). However, a broadly accepted theory for the function of sleep has not been defined yet.

The finding that the glymphatic system is mostly active during sleep and not during wakefulness proposes sleep as the fundamental process that allows the clearing of potentially neurotoxic waste products from the brain.

Xie and colleagues were the first to describe the relationship between the glymphatic system and sleep in 2013 (Xie et al., 2013). They observed that the brain influx of CSF tracers is increased by 95% in asleep and anaesthetized mice compared to awake animals. Similar evidence was produced by Ma group in 2019 (Ma et al., 2019). In addition, MRI experiments in human subjects showed increased fluid movement in the white matter during sleep (Bernardi et al., 2016). Conversely, norepinephrine (NE), a neuromodulator that promotes arousal, has a suppressive effect on the glymphatic system activity (O'Donnel et al., 2019). In general, the fundamental role of sleep for glymphatic system removal of brain metabolites has been demonstrated both in animal models and humans (Ju et al., 2017).

Glymphatic system activation happens mostly in the non-rapid-eye movement (nREM) phase of sleep, which is characterized by slow high amplitude electrical waves (1-4 Hz) of brain activity. Interestingly, anaesthetics associated with such slow wave of activity (SWA) like dexmedetomidine increase glymphatic influx, while the ones associated with low amplitude delta waves like isoflurane do not (Hablitz et al., 2019).

However, the mechanism that regulates the switch between brain waste clearance during sleep and wakefulness remains to be addressed. Additionally, it is also unclear why clearance processes in the brain do not happen continuously to avoid the accumulation of toxic waste. A possible explanation is that the rapid movement of the

large volume of CSF-ISF required for brain clearance may interfere with the synaptic activity happening during awake consciousness.

Interestingly, disturbance in sleep, which is reported to increase dramatically with age, has been identified as a risk factor for many neurodegenerative diseases and mood disorders like PD, AD (Kang et al., 2017), and dementia (Lim et al., 2013). In accordance with this, Winer and colleagues observed that impaired sleep functions (decreased slow waves and impaired coupling of neuronal activity during nREM sleep) correlated with a higher level of amyloid beta (Aβ) and tau deposition in the brain of patients with Alzheimer's disease (Winer et al., 2019).

3.2.3 Age

In 2014 Kress group demonstrated that the glymphatic clearance in mice brains declines by 80-90% with ageing (Kress et al., 2014). The vascular remodelling that naturally occurs in ageing is one of the factors that may explain such effect. Indeed, the stiffening of brain arteries and the reduced elasticity of arterial walls result in enhanced arterial pulse wave velocity and pressure that are mechanically transmitted also to distal vessels. Such an increase in intracranial pulsatility might significantly impair the physiological activity of the glymphatic system (Hachinski et al., 2016). Accordingly, Bedussi and colleagues observed that glymphatic system dysfunctions are implicated in rat models for hypertension on brain microvessels (Bedussi et al., 2017).

Ageing affects also AQP4 pattern of expression. Indeed, vascular polarization at astrocytic endfeet is lost in the ageing brain especially along penetrating arterioles (Kress et al., 2014). This phenomenon correlates with the hypertrophy of reactive astrocytes during neuroinflammation, another typical characteristic of ageing brains (Sabbatini et al., 1999).

Additionally, ageing is also associated with a reduction in sleep quality and quantity, with a progressive reduction in SWA in humans already from thirty years of age (Bohnen et al., 2019). Altogether, these data suggest that the glymphatic system activity naturally declines with age [Figure 6].

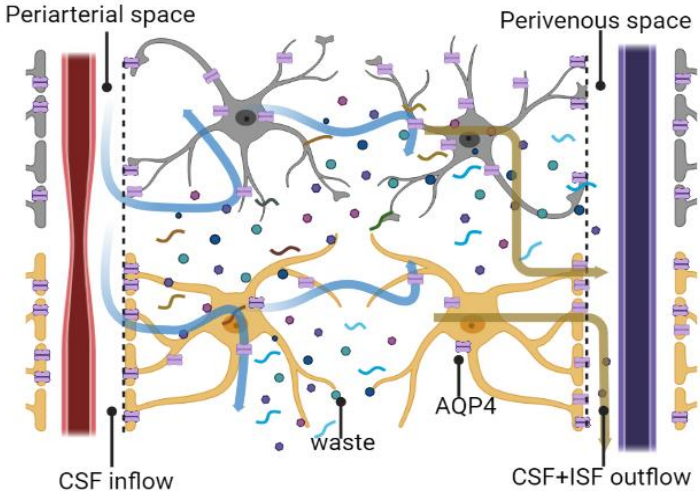

Figure 6: The clearance activity of the glymphatic system is impaired in aged brain. CSF convective bulk flow (blue arrows) is impaired in aged brain, because of alteration in vessel architecture, changes in astrocyte morphology in response to inflammatory stimuli, and modification in AQP4 expression pattern. Consequently, CSF-ISF outflow (brown arrows) is reduced, and waste accumulates in the brain parenchyma. Created with BioRender.com.

3.3 Dysfunctions of the glymphatic system and neurodegenerative disorders

The evidence that the activity of the glymphatic system declines with age is important, as age has been identified as the highest risk factor for neurodegenerative diseases (Driver et al., 2009). The misfunctioning of this clearance pathway might indeed contribute to the accumulation of misfolded proteins in the brain tissue. Accordingly, while previous work about protein degradation has focused mainly on intracellular processes like proteasomal and lysosomal degradation, recent analyses have revealed the presence in the CSF and ISF of several disease-related protein species: misfolded amyloid beta and tau in AD (Frost et al., 2009; Weller et al., 2008), phosphorylated α-synuclein in PD (Kordower et al., 2008), and misfolded superoxide dismutase 1 (SOD1) in mouse modelling ALS (Grad et al., 2014). Additionally, the emerging concept of a prion-like spread of protein aggregates (Li et al., 2008; Jucker et al., 2011) could be supported by the activity of the glymphatic clearing system through the brain parenchyma. Moreover, many neurodegenerative disorders display an alteration of sleep pattern.

Clearly, dysfunctions/low function of the glymphatic system could be involved in the development of neurodegenerative diseases.

3.3.1 Glymphatic system and Parkinson's disease

The discovery that the glymphatic system is deeply implicated in the removal of extracellular amyloid β in AD patients and animal models (Yang et al., 2011; Michaud et al., 2013; Da Mesquita et al., 2018) pushed researchers to investigate whether such clearance pathway could be involved in other neurodegenerative disorders, as Parkinson's disease.

The observation that up to 75-80% of PD patients display sleep disturbances over the course of the disease (Goetz et al., 2010; Chahine et al., 2016), like REM-sleep behaviour disorder (RBD), changes in cortical sleep-related activity while (Fantini et al., 2003), reduced sleep quality (Gjerstad et al., 2008), and altered expression of clock genes that regulate circadian rhythm (Breen et al., 2014) is supportive. Interestingly, such sleep disturbances usually precede the onset of typical motor symptoms. Accordingly, idiopathic RBD is now considered a prodromal predictor for the

development of PD and other synucleinopathies, like LBD and MSA (Schenck et al., 2013).

A direct involvement of the glymphatic system in the clearance of α-synuclein is still under investigation. In 2013 Kalaitzakis group observed that α-synuclein aggregates were increased in the brain tissue of PD patients with sleep disturbances as compared to those without alterations in the sleep pattern (Kalaitzakis et al., 2013). Additionally, several recent works have assessed that α-synuclein presence in the CSF of PD patients is reduced by 13% compared to controls, suggesting an impaired brain clearance of the protein in PD patients (Mollenhauer et al., 2011; van Dijk et al., 2013; Gao et al., 2015).

In the last twenty years, glymphatic system activity was visualized in humans by means of intrathecal injections of gadolinium-based contrast agents followed by MRI (Absinta et al., 2017). However, such approach cannot be applied to large cohorts of patients necessary to gain meaningful insights because of possible gadolinium-linked neurotoxic complications (Patel et al., 2020). The development of a novel minimal-invasive imaging technique called diffusion tensor image analysis along the perivascular space (DTI-ALPS) has allowed to successfully assess glymphatic function without the use of a contrast agent (Taoka et al., 2017). Thanks to this technique, a reduced glymphatic function has been demonstrated comparing 68 patients with PD and 129 healthy controls. Additionally, 119 patients with RBD showed a moderate decline in the glymphatic system activity, which was less relevant compared to PD patients (Si et al., 2022). Interestingly, this finding suggests that the impairment of the glymphatic system may start in the prodromal phase of PD and then worsen throughout the disease.

Other evidence pointing towards a link between the glymphatic system and PD came from animal models. Delayed glymphatic drainage was observed in mice injected with α-synuclein fibrils (Ding et al., 2021). A53T α-synuclein mouse model of PD displays a decrease in the influx of fluorescent cerebrospinal fluid tracer compared to wild type, together with perivascular aggregation of α-synuclein and mislocalization of AQP4 in the substantia nigra. Additionally, blocking of meningeal lymphatic drainage through ligation of cervical LVs worsened the phenotype in A53T mouse model, leading to further reduction of glymphatic clearance, increased α-synuclein deposition, astrogliosis and neuroinflammation, dopaminergic neurodegeneration and more severe motor defects (Zou et al., 2019) [Figure 7]. This evidence suggests that the glymphatic system plays an important role in the pathology and progression of PD.

To date, the most accredited hypothesis that links glymphatic system and PD is that early intra- and extracellular aggregation of α-synuclein perturbs glymphatic clearance,

which in turn further increases α-synuclein deposition, leading to a vicious self-amplifying circle of protein aggregation, inflammation and astrogliosis that exacerbates Parkinson's disease pathology.

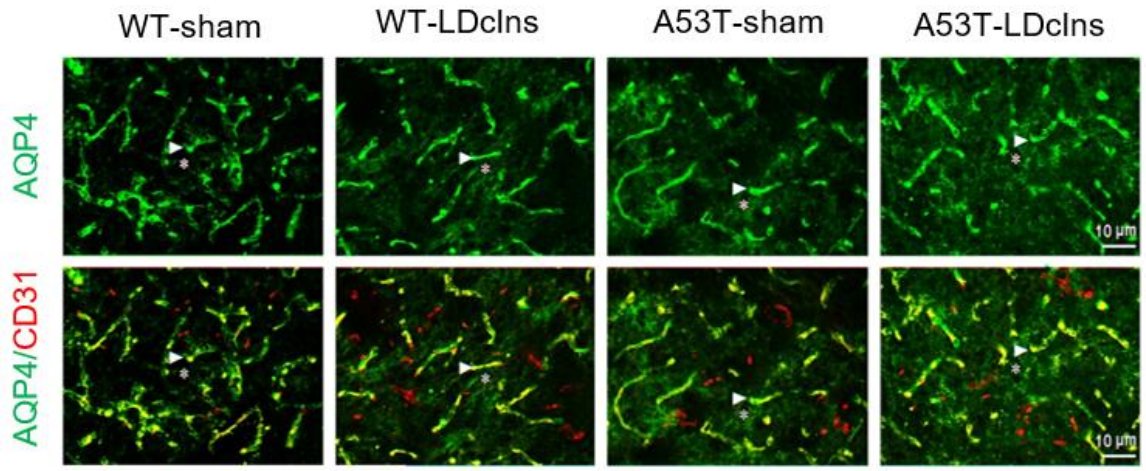

Figure 7: AQP4 vascular polarization is perturbed in A53T α-synuclein mouse model of PD and worsens after ligation of cervical lymphatic vessel (LDclns). Immunofluorescence revealed that AQP4 (green) is correctly located at astrocyte endfeet (arrowhead) surrounding CD31+ vessels (red) in the substantia nigra of WT-sham mice, while AQP4 signal was abnormally detected also in the neuropil domains (stars) in the other three groups, becoming especially prominent in A53T-LDclns condition. Adapted from Zou et al., 2019.

4 Familial forms of Parkinson's disease

Despite most forms being sporadic (meaning occurring in individuals with no family history of PD), a critical step in the understanding of the pathological mechanisms underlying PD came from the identification of genetic forms of the disorder, which represent about 10-15% of cases (Kalia et al., 2015). However, genetic contribution is present also in sporadic (also referred to as idiopathic) PD patients, in the form of gene-environment interaction and *de novo* causative mutations.

As sporadic and familial cases are almost clinically indistinguishable (Baba et al., 2006), modelling genetic PD can produce useful information on the pathogenesis and aetiology of idiopathic cases as well.

To date, 28 distinct chromosomal regions have been related to Parkinson's disease, but only eight of those contain genes that have conclusively been linked to monogenic PD, the most studied being: SNCA (α-synuclein) and PARK8 (leucine-rich repeat kinase 2, LRRK2) for autosomal dominant forms, PARK2 (Parkin), PARK6 (PTEN induced kinase 1, PINK1), and PARK7 (DJ-1) for autosomal recessive ones (Klein et al., 2012).

4.1 Autosomal dominant PD: SNCA and LRRK2

SNCA, encoding α-synuclein, was the first gene to be associated with Parkinson's disease (Polymeropoulos et al., 1997). At least five missense mutations (resulting in α-synuclein A53T, E46K, H50Q, G51D, and A30P) have been linked to autosomal dominant PD, but also several cases of duplication and triplication of the wild type SNCA gene have been observed (Appel-Cresswell et al., 2013; Krüger et al., 1998; Lesage et al., 2013; Zarranz et al., 2004; Singleton et al., 2003). Patients commonly display motor symptoms of typical late-onset PD with Lewy pathology (Farrer et al., 2001).

Even though SNCA dominant mutations are extremely rare, accounting for about 1% of the familial PD cases (George JM, 2002), the discovery that α-synuclein is one of the major components of LBs generated the idea of a common pathological mechanism for monogenic and sporadic Parkinson's disease. In support of this theory, SNCA gene duplications have been observed in idiopathic PD patients, and a polymorphism in its 3' UTR and promoter region were identified as risk factors (Narhi et al., 1999; Mueller et al., 2005). Such evidence suggests a critical dose-effect for α-synuclein expression both in sporadic and familial forms of PD (Eriksen et al., 2005).

More than 50 mutations have been identified in LRRK2 gene, accounting for 4% of idiopathic and 10% of hereditary PD cases with autosomal dominant inheritance, making it the most common cause of dominant Parkinson's disease (Berg et al., 2005). LRRK2 G2019S substitution is the most frequently observed in the Caucasian population (Obergasteiger et al., 2020). Clinical manifestations of LRRK2-PD resemble motor- and non-motor features of the sporadic disorder, while Lewy pathology is not always present (Ishihara et al., 2006).

4.2 Autosomal recessive PD: Parkin, PINK1, DJ-1

PINK1, Parkin and DJ-1 proteins are all directly or indirectly involved in mitochondria quality control and oxidative stress and have been associated with early-onset recessively inherited Parkinson's disease. Interestingly, all these PD subtypes present overlapping clinical features, with SN neurodegeneration, gliosis, and a general absence of Lewy bodies, especially in individuals carrying Parkin mutations (Farrer et al., 2001).

Mutations in PARK2, encoding Parkin protein, constitute the most common cause of early-onset familial PD. Indeed, homozygous missense mutations, copy number variations and deletions with loss of function (LOF) effect are observed in 50% of the hereditary PD forms and about 15% of the idiopathic cases (Lücking et al., 2000; Periquet et al., 2003). Both homozygous and compound heterozygous PARK2

mutations were identified in PD patients, and Ruffmann and colleagues identified in 2012 the first pure heterozygous Parkin patient, carrying R275W substitution (Ruffmann et al., 2012). Such evidence indicates that heterozygous mutations in PARK2 gene may not only represent a risk factor for the disease but can also result in symptomatic manifestations (Castelo Rueda et al., 2021).

Homozygous point mutations, insertions, and deletions with LOF effect in PINK1 and DJ-1 have also been observed in early-onset PD patients, but at a much lower rate compared to Parkin-linked cases (Valente et al., 2004; Lockhart et al., 2004). Heterozygous mutations in PINK1 are considered a risk factor for sporadic PD (Abou-Sleiman et al., 2006), and DJ-1 has been identified as one of the components of LBs (Clark et al., 2004), highlighting once again the correlation between monogenic and sporadic forms of Parkinson's disease.

Other genes that have been associated with inherited juvenile PD include ATP132A, C9ORF72, FBX07, PLA2G6, POLG1, SCA2, SCA3, SYNJ1, and RAB39B. Parkinson's disease caused by mutations in these genes is rare and shows quite uncommon symptomatic features, such as cognitive impairment, ataxia, and ophthalmologic dysfunctions (Puschmann, 2013).

4.3 Genetic risk factors for PD: GBA

In the last decades, genetic elements have been recognised as important risk factors for the development of Parkinson's disease (Noyce et al., 2012).

An example is the GBA gene, that encodes β-glucocerebrosidase (CGase). Compound heterozygous and homozygous mutations are causative of Gaucher disease, a rare lipid storage disorder. Instead, heterozygous mutations have been linked to an increased risk of Parkinson's disease (Gan-Or et al., 2008). Indeed, the accumulation of misfolded CGase and its lipid substrates causes ER stress and activates UPR response, possibly resulting in the misfolding of other proteins, including α-synuclein, thus increasing the risk of PD (Maor et al., 2013).

5 Parkin is a multifunctional E3 ubiquitin ligase

As briefly mentioned in chapter 4.2, mutations in PARK2 have been recognised as the most common cause of autosomal recessive PD. PARK2 is located on chromosome 6q25.2-q27 and encodes a 52 kDa protein called Parkin, a multifunctional E3 ubiquitin ligase that plays a variety of roles in the cell including the degradation of proteins and the maintenance of mitochondria homeostasis and integrity (Seirafi et al., 2015). Parkin is highly expressed in the brain, heart, and skeletal muscle, and it is present both in the cytosol and marginally in the cell nucleus (Kitada et al., 1998).

5.1 Structure and activation of Parkin

From the structural point of view, Parkin is composed of 465 amino acids and presents five different domains with specific functions. The ubiquitin-like domain (UBL, residues 1-76) is located at the N-terminal and is followed by three zinc-coordinating Really Interesting New Gene (RING) domains: RING0 (residues 141-216), RING1 (residues 217-327), IBR (residues 328-378), and RING2 (residues 411-465) (Seirafi et al., 2015). Parkin contains two additional linker interdomains that are flexible. The first one follows the UBL domain and is composed of about 70 amino acids with unknown function. The second is located between IBR and RING2 domains and is constituted of disordered segments and an α-helix that binds RING1. This structure is called repressor element of Parkin (REP) as it negatively regulates the activity of the protein (Dove et al., 2013) [Figure 8 A].

Functionally, Parkin can be classified as a RING-between-RING (RBR) E3 ubiquitin ligase (Wenzel et al., 2011). E3 ubiquitin ligases participate in the last step of the ubiquitination process, interacting with ubiquitin-charged E2 enzymes and finally transferring activated ubiquitin to the substrate protein (Berndsen et al., 2014).

In Parkin, RING1 domain is the putative binding site of the E2 enzyme, while RING2 is the active domain, with the catalytic cysteine residue for ubiquitin binding located at position 431 (Hristova et al., 2009). While UBL and REP domains are important for Parkin activation, functions of IBR and RING0 remain elusive (Beasley et al., 2007).

Interestingly, Parkin is engaged in both monoubiquitination, as well as K48- and K63-linked polyubiquitination (Peng et al., 2003). While K48-linked ubiquitin chains target proteins to the proteasome for degradation, K63-linked and other less common types of ubiquitination (K6 and K11) result in proteasome-independent regulation of protein trafficking and localization (Komander et al., 2012). Clearly, Parkin role is not solely restricted to protein degradation.

Parkin activity is strictly controlled by different levels of autoinhibition. First, access to RING2 catalytic domain is structurally blocked by RING0. Additionally, UBL and REP domains occlude E2 binding site located in RING1 domain. Deletions of all these domains *in vitro* result in increased Parkin activation (Wauer et al., 2013). Finally, the long distance between RING1 and RING2 prevents the transfer of activated ubiquitin from E2 enzyme to Parkin catalytic cysteine [Figure 8 B]. Multiple effectors can promote the activation of Parkin. In particular, UBL domain plays an important role in this process: indeed, binding of UBL binding partners such as Eps15, proteasomal subunits, and ataxin3 causes the dissociation of UBL from RING1 allowing the switch from inactive to active conformation with a so-called “butterfly” transition (Chaugule et al., 2011; Trempe et al., 2013) [Figure 8 C].

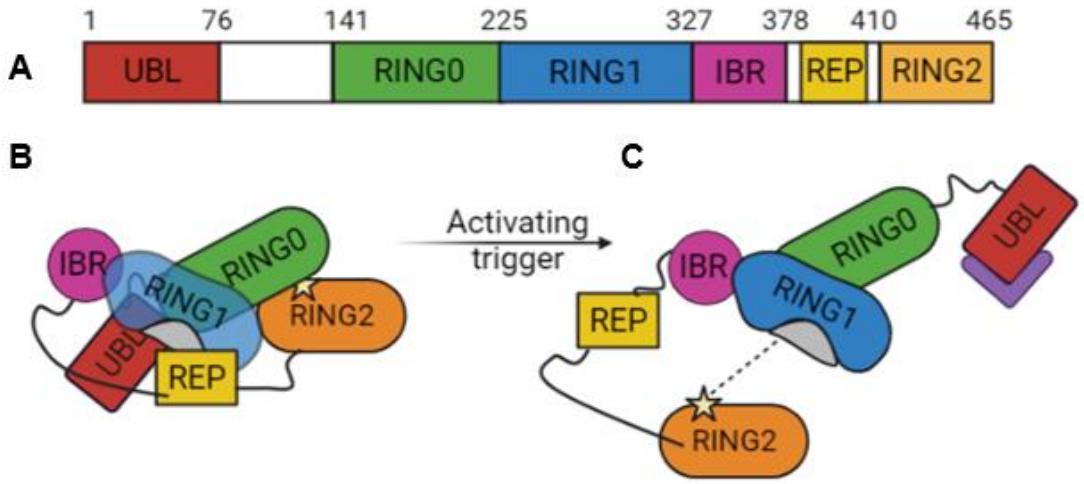

Figure 8: Parkin structural organization reveals its autoinhibition mechanism. A) Architecture of Parkin protein domains. Linkers and sites with unknown function are in white. In its autoinhibited state (B), E2 binding site on RING1 (grey) is structurally blocked by REP and UBL domains, and catalytic cysteine 431 on RING2 (star) is obstructed by RING0. (C) Activating stimuli, such as binding of UBL by specific substrates (purple) trigger a "butterfly" conformational change that exposes Parkin active sites and reduces the distance (dashed line) between cysteine 431 and E2 binding site, allowing the transfer of activated ubiquitin. Created with BioRender.com.

5.2 The role of Parkin in Parkinson's disease

More than 100 PD-linked mutations have been found in Parkin, the most common being exons 3/4 deletion and R275W substitution (Grünewald et al., 2013). Mutations in PARK2 typically result in the loss of protein function (LOF). LOF can result upon conformational changes, impaired zinc coordination (C212Y, C289G and C441R) and folding (R42P, K211N and TR51P), disrupted catalytic (C431F and G430) and binding (T240R) sites, altered solubility and localization (R275W and C418R), increased or decreased ubiquitination and autoubiquitination activity (T415N), modification of substrate recognition and binding, and impaired mitochondrial translocation (K161N) (Cookson et al., 2003; Siram et al., 2005; Wang et al., 2005; Hampe et al., 2006).

Clinically, Parkin-linked PD is indistinguishable from sporadic cases (Lücking et al., 2000). Most patients display typical motor and non-motor symptoms, with early onset (21-50 years) and slow disease progression (Corti et al., 2011). Typically, Lewy body pathology is not observed in the brains of patients carrying Parkin mutations (Lohmann et al., 2009). Parkin alterations are observed also in sporadic cases of the disorder. Indeed, brain specimens collected from idiopathic PD patients revealed decreased Parkin expression and activity compared to healthy controls (Chung et al., 2004), decreased Parkin solubility, increased levels of ubiquitinated proteins, and upregulation of PARIS (Shin et al., 2011), a substrate of Parkin that is linked to mitochondria turnover.

5.2.1 Parkin and protein aggregation

As an E3 ubiquitin ligase, Parkin is deeply involved in the process of protein quality control and degradation through the ubiquitin proteasome system. Being one of the mechanisms linked to the development of Parkinson's disease, the theory that accumulation of proteins caused by loss of Parkin function could lead to degeneration is very appealing.

To date, more than 30 putative substrates of Parkin have been identified, but none of them was found to be exclusively expressed in DA neurons and only a few of them (Cyclin E, FBP1, Hsp70, P38) accumulate in PD patients' brains (Zhang et al., 2016). One of the most interesting substrates is PARIS (ZNF46). PARIS is a transcriptional repressor of peroxisome-activated receptor gamma coactivator 1-alpha (PGC-1α), a key regulator of many aspects of cellular metabolism and mitochondrial biogenesis (Scarpulla et al., 2008). Interestingly, PARIS accumulates in brain specimens from autosomal recessive and sporadic PD patients, and mouse models lacking Parkin show PARIS aggregation in the ventral midbrain region (Shin et al., 2011). This evidence suggests an important link between Parkin activity and protein aggregation both in familial and idiopathic Parkinson's disease.

The non-proteolytic ubiquitin chains catalysed by Parkin can be involved in the neurodegeneration as well (Peng et al., 2003). Indeed, it was observed that K63-linked polyubiquitination of several proteins including synphilin-1 (a binding partner of α-synuclein) and DJ-1 in their misfolded state promotes their sequestration into juxtanuclear inclusion bodies called aggresomes (Lim et al., 2005; Olzmann et al., 2007). Additionally, K63-linked polyubiquitin triggers the macroautophagy-mediated clearance of aggresomes (Tan et al., 2008).

This dual role of Parkin in mediating both proteasome-associated (K48-linked) and macroautophagy-associated (K63-linked) polyubiquitination indicates that Parkin acts as an important bridge element between the two major degradation pathways of the cell. Alterations in Parkin expression and activity can influence the delicate equilibrium of these processes, eventually leading to protein accumulation and neurodegeneration.

5.2.2 Parkin and the mitochondria

Besides its importance in the UPS system, Parkin modulates mitochondria homeostasis, biogenesis, quality control and degradation (Harper et al., 2018).

Indeed, Parkin can translocate to damaged mitochondria upon membrane depolarization and promote their autophagy-mediated degradation, a process called mitophagy, in a PINK1-dependent manner. PINK1 works as a sensor of mitochondrial damage (Rüb et al., 2017): in healthy mitochondria PINK1 is constitutively imported

across the mitochondrial outer and inner membranes (MOM, MIM) using TOMM and TIMM23 transporters, respectively. Inside the mitochondria PINK1 is cleaved and then released back into the cytosol, where it is targeted for proteasomal degradation. Upon mitochondria depolarization instead, PINK1 is retained on the outer membrane where it accumulates and forms large complexes. Stabilized PINK1 phosphorylates ubiquitin and Parkin on serine 65 (Ser65) (Kazlauskaite et al., 2014; Koyano et al., 2017). Chains of phosphorylated ubiquitin on the MOM allow the retain of Parkin on the mitochondrial membrane. Phosphorylated Parkin is hyperactive and ubiquitinates several mitochondrial substrates, as for example myosin VI (MYO6) (Kruppa et al., 2018).

At this point, ubiquitinated proteins and ubiquitin chains are recognized by autophagy receptors, leading to the engulfment of the damaged mitochondria into the autophagosome, which will eventually fuse with the lysosome for cargo degradation. However, although Parkin importance in mitophagy is highly demonstrated, the relevance of this process in conditions of moderate stress or in non-dividing cells, like neurons, is still unclear (Grenier et al., 2013).

Indeed, the majority of studies on post-mortem brain samples of PD patients did not report overt changes in mitochondrial network and morphology (Zanellati et al., 2015). Despite the fact that mitochondria of DA neurons derived from patients with Parkin-linked PD showed swelling and cristae degeneration (Shaltouki et al., 2015), no or little studies have been performed on mitophagy in these cells.

Parkin is important not only for mitochondria elimination but is also involved in their biogenesis. Indeed, Parkin ubiquitinates PARIS, a transcriptional repressor of PGC-1α, one of the key regulators of mitochondrial biogenesis and function. PARIS ubiquitination leads to its proteasomal degradation, allowing PGC-1α transcription and subsequent expression of downstream genes such as Nrf-1 and Nrf-2, which increase cellular respiration, energy utilization and mitochondrial biogenesis (Zheng et al., 2017). LOF mutations in Parkin mouse models cause PARIS accumulation and a reduction in the size and the number of mitochondria in ventral midbrain neurons, a phenotype that was rescued by knockdown of PARIS (Stevens et al., 2015). Additionally, low levels of PGC-1α have been detected in the substantia nigra of PD patients (Zhen et al., 2010).

Parkin also protects mitochondrial genome integrity by interacting with mitochondrial transcription factor A (TFAM), thus increasing mitochondrial DNA transcription, and stimulating its repair. Indeed, higher susceptibility of mtDNA to ROS and reduced mtDNA repair capacity was observed by Rothfuss and colleagues in Parkin-deficient fibroblasts derived from a PD patient (Rothfuss et al., 2019), indicating that Parkin-

dependent protection of mitochondria genome from oxidative stress is lost in Parkinson's disease.

5.2.3 Other functions of Parkin

Several studies have also reported that Parkin can promote cell survival through different pathways.

For example, Parkin has been shown to activate pro-survival nuclear factor-kB (NF-κB) signalling cascade under stress conditions, by ubiquitination of NF-κB essential modulator (NEMO) and regulatory kinase IκB (IKK) (Hwang et al., 2010).

Additionally, PARK2 is now considered a tumour-suppressor gene. Indeed, PARK2 deletions are observed in 30% of human tumours, and Parkin null mice are more susceptible to tumorigenesis (Wahabi et al., 2018). Parkin is thought to exert its anti-tumorigenic effect by acting as a transcriptional repressor of p53 both binding to its promoter (daCosta et al., 2009) and by direct interaction with p53 protein (Zhang et al., 2011).

Finally, Parkin plays a role in innate immunity and pathogens defence promoting xenophagy, a process in which bacteria (for example *Mycobacterium tuberculosis* and *Salmonella enterica*) are tagged with ubiquitin chains and are degraded by the autophagy/lysosomal pathway (Manzanillo et al., 2013).

5.3 Parkin-null animal models of Parkinson's disease

To better understand the role of Parkin in the pathological mechanisms of PD, numerous animal models have been generated.

KO of Park2 in *Drosophila* reduces longevity, induces male sterility due to defects in spermatogenesis, and increases susceptibility to stressors (Pesah et al., 2004). Mutant flies show moderate motor impairment in flight and climbing ability. The major flight muscles (IFM) revealed strong degeneration and accumulation of swollen mitochondria with disintegrated cristae. However, overt degeneration of dopaminergic neurons was not observed in Parkin null *Drosophila* brains (Greene et al., 2003). Degeneration at the muscle level is an interesting feature that is observed almost uniquely in *Drosophila* models with Parkin knock-out.

Parkin depletion in mice does not result in any relevant phenotype. In general, Parkin mutant mice do not show overt DA neurons loss, nor motor impairments (Goldberg et al., 2003). Some alterations in non-motor behaviour and defects in synaptic plasticity have been reported in Park2-deficient mice (Hanson et al., 2010), but the results are sometimes non-coherent. Mice lacking Parkin do not display evident defects in

mitochondria structure and organization, but mitochondrial respiratory capacity is decreased (Palacino et al., 2004).

6 Parkin R275W

In 2001 Farrer et colleagues identified a novel 924C>T point mutation in exon 7 of PARK2 that leads to the substitution of arginine with tryptophan at position 275 (R275W) in the RING1 domain of Parkin protein. R275W mutation was observed in a patient together with a 40-base pair (bp) deletion in exon3 (Ex3Δ40).

Clinically, this patient displayed early onset PD and the degeneration of dopaminergic neurons. Autoptic analysis revealed the presence of α-synuclein-positive LBs in the brain, suggesting that R275W/Ex3Δ40 Parkin-pathology was comparable to that seen in mild to moderate sporadic PD.

Conversely, brain autoptic analysis of a 93-year-old asymptomatic carrier of PARK2 Ex3Δ40 only did not show alterations in the substantia nigra nor Lewy pathology, suggesting that hemizygous Ex3Δ40 confers susceptibility to PD but it is not sufficient to cause the disease, while R275W compound heterozygosis leads to early-onset pathology with LBs (Farrer et al., 2001).

In 2012 Ruffmann and his group identified the first pure heterozygous R275W patient with clinical features typical of sporadic PD, like late onset (62 years old), severe neuronal loss in the substantia nigra, and diffuse Lewy pathology (Ruffmann et al., 2012).

As mentioned in 6.2, Parkin-related forms of Parkinson's disease typically display early onset and absence of Lewy pathology. Thus, the description of a novel heterozygous mutation in Parkin that causes a form of the disease that is consistent with sporadic PD, rather than familial PD, is of great interest and could help uncover pathological aspects of idiopathic disease.

6.1 Parkin R275W *in vitro* characterization

Unlike other common PARK2 mutations that result in the complete ablation of enzyme function, R275W Parkin retains a residual E3 ubiquitin ligase activity at least on some of its substrates (Lee et al., 2010).

The first characterization of Parkin R275W was performed by Cookson and colleagues in 2003. They observed that, upon overexpression in HEK 293 cells, wild type Parkin had a homogeneous distribution in the cytosol and was also present in the nucleus, while mutant Parkin formed inclusions both in the cytosol and in the nucleus that did not overlap with DNA. Additionally, they also noticed that Parkin R275W could generate large perinuclear structures identified as aggresomes (Cookson et al., 2003),

as they were surrounded by vimentin and contained ubiquitin (Johnston et al., 1998). The same pattern was observed when wild type or R275W Parkin were overexpressed in hippocampal neurons.

Similar results were obtained by analysing the impact of R256C substitution, falling as well in the RING1 domain. Other mutations like A82E, G328E, C431F, and Ex3Δ40, falling in different domains, did not influence Parkin subcellular distribution. These data suggest that the RING1 domain is important for protein folding and its correct localization (Cookson et al., 2003).

RING1 mutations may indeed cause the misfolding of the protein leading to its accumulation in intracellular and intranuclear inclusions. This scenario depicts a gain of toxic function rather than a LOF as a pathological mechanism for Parkin R275W PD. Accordingly with this idea, several recent studies have proved that about half of PD patients carrying R275W Parkin mutation display Lewy pathology in several brain areas (Madsen et al., 2021).

In conclusion, it is possible to hypothesize that depending on the affected domain, each Parkin mutations can trigger the disease via loss of- and/or gain of function (GOF) mechanisms, explaining the different genetic profiles of the mutations.

6.2 Parkin R275W *Drosophila melanogaster*

Drosophila melanogaster has revealed itself to be a useful tool to investigate familial forms of PD and it has been particularly implied to model Parkin-linked forms of the disease.

Overexpression of R275W human Parkin in *Drosophila* causes selective and progressive degeneration of dopaminergic neuronal clusters, decreased Parkin solubility and prominent climbing defects in mutant flies compared to wild type. R275W flies also display increased sensitivity to rotenone-induced neurotoxicity. Additionally, *Drosophila* mutants also showed marked fibre degeneration in the flight muscles, accompanied by severe and pleiomorphic mitochondrial pathologies, characterized by the presence of vacuolar structures surrounded by layers of membranes, disorganized cristae, and disrupted membranes. Interestingly, Parkin R275W mutants displayed the same pathological features as Parkin-null flies, suggesting that Parkin R275W expression *in vivo* could be pathogenic even in the presence of wild type protein, consistent with a dominant-negative effect for the mutation. Additionally, it was observed that R275W flies present a stronger defect in climbing and different mitochondrial abnormalities compared to Parkin-deficient *Drosophila* [Figure 9], suggesting that Parkin R275W toxic effects may be exerted through a mechanism

dissimilar from that caused by overt loss of Parkin expression and activity (Wang et al., 2007).

Interestingly, none of the phenotypes described above was observed in *Drosophila* that overexpressed human G328E Parkin, a mutation that occurs outside the RING1 domain (Wang et al., 2005). Conversely, Sang group observed that overexpression of other mutants with a substitution within the RING1 finger domain (i.e., T240R and Q311X) caused neurodegeneration of DA neurons and progressive motor impairment in *Drosophila* (Sang et al., 2007). Altogether, these studies suggest that the localization of the substitution is important to determine the pathogenicity of Parkin mutation.

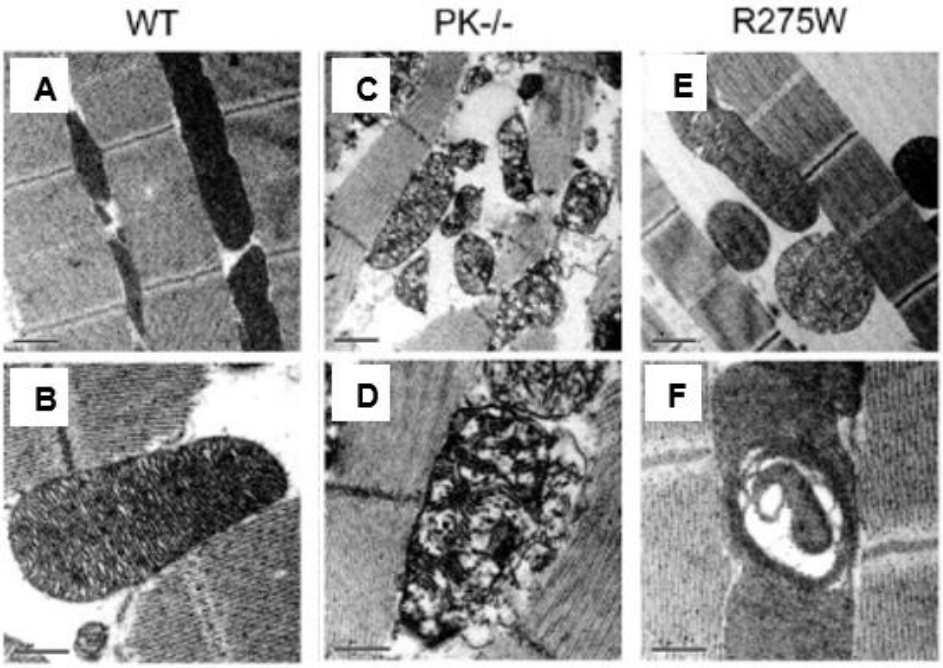

Figure 9: Mitochondrial abnormalities in Parkin-null and Parkin R275W *Drosophila* reveal mutation-dependent peculiarities. Transmitted electron microscopy (TEM) analysis of flight muscle of flies overexpressing wild type human Parkin (WT) (A, B), R275W (E, F) or lacking endogenous Parkin (PK-/-) (C, D). Scale bar = 1 µm for A, C, E. Scale bar = 0.5 µm for B, D, F. Adapted from Wang et al., 2007.

AIMS OF THE PROJECT

The main aim of this project was the *in vivo* and *ex vivo* characterization of the functional impact of R274W Parkin variant. To this goal, we generated the first mouse line carrying the substitution corresponding to the human R275W mutation both in hetero- and homozygosity.

More in detail our project aims to:

1) Characterize the effect of R274W mutation in a mouse model. Current genetic models of Parkinson's disease fail to recapitulate the major hallmarks of the disorder, such as age-dependent motor impairment and dopaminergic neurons loss, neuroinflammation, mitochondrial damage, and protein aggregation. All these aspects were characterized in our novel mouse model.
2) Improve understanding of Parkin R274W molecular mechanism. It is well known that Parkin is important for the mitochondria. We explored the impact of the mutation on pathways related to mitochondria biogenesis, but also protein aggregation and triggering of cellular stress.
3) Obtain new vision about Parkin function: current knowledge links Parkin with several aspects of mitochondrial homeostasis and protein degradation. Here we investigated an unexpected role for Parkin in modulating AQP4 localization in the glymphatic system.
4) Offer novel information about the effect of Parkin R274W in the skeletal muscle.
5) Gain new insight into the genetic of Parkin mutation. PARK2 mutations are usually recessive. However, heterozygous cases are also observed. Our characterization will help uncover the link between Parkin-linked dominant gain of toxicity and PD.

The ultimate goal was to verify whether the transgenic Parkin R274W mouse we generated could be a robust and predictive animal model able to recapitulate the main features observed in human patients. Ideally, our model could serve not only to study pathogenic mechanisms but also to test new therapeutic approaches.

RESULTS

1 Parkin R274W in homozygous mice brains

We generated by CRISPR/Cas9 technology the first C57BL/6N mouse line carrying R274W Parkin mutation (corresponding to the human R275W substitution). Full characterization of homozygous and heterozygous mice was performed at 6, 12, and 18 months.

1.1 Homozygous mice display age-dependent motor impairment, DA neurons loss and astrogliosis

We assessed motor performance of homozygous mice at 6, 12, and 18 months and compared the results with age-matched wild type (WT). Male and female animals were included in our cohorts in a 1:1 ratio.

We evaluated motor coordination on the rotarod at increasing acceleration (4-32 rpm), on the balance beam (12 and 6 mm), and on the pole test.

An impairment in coordination in R274W+/+ mice was observed already at 6 months on the 12 mm balance beam [Figure 10 B]. Such defects were more evident at 12 months, were homozygous mice performed significantly worse than age-matched wild type both in the 6 mm balance beam [Figure 10 E] and in the pole test [Figure 10 F]. Finally, coordination impairment was overt in 18-month-old R274W+/+ mice, which showed defects also in the accelerated rotarod test [Figure 10 G, H]. At 18 months, neither wild type nor homozygous mice were able to perform on the pole test and on the 6 mm balance beam. No differences were detected in anxiety phenotype nor in the weight of mutant animals compared to age-matched wild type [Supplementary Figure S1].

Such evidence indicate that R274W+/+ mice display an age-dependent phenotype of motor impairment in coordination.

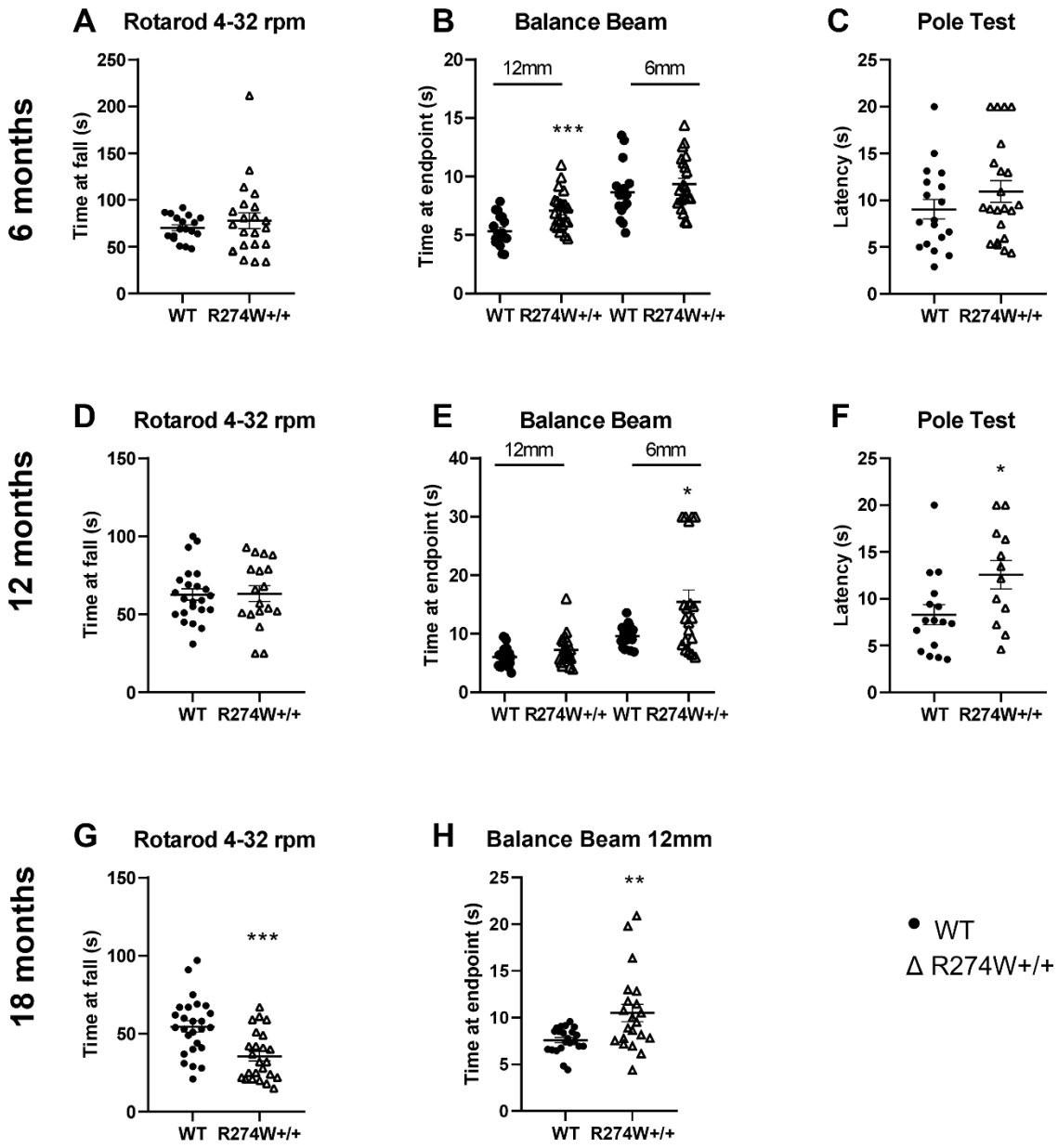

Figure 10: R274W+/+ mice show age-dependent impairment in motor coordination. We tested male and female mice at the indicated ages. We observed defects on the rotarod at increased acceleration at 18 months (G), in the balance beam at 6 (B), 12 (E), and 18 (H) months, and on the pole test at 12 months (F). Old mice were not able to perform on the 6 mm balance beam nor on the pole test. Data are the means ± SEM; n WT = 16-22; n R274W+/+ = 16-22; *, **, *** p<0.05, 0.01, 0.001 vs. wild type.

To define the time-course of nigral degeneration, we evaluated the number of dopaminergic neurons in the substantia nigra along ageing by means of confocal-assisted stereological cell count.

Homozygous mice displayed a reduction in DA neurons of 23%, 30%, and 40% at 6, 12, and 18 months respectively compared to age-matched wild type [Figure 11 A, B]. Additionally, we also observed by means of HPLC analysis a reduction in the amount of dopamine (DA) present in the striatum of mutant mice compared to wild type at 12

months of age [Figure 11 C]. The decrease of tyrosine hydroxylase (TH) expression by dopaminergic neurons in the SN pc of mutant animals was also assessed at 6, 12, and 18 months of age by immunofluorescence analysis [Figure 12].

This phenotype of overt neurodegeneration was also accompanied by astrogliosis, as suggested by increased GFAP fluorescent signal observed in the striatum and substantia nigra of homozygous mice compared to wild type [Figure 13]. Indeed, the glial fibrillary protein GFAP is a common marker of astrocytes which expression is increased during inflammatory-driven astrocytes proliferation. Augmented intensity of GFAP signal was also detected in homozygous cortex compared to age-matched wild type in all the ages analysed [Supplementary Figure S2].

Altogether, our data show that Parkin R274W+/+ mice present an age-dependent PD-related phenotype starting at 6 months of age.

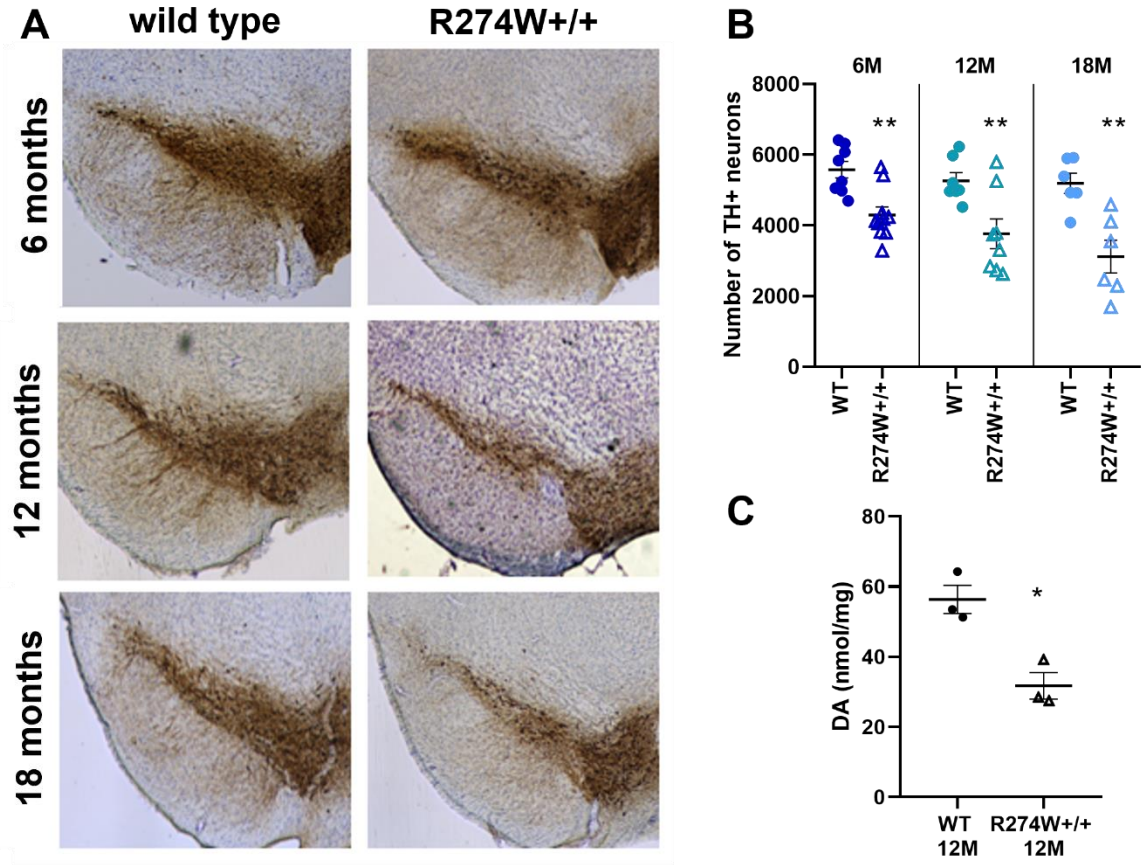

Figure 11: R274W+/+ mice show an age-dependent loss of dopaminergic neurons. (A) TH immunoperoxidase labelling (brown) in the SN pc of WT and R274W homozygous mice at 6, 12, and 18 months of age. Nuclei are shown in blue. (B) The graph shows quantification of DA neurons in the substantia nigra of wild type and mutant mice at 6, 12, and 18 months. Data are the means ± SEM; two-sided t-test was performed to compare intra-age data vs. wild type; n 6M = 8-9; n 12M = 6-8; n 18M = 6; **, $p<0.01$ (C) HPLC analysis on striatum revealed that dopamine released in the striatum is decreased in homozygous mice compared to wild type at 12 months. Data are the means ± SEM; n = 3; *, $p<0.05$ versus wild type. In collaboration with Prof. Michele Morari.

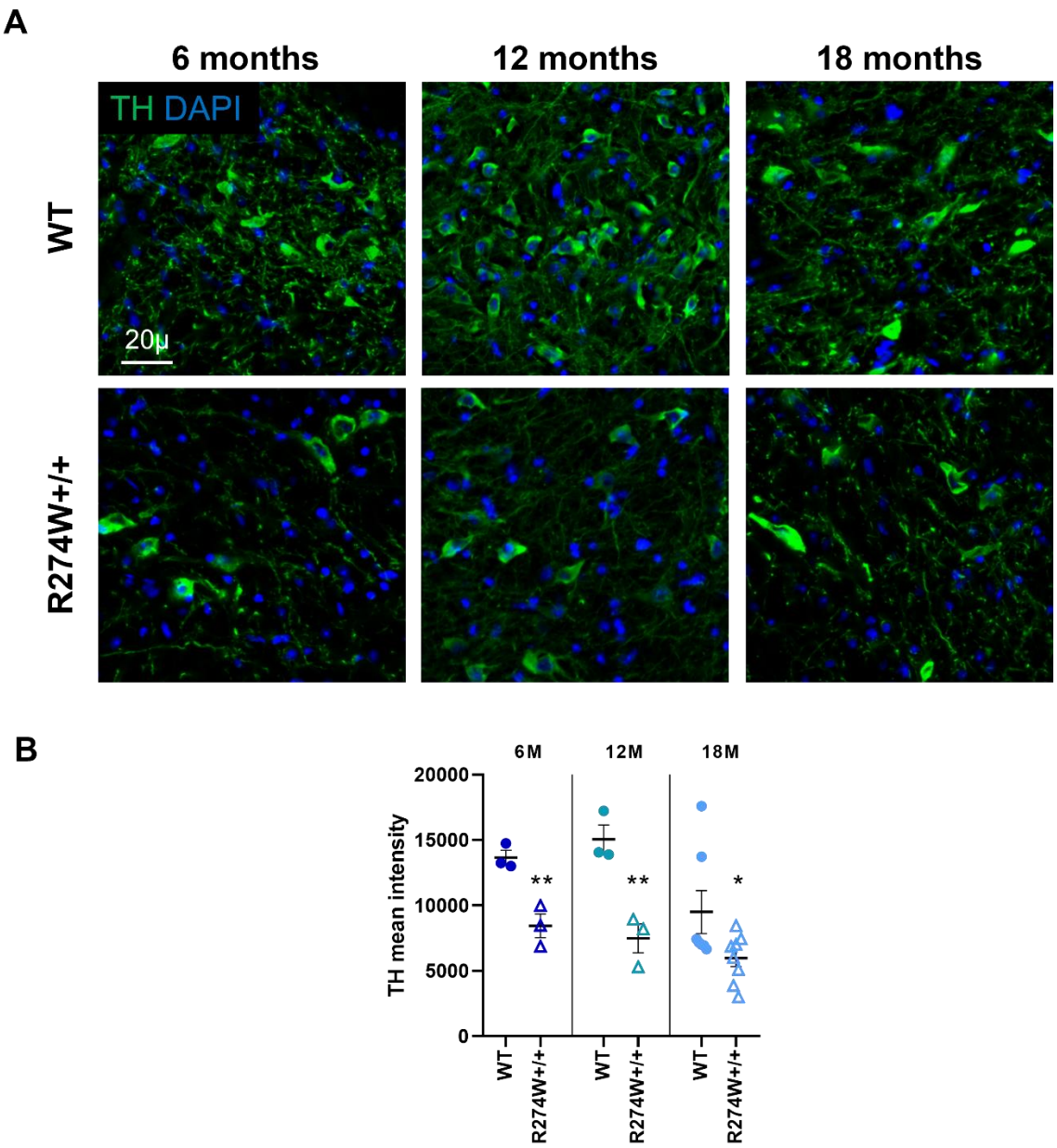

Figure 12: R274W+/+ mice brains display age-dependent TH loss. (A) Representative images of SN pc sections from 6-, 12-, and 18-month-old wild type and Parkin R274W+/+ mice stained with anti-TH antibody and DAPI to visualize nuclei. Scale bar = 20 µm. (B) The graph reports the TH mean intensity for each brain region folded on wild type mean; data are expressed as means ±SEM; two-sided t-test was performed comparing intra-age data vs. wild type; n 6M = 3, n 12M = 3, n 18M = 6; *, ** $p<0.05$, 0.001.

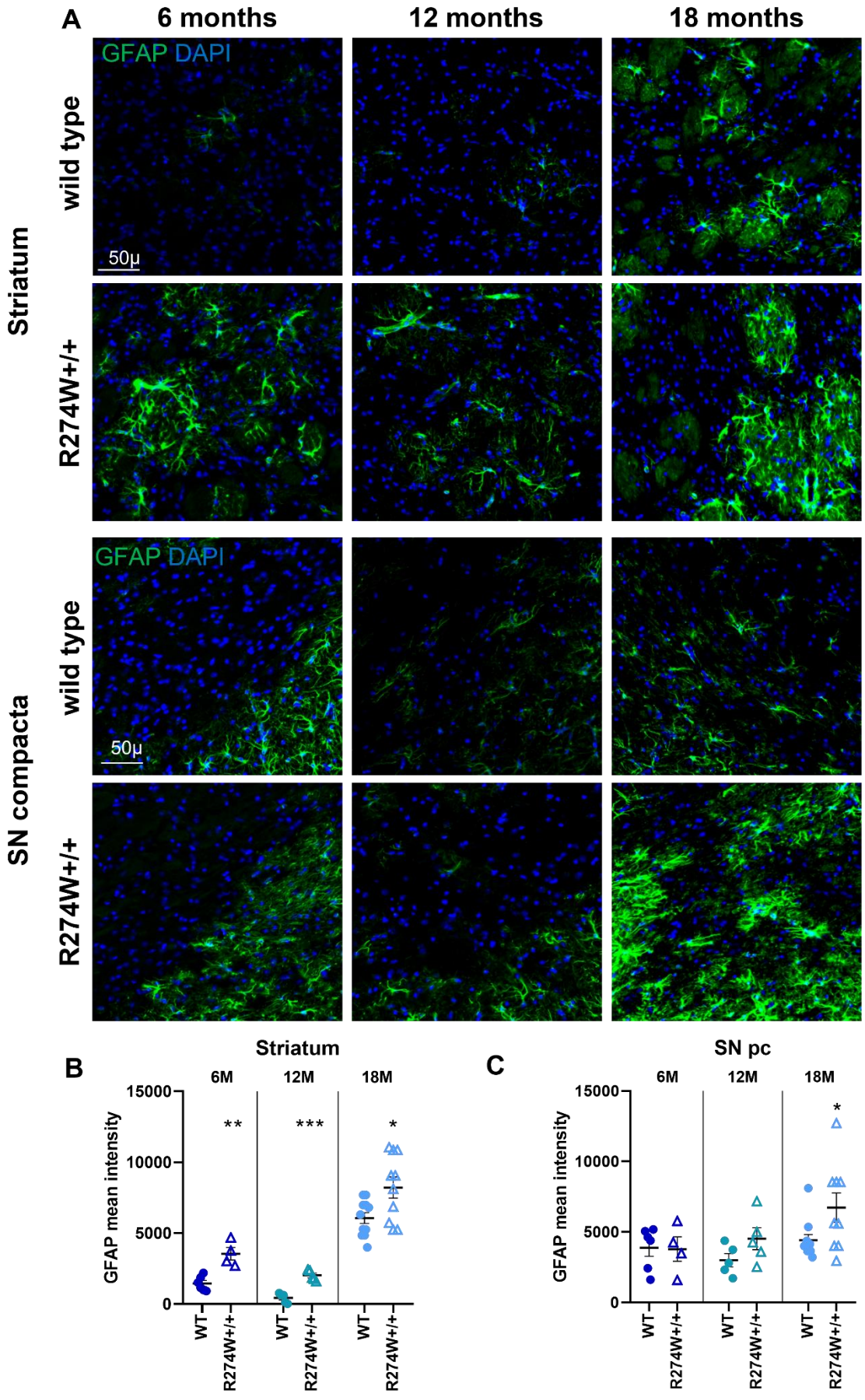
A
6 months
12 months
18 months
Striatum
wild type
R274W+/+
GFAP DAPI
50µ
SN compacta
wild type
R274W+/+
GFAP DAPI
50µ
B
Striatum
6M
12M
18M
GFAP mean intensity
15000
10000
5000
0
**
***
*
WT
R274W+/+
C
SN pc
6M
12M
18M
GFAP mean intensity
15000
10000
5000
0
*
WT
R274W+/+

Figure 13: Parkin R274W+/+ mice brains display an age-dependent astrogliosis. (A) Representative images of striatum and SN pc sections from 6-, 12-, and 18-month-old wild type and homozygous mice stained with anti-GFAP antibody (green) and DAPI (blue). Scale bar = 50 µm. The graphs (B, C) report GFAP mean intensity in the striatum and SN pc respectively. Data are the means ± SEM; n 6M = 5-4, n 12M = 4-4; n 18M = 9-10; two-sided t-test was performed comparing intra-age data vs. wild type; *, **, ***, p<0.05, 0.01, 0.001.

1.2 R274W mutation in Parkin causes defects in mitochondrial biogenesis

Given the fundamental role of Parkin in the regulation of mitochondrial turnover, we examined mitochondria levels in DIV14 cortical neurons derived from wild type and homozygous mice. To this aim, we used an antibody that recognizes the MOM receptor Tomm20 and analysed our samples by biochemical means.

First, we observed by western blotting that mitochondrial mass is decreased in R274W+/+ neurons compared to wild type [Figure 14].

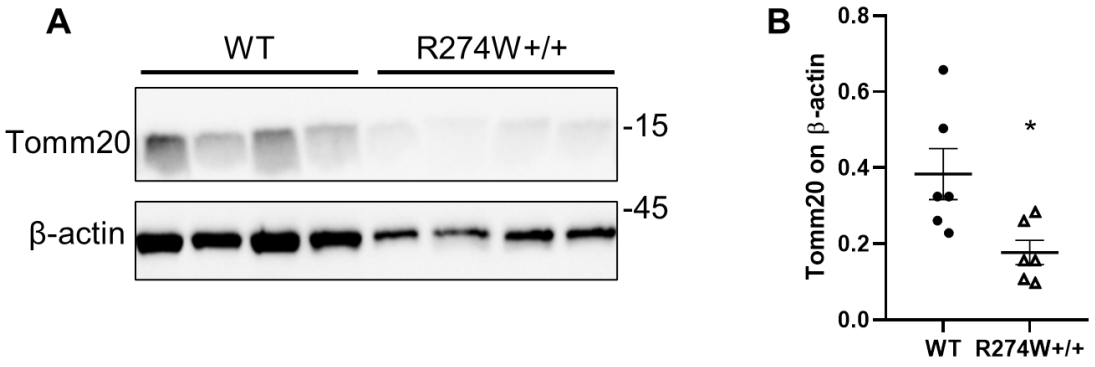

Figure 14: Mitochondrial mass is reduced in R274W+/+ neurons. Tomm20 was used as a probe to assess mitochondria quantity in neurons derived from WT or homozygous mice via western blotting. The graph (B) shows quantification of Tomm20 protein level normalized on β-actin amount. Data are the means ± SEM; n = 6; *, p<0.05 versus wild type.

We observed a similar result in primary fibroblasts generated from wild type and homozygous mice [Figure 15 A, B]. Interestingly, performing high resolution respirometry we also noticed a decreased respiratory capacity [Figure 15 F] in homozygous cells compared to wild type. In mutant fibroblasts we also noticed the accumulation of PARIS [Figure 15 C], a known Parkin substrate involved in the control of mitochondrial biogenesis.

Indeed, PARIS is normally sent to proteasomal degradation by Parkin-dependent ubiquitination. When Parkin is less present or non-functional, PARIS is able to translocate into the nucleus, where it represses the transcription of PGC-1α, a master regulator of mitochondrial biosynthesis, with consequent reduced expression of several downstream genes that regulate mitochondria biogenesis [Figure 15 D].

Noteworthy, PGC-1α mRNA levels are reduced in homozygous fibroblasts compared to wild type [Figure 15 E], indicating that R274W mutation in Parkin impairs PARIS-PGC-1α pathway of mitochondrial biogenesis.

Finally, we demonstrated that overexpression of PGC-1α is sufficient to restore mitochondria content in mutant fibroblasts [Figure 15 G, H].

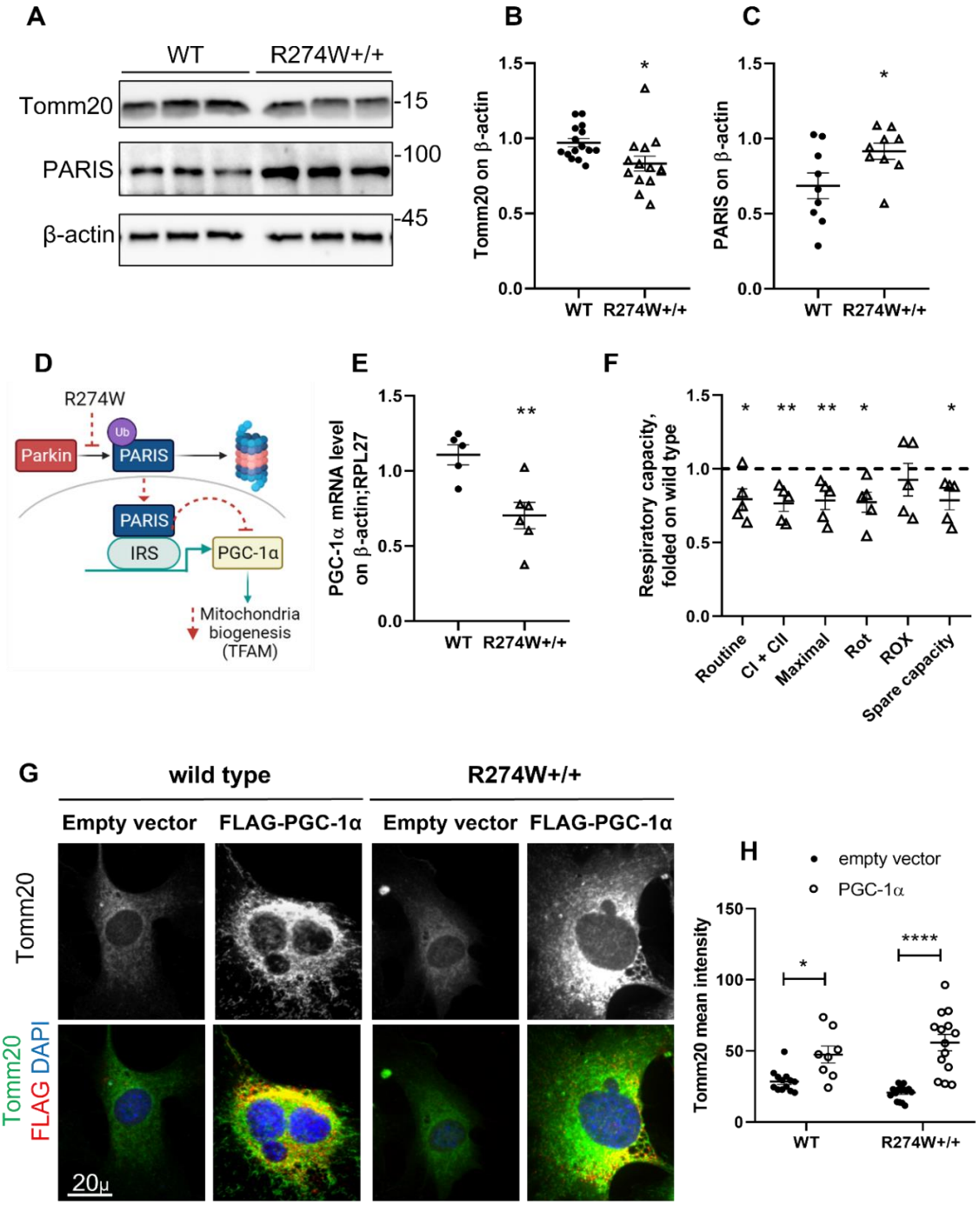

Figure 15: Mitochondrial biogenesis through the PARIS-PGC-1α pathway is impaired in R274W+/+ fibroblasts. (A) We analysed by western-blotting protein lysates prepared from wild type and Parkin R274W+/+ primary fibroblasts. The graphs report Tomm20 (B) and PARIS (C) levels expressed as optical density and normalized on β-actin amount. Data are expressed as means ±SEM, (B) n = 15-14; (C) n = 9; *, p<0.05 versus wild type. (D) Parkin controls PARIS degradation via the proteasome. PARIS represses the transcription

of PGC-1α, a master regulator of mitochondrial biogenesis. Parkin LOF induces PARIS accumulation, down-regulates PGC-1α transcription, and eventually leads to decreased mitochondrial biogenesis. (E) We assessed PGC-1α mRNA level in wild type and Parkin R274W+/+ primary fibroblasts by qRT-PCR. The graph represents the relative expression of PGC-1α mRNA level, normalized on β-actin and RPL27 mRNA amount. Data are expressed as means ±SEM, n = 5-6; **, p<0.01 versus wild type.
(F) In collaboration with Dr. Irene Pichler, we assessed oxygen consumption in wild type and homozygous primary fibroblasts by high resolution respirometry. The graph reports routine activity (routine respiration), complex I and complex II-dependent activity (upon treatment with malate, glutamate, and succinate), maximal respiration (maximal uncoupled respiration after uncoupler addition), respiration after inhibition of complex I (upon Rotenone inhibition), residual oxygen consumption due to oxidative side reactions (after addition of antimycin A) and difference between maximal respiration and routine respiration (spare capacity). Data are expressed as means ±SEM; n = 5; *, **, p<0.05, 0.01 versus wild type.
(G) We transfected primary fibroblasts derived from wild type and Parkin R274W+/+ mice with empty vector or with FLAG-PGC-1α vector. Cells were stained with anti-FLAG (red) and anti-Tomm20 (green) antibodies and DAPI to visualize the nuclei. Scale bar = 20 µm. The graph (H) shows that overexpression of PGC-1α increases Tomm20 levels (transfection $F(1, 47)= 45.15$, $p<0.0001$, ****) with more efficacy on R274W+/+ fibroblasts than WT (interaction $F(1, 47)= 4.132$, $p=0.0478$, *; Bonferroni *post hoc* test: WT empty vector vs FLAG-PGC-1α p-value<0.05, and R274W+/+ empty vector vs FLAG-PGC-1α p-value<0.0001).

2 Parkin R274W in heterozygous mice brains

To deepen our understanding on the pathological mechanism of R274W mutation in Parkin, we profiled heterozygous mice at 6, 12, and 18 months.

2.1 Heterozygous mice display age-dependent motor impairment, DA neurons loss and astrogliosis

In parallel to what we did for homozygous mice, we tested WT and R274W+/- mice at 6, 12, and 18 months of age for motor coordination on the rotarod at increasing acceleration (4-32 rpm), the balance beam (12 and 6 mm), and the pole test. Our cohorts included male and female animals in a 1:1 ratio.

We observed decreased coordination in heterozygous mice compared to age-matched wild type on the rotarod 4-32 rpm at 12 [Figure 16 D] and 18 months [Figure 16 G], and on the balance beam at all the time points tested [Figure 16 B, E, H]. Decreased performance on the pole test was detected at in mutant mice at 12 months [Figure 16 F]. At 18 months, neither wild type nor heterozygous mice were able to perform on the pole test and on the 6 mm balance beam. No differences were detected in anxiety phenotype nor in the weight of mutant animals compared to age-matched wild type [Supplementary Figure S3].

Altogether, our data show that R274W+/- mice display age-dependent defects in motor coordination that mirror the phenotype of homozygous mice.

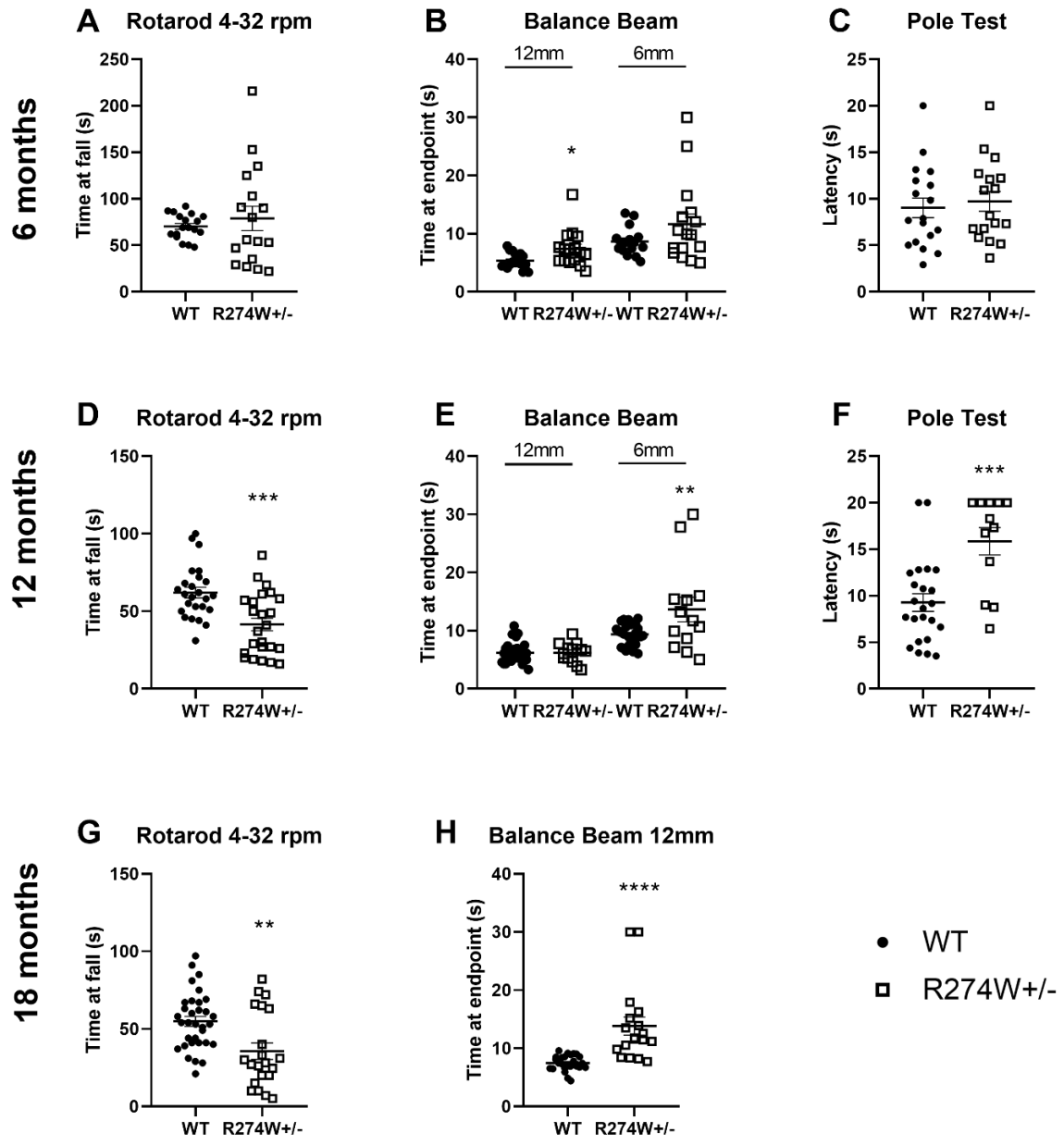

Figure 16: R274W+/- mice show age-dependent impairment in motor coordination. We tested male and female mice at the indicated ages. We observed defects on the rotarod at increased acceleration at 12 (D), and 18 months (G), on the balance beam at 6 (B), 12 (E), and 18 months (H), and on the pole test at 12 months (F). Old mice were not able to perform on the 6 mm balance beam nor on the pole test. Data are the means ± SEM; n WT = 17-23, n R274W+/- = 17-22; *, **, ***, ****, p<0.05, 0.01, 0.001, 0.0001 vs. wild type.

To analyse whether motor defects result from nigral neurodegeneration we evaluated the density of dopaminergic neurons in the substantia nigra of wild type and heterozygous mice along ageing by means of TH immunofluorescence.

The intensity of TH staining was reduced by 55%, 40%, and 49% at 6, 12, and 18 months respectively compared to age-matched wild type [Figure 17 A, B].

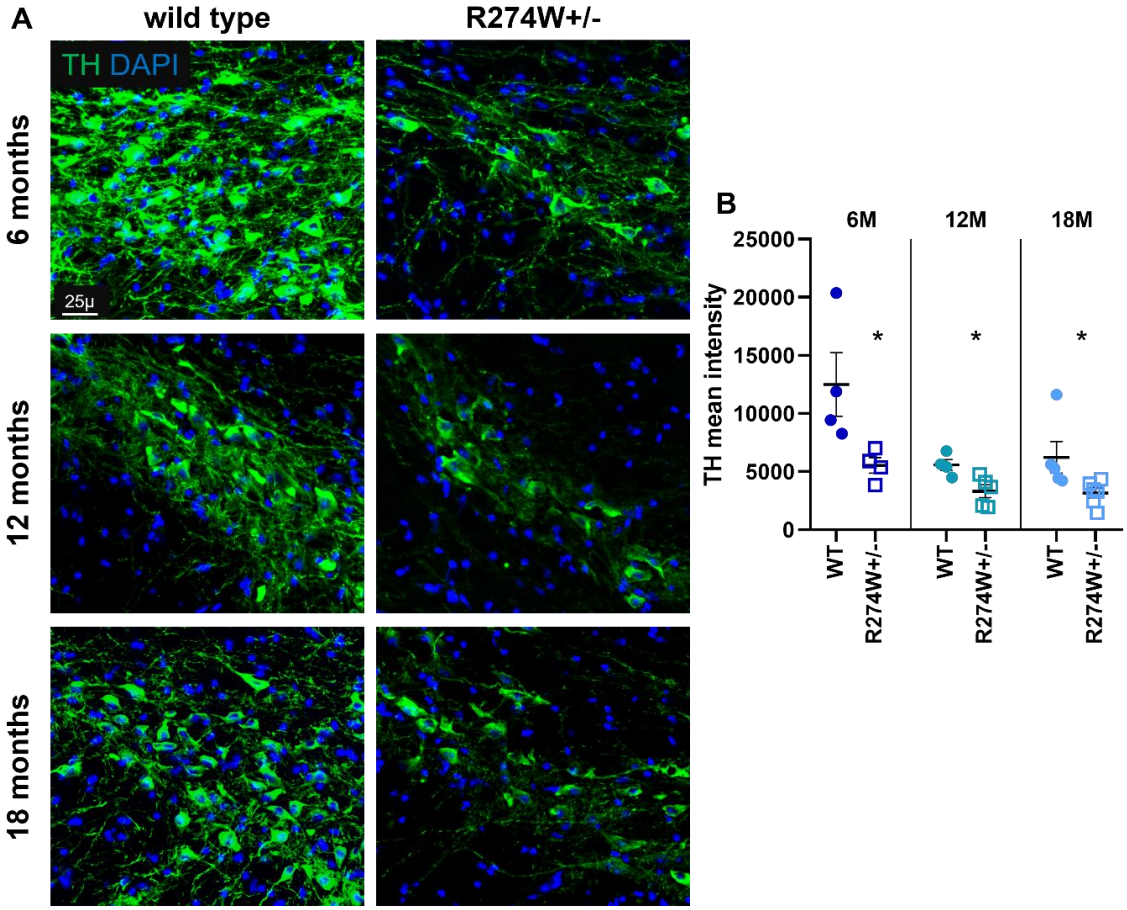

Figure 17: Parkin R274W+/- mice brains exhibit TH loss. (A) Representative images of substantia nigra pars compacta sections from 6-, 12-, and 18-month-old wild type and heterozygous mice stained with anti-TH antibody (green) and DAPI to visualize nuclei (blue). Scale bar = 25 µm. (B) The graph reports the TH mean intensity for each age; data are expressed as means ±SEM; n 6M = 4, n 12M = 4-5, n 18M = 5; two-sided t-test was performed comparing intra-age data vs. wild type; *, $p<0.05$.

Next, we noticed a significant increase in GFAP fluorescent signal in heterozygous striatum and substantia nigra compared to wild type [Figure 18], indicating that both neurodegeneration and astrogliosis are a consequence of Parkin R274W mutation. We noticed increased astrogliosis also in heterozygous cortex compared to WT in all considered ages [Supplementary Figure S4].

Altogether, our data show that heterozygous mice present an age-dependent PD-related phenotype starting at 6 months of age.

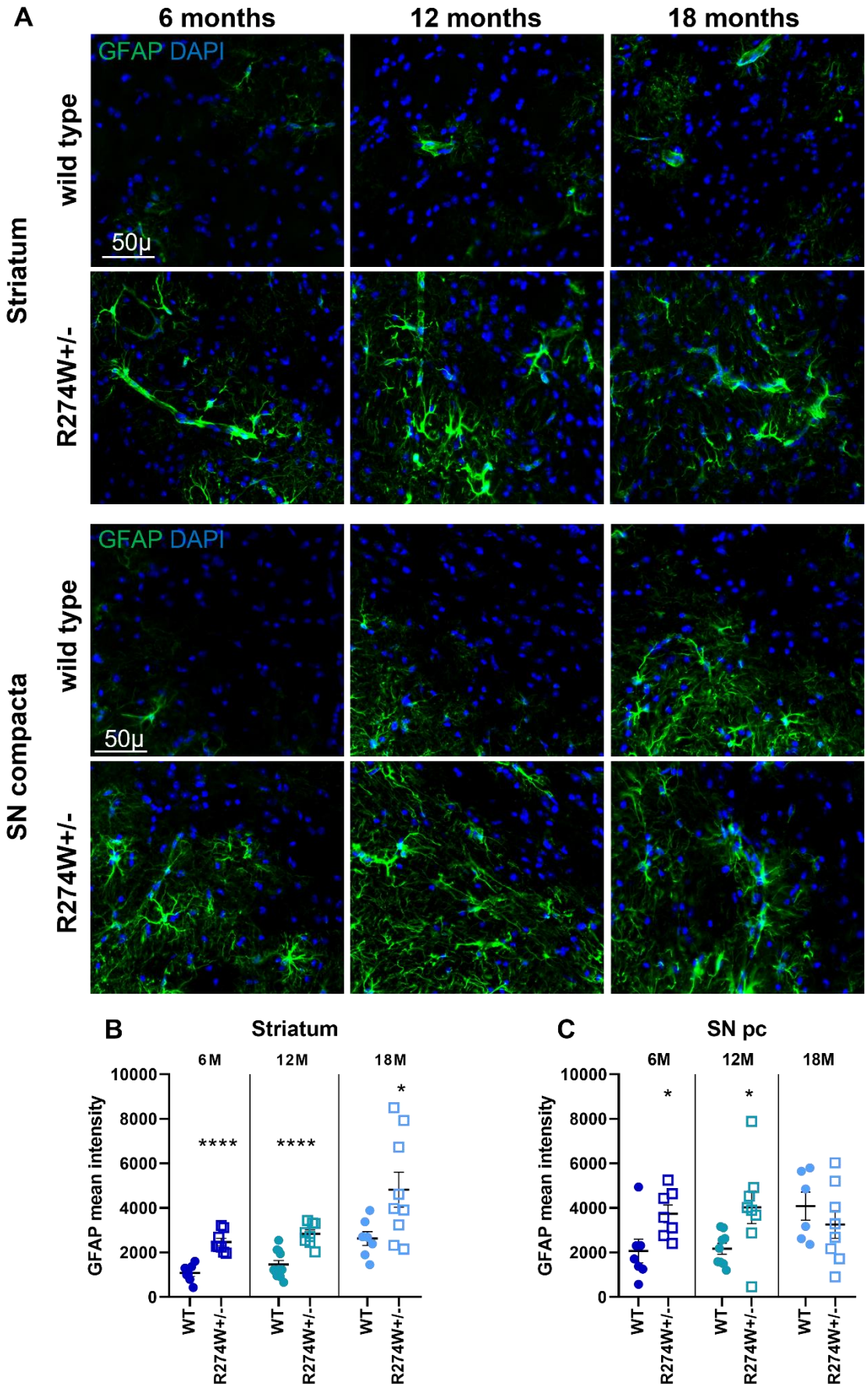

Figure 18: Parkin R274W+/- mice brains show astrogliosis. (A) Representative images of striatum and SN pc sections from 6-, 12-, and 18-month-old wild type and heterozygous

mice stained with anti-GFAP antibody (green) and DAPI (blue) to visualize nuclei. Scale bar = 50 µm. The graphs (B, C) report GFAP mean intensity in the striatum and SN pc respectively. Data are the means ± SEM; n 6M = 7, n 12M = 7-8, n 18M = 6-8; two-sided t-test was performed comparing intra-age data vs. wild type; *, * ***, p<0.01, 0.05, 0.0001.

3 Parkin R274W exerts a gain of toxic function

Our discovery that the phenotype of homozygous and heterozygous mice is comparable both for motor impairment, neurodegeneration and astrogliosis suggest that the pathologic mechanism for R274W Parkin is different from a simple loss of function.

3.1 Parkin R274W alters protein solubility through a dominant-negative mechanism

To better define the features of mutant Parkin, we characterized the level of expression and the solubility profile of WT and R274W Parkin in mice brains. To this aim we evaluated the amount of protein and its solubility in 1% Triton-X100.

We observed that in homozygous brains Parkin is less expressed compared to wild type at 6, 12, and 18 months [Figure 19 A, B]. Additionally, Parkin accumulates in the insoluble fraction of mutant brains in all the time points analysed [Figure 19 C, D], indicating that the aminoacidic substitution alters the solubility of the protein. The same effect was observed in primary cortical neurons derived from wild type or homozygous mice [Figure 20].

Interestingly, all these observations were replicated on heterozygous brain samples at 12 months compared to age-matched wild type [Figure 21], suggesting that a single mutant allele is sufficient to alter Parkin solubility profile leading to its detergent-resistant accumulation.

This hypothesis was confirmed by experiments performed in HEK293 cells, which normally express relevant levels of Parkin. Overexpression of human R275W and not of WT Parkin causes the accumulation of the protein in the insoluble fraction [Figure 22 A, B], mirroring what happens in heterozygous mice brains. The formation of R275W Parkin aggregates was also observed in HEK293 cells by means of immunofluorescence staining, as already showed by Cookson work in 2003 (Cookson et al., 2003) [Supplementary Figure S5].

Given the phenotype of altered solubility observed both in homo- and heterozygous genotypes, we wondered whether R274W mutation may act through a dominant negative effect, thus also affecting the solubility of WT protein.

To better understand this aspect, we overexpressed in HEK293 cells WT-myc Parkin together with WT-flag Parkin or R275W-flag Parkin, and then compared the distribution of WT-myc Parkin in Triton-X100 soluble and insoluble fractions.

Coherently with our hypothesis, we observed that Parkin WT-myc is more insoluble when co-expressed with mutant Parkin [Figure 22 B, C], indicating that R275W protein affects the biochemical characteristics of wild type Parkin.

Altogether, these results suggest that R274W mutation alters Parkin solubility both in homo- and heterozygous condition, supporting a dominant gain of toxic function for this aminoacidic substitution.

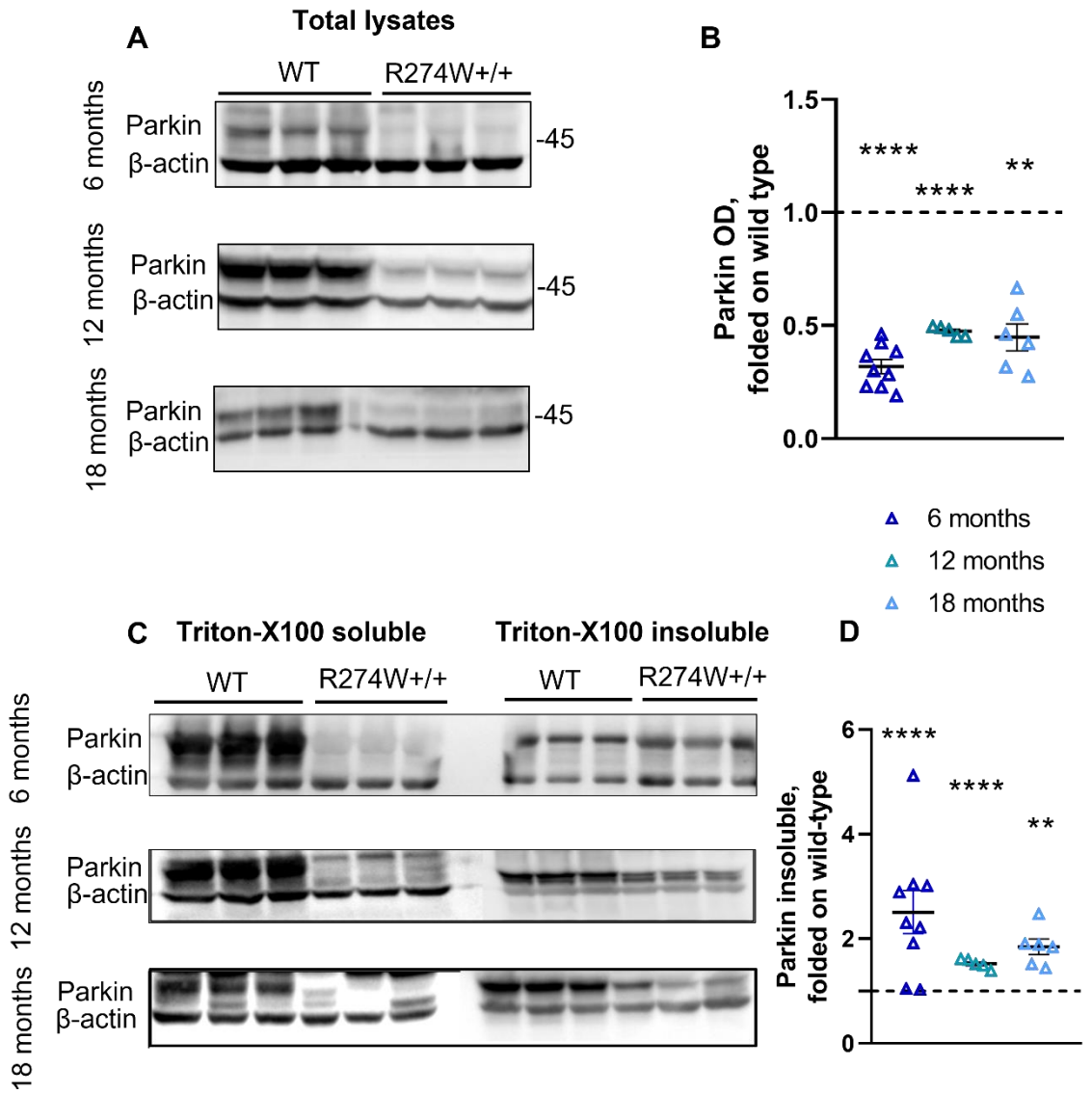

Figure 19: Parkin is less expressed and more insoluble in R274W+/+ brains. Biochemical analysis of brain specimens from 6, 12, and 18-month-old mice revealed reduced protein level (A) and increased presence in Triton-X100 insoluble fraction of Parkin in homozygous mice compared to wild type (C). The graphs show quantification of protein levels normalized on β-actin (B) and protein insolubility (D) normalized on β-actin and total

Parkin level, folded on reference wild type mean. Data are the means ± SEM; n 6M = 9; n 12M = 5; n 18M = 6; **, ****, p<0.01, 0.0001 vs. wild type.

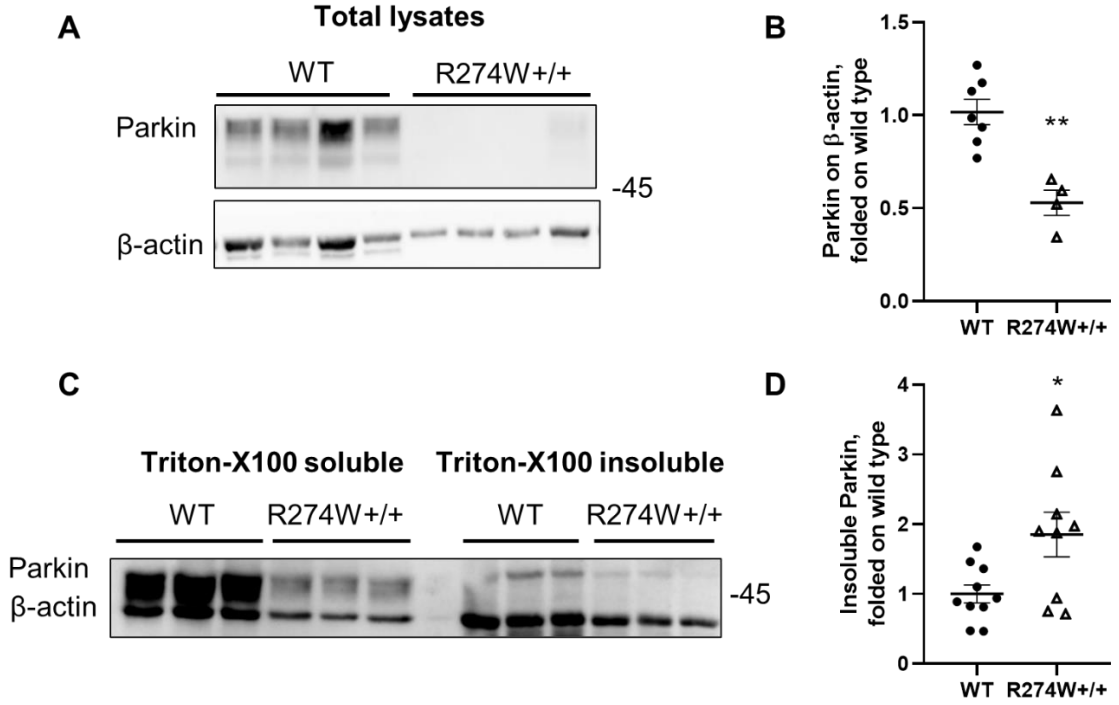

Figure 20: Parkin is less expressed and more insoluble in R274W+/+ neurons. Biochemical analysis of cortical neurons from E18.5 mice showed reduced Parkin level (A) and its increased insolubility in Triton-X100 fraction (C) in homozygous mice compared to wild type. (B) The graph shows quantification of Parkin levels normalized on β-actin folded on wild type mean. (D) The graph shows quantification of Parkin in Triton-X100 insoluble fraction, normalized on β-actin and total Parkin level, and folded on wild type mean. Data are the means ± SEM; (A) n = 8; (C) n = 10-9; *, **, p<0.05, 0.01 vs. wild type.

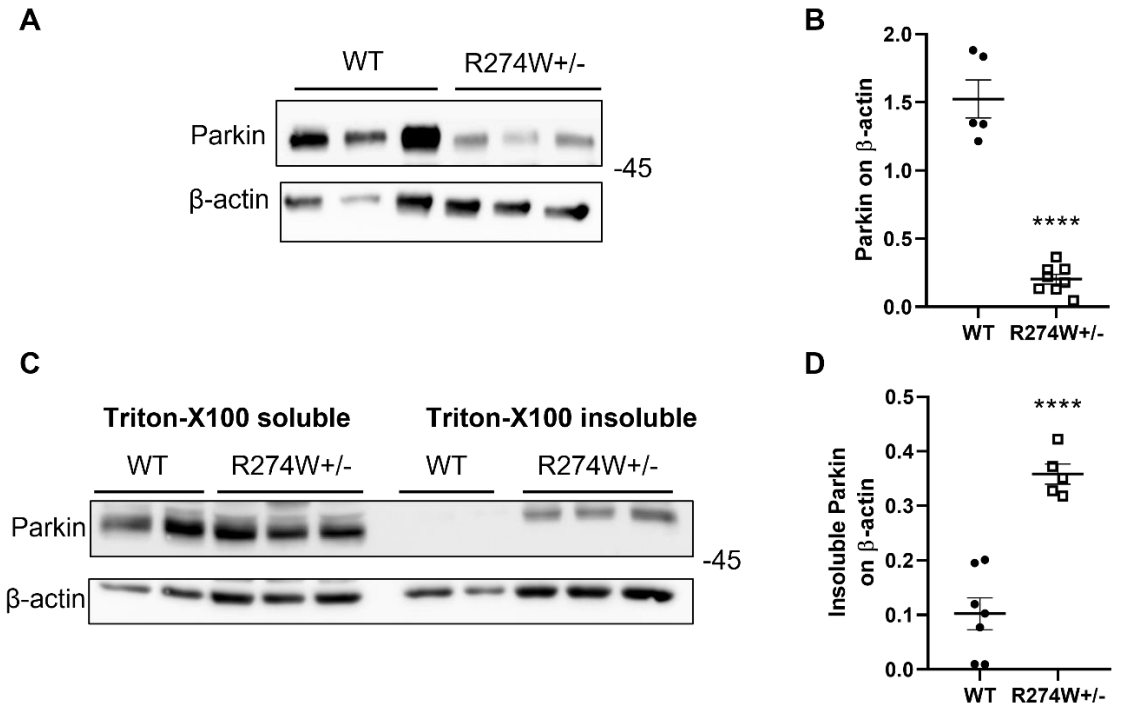

Figure 21: Parkin is less expressed and more insoluble in R274W+/- brains. Biochemical analysis of brain specimens from 12-month-old mice revealed reduced Parkin level (A) and increased presence in Triton-X100 insoluble fraction (C) in heterozygous mice compared to wild type. The graphs show quantification of Parkin levels normalized on β-actin (B) and insolubility (D) normalized on β-actin and on total Parkin level. Data are the means ± SEM; n= 7-5; ****, p<0.0001 vs. wild type.

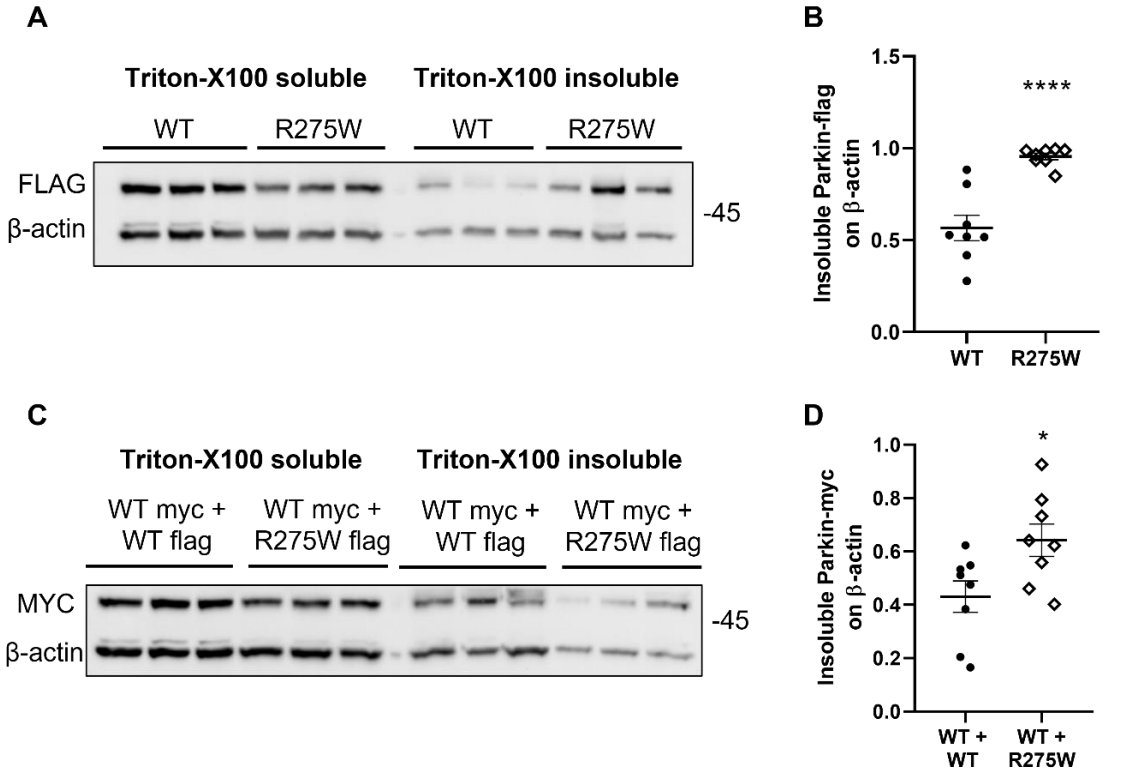

Figure 22: Parkin R275W exerts a dominant negative effect on the solubility of WT protein in HEK293 cells. (A) We assayed the solubility profile of Parkin-flag WT and

R275W in samples prepared from transfected HEK293 cells (WT = Parkin endogenous/wild type; R275W = Parkin endogenous/R275W). (C) We overexpressed in HEK293 cells WT-myc + WT-flag or WT-myc + R275W-flag Parkin and compared the solubility profile of WT-myc protein in Triton-X100 soluble and insoluble fraction. The amount of WT-myc Parkin in the insoluble fraction increases when it is co-expressed with R275W-flag and not WT Parkin. (B, D) The graphs report the amount of Parkin in the Triton-X100 insoluble fraction, normalized on β-actin and total Parkin level. Data are expressed as means ±SEM; n = 8; *, ****, $p<0.05$, 0.0001 versus wild type.

3.2 Signs of protein aggregation are observed in mutant mice brains

Next, we decided to examine homozygous and heterozygous mice brains for histological hallmarks of protein aggregation. To this aim, we performed an immunoperoxidase labelling in the brains of 18-month-old WT and mutant mice for markers of protein aggregation such as ubiquitin and p62 (an autophagosome cargo protein).

The midbrain of mutant mice revealed an increased number of ubiquitin and p62 positive cells and an enhanced signal intensity compared to wild type both for homozygous [Figure 23] and heterozygous mice [Figure 24], while no differences were observed in other brain regions [Supplementary Figure S6, S7].

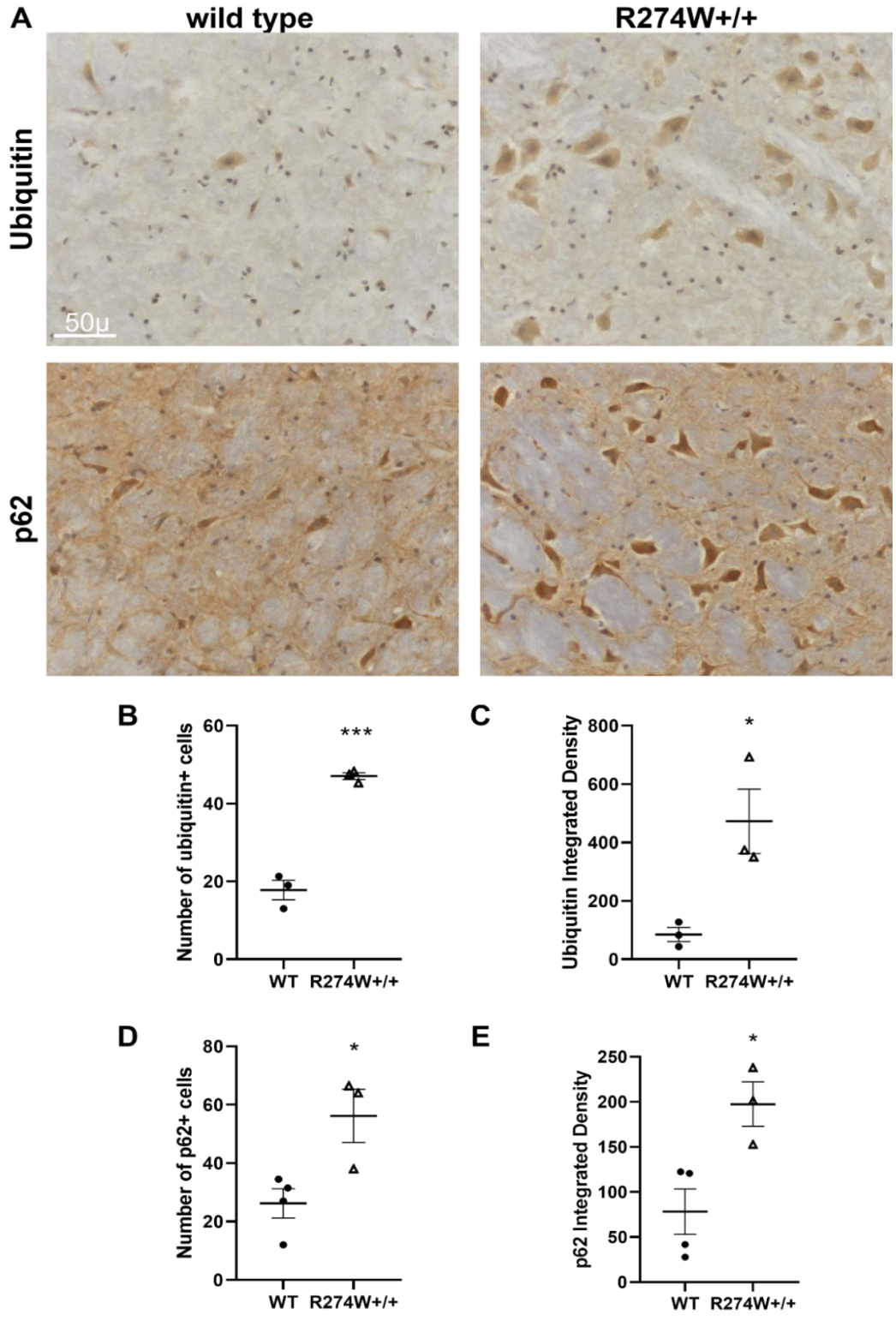

Figure 23: Midbrain of homozygous mice reveals strong immunostaining for ubiquitin and p62, common markers of aggresomes. (A) Immunoperoxidase labelling for ubiquitin or p62 (brown) in the midbrain of 18-month-old wild type or R274W+/+ mice. Nuclei are seen in blue. Graphs show the number of cells that are positive to ubiquitin (B) or p62 (D) and corresponding signal intensity (C, E). Data are the means ± SEM; n = 4-3; *, ***, p<0.05, 0.001 vs. wild type.

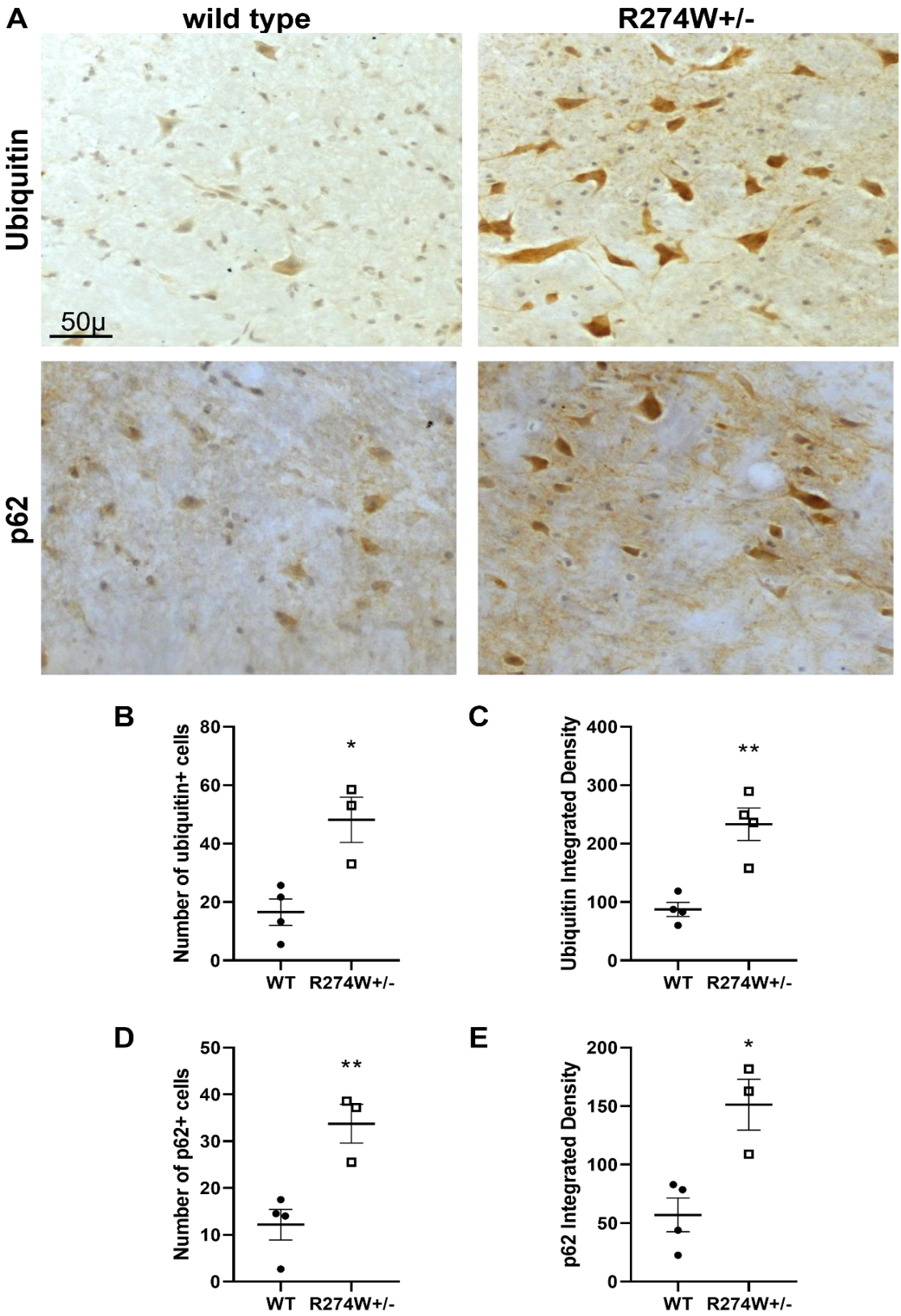

Figure 24: Midbrain of heterozygous mice reveals strong immunostaining for ubiquitin and p62, common markers of aggresomes. (A) Immunoperoxidase labelling for ubiquitin or p62 (brown) in the midbrain of 18-month-old wild type or R274W+/- mice. Nuclei are seen in blue. Graphs show the number of cells that are positive to ubiquitin (B) or p62 (D) and corresponding signal intensity (C, E). Data are the means ± SEM; n = 4-3; *, **, $p<0.05$, 0.01 vs. wild type.

3.2.1 Parkin R274W is associated with Lewy pathology in heterozygous brains

α-synuclein phosphorylated on serine 129 (pS129 α-syn) is the most well-known and abundant component of Lewy bodies in human PD patients.

The immunostaining with anti pS129 α-syn antibody on wild type, hetero-, and homozygous brains of 18-month-old mice indicated an increased signal in mutant tissue. Interestingly, in the midbrain of R274W+/- mice we detected the presence of cellular inclusions that resemble Lewy bodies, together with a strong pS129 α-syn immunostaining in the neurites. These observations were not replicated in R274W+/+ midbrain [Figure 25].

Such evidence suggests that heterozygous R274W Parkin mutation is associated with Lewy pathology, resembling what is observed in human patients.

Consistently, we observed that α-synuclein is more insoluble in heterozygous brains at 12 months compared to age-matched wild type. Such an increase was not detected in homozygous brains obtained from mice of the same age [Figure 26].

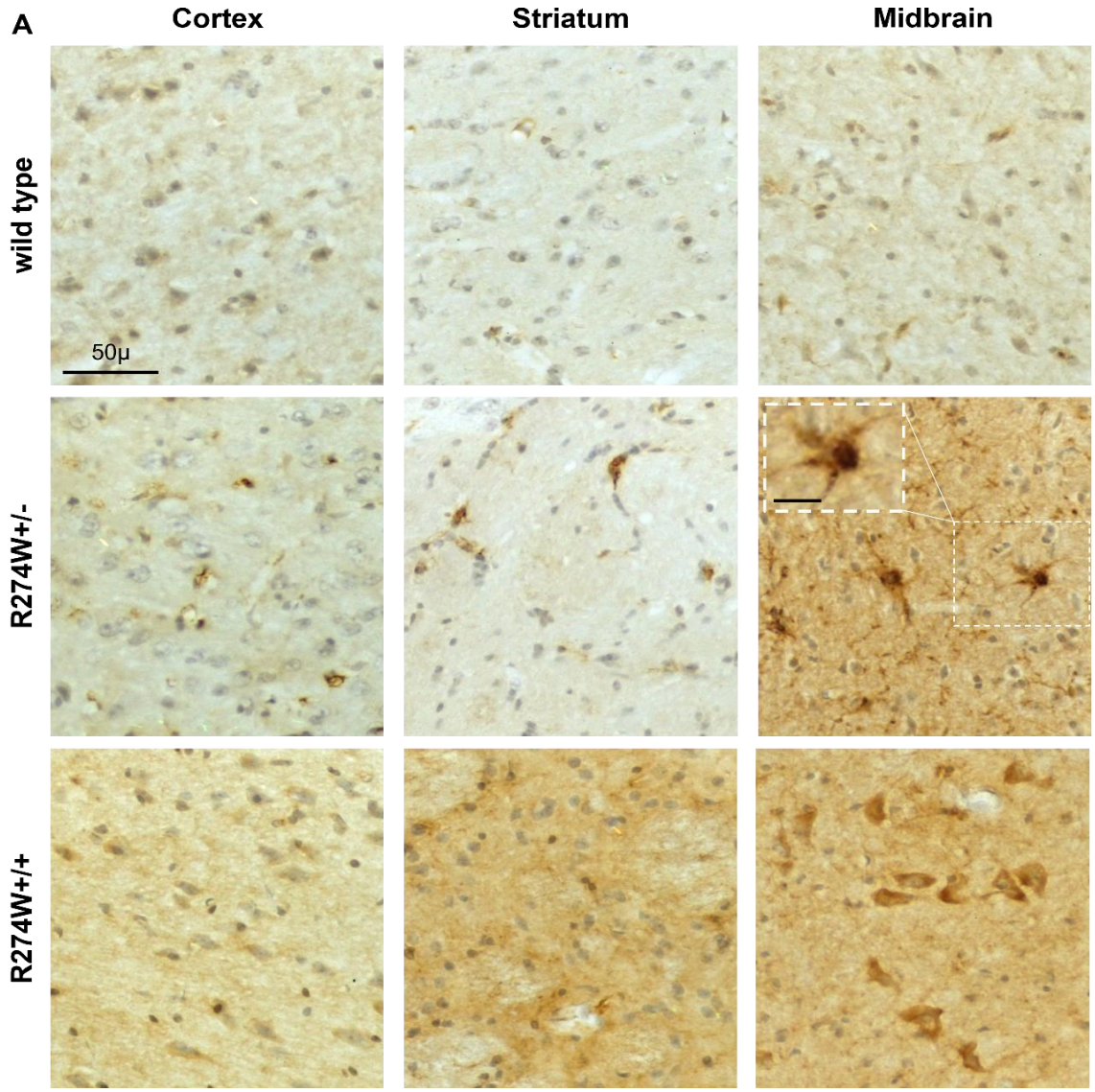

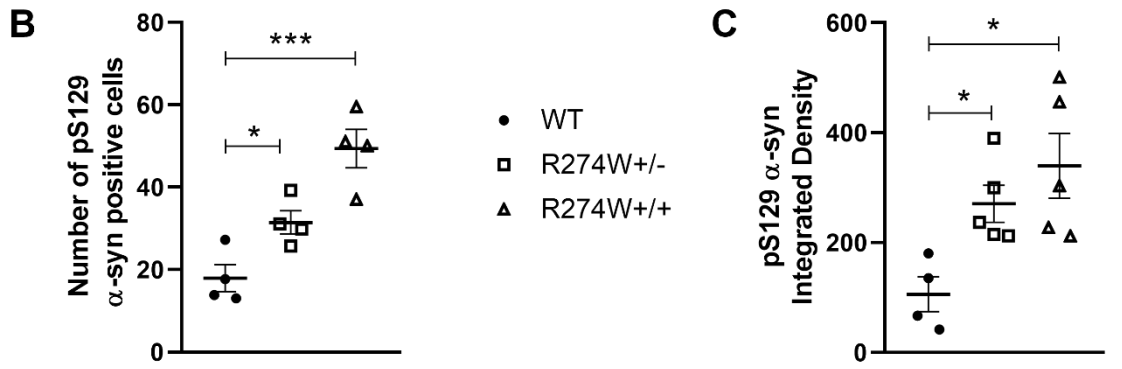

Figure 25: Lewy body-like inclusions are observed in the midbrain of hetero- but not homozygous mice. (A) Immunoperoxidase labelling for S129 phosphorylated α-synuclein (pS129 α-syn) (brown) in the midbrain of 18-month-old wild type, R274W+/- or R274W+/+ mice. Nuclei are seen in blue. pS129 α-synuclein-positive inclusions are observed in the midbrain of heterozygous brain both in cell body and neurites, and at smaller extent in the cortex and striatum. Increased immunoreactivity is detected in the midbrain of both mutant genotypes, (B, C), but no Lewy body-like structures are seen in homozygous animals. (A) n = 6; (B, C) n = 4. Scale bar = 50µm. Scale bar of dashed white square = 25 µm.

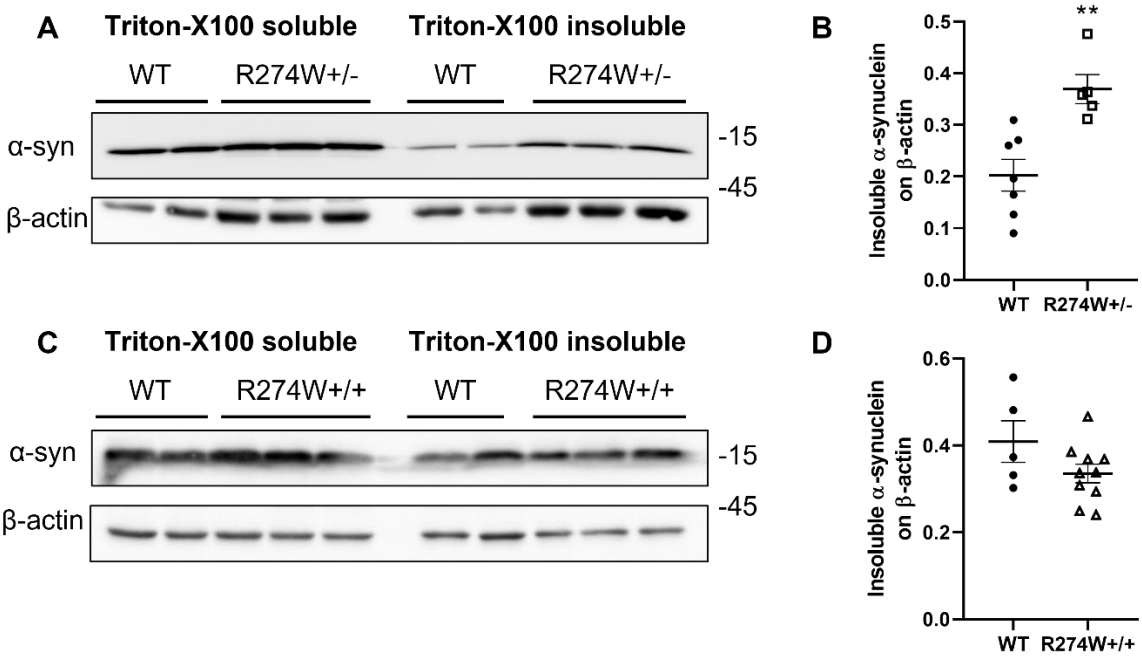

Figure 26: α-synuclein is more insoluble in heterozygous brain. (A, C) We analysed the solubility profile of α-Synuclein in wild type, hetero- and homozygous hemispheres at 12 months through western blotting. (B, D) The graphs show levels of α-synuclein in Triton X-100 insoluble fraction in heterozygous (B) and homozygous (D) brains normalized on β-actin and total α-synuclein amount. Data are expressed as means ±SEM; (B) n = 7-5, (D) n = 5-10; ** $p<0.01$ versus wild type.

3.3 ER stress and UPR activation are observed in mutant brains

Protein aggregation triggers ER stress and subsequent unfolded protein response through BiP overexpression (Leitman et al., 2013; Gardner et al., 2013). To verify whether Parkin R274W triggers UPR activation, we evaluated the expression of BiP, in the brain of 12-month-old wild type, hetero-, and homozygous mice by western blotting. We observed a significant increase in the levels of BiP expression in both mutant genotypes compared to wild type [Figure 27 A, B], indicating the presence of ER stress in homo- and heterozygous brains.

Coherent with this finding we also detected an increase in BiP mRNA levels in homozygous cortex at 6, 12, and 18 months compared to age-matched wild type [Figure 27 E].

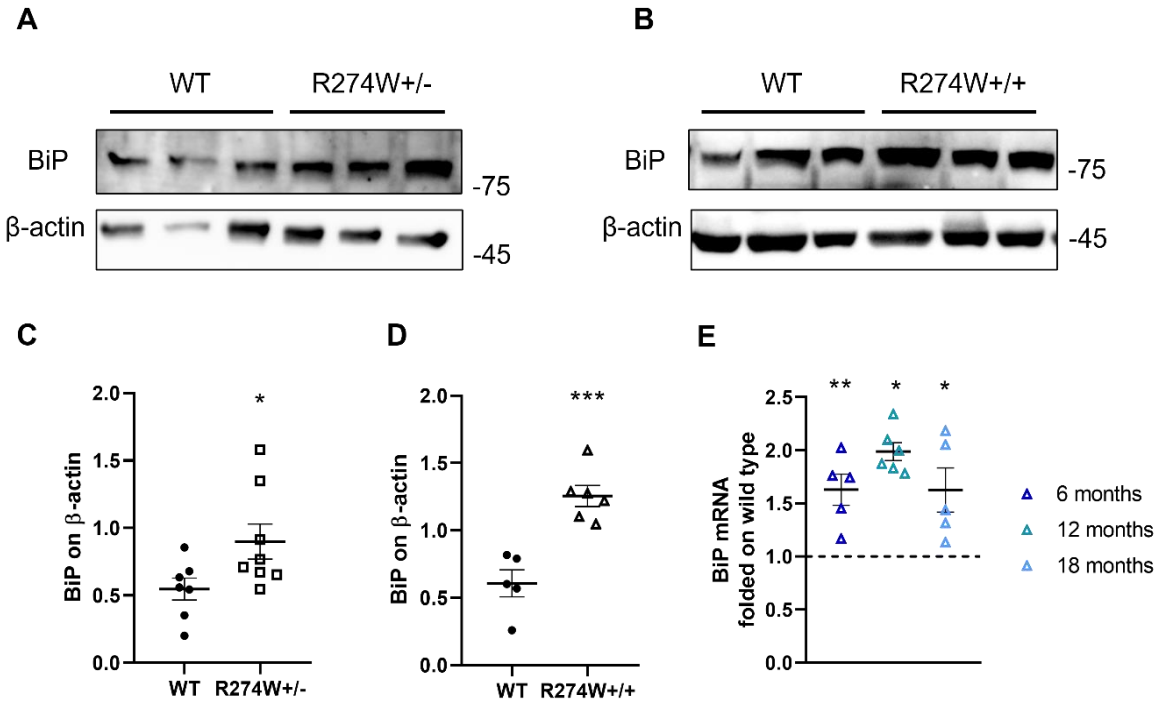

Figure 27: R274W Parkin triggers UPR activation. We assessed BiP amount in hemispheres derived from WT, hetero- (A) and homozygous (B) mice at 12 months of age. The graphs (C, D) show the levels of BiP normalized on β-actin amount. BiP is increased in R274W+/- (C) and R274W+/+ (D) mice compared to age-matched wild type. Data are the means ± SEM; (C) n = 7-8; (D) n = 5-6; *, **, p<0.05, 0.01 vs. wild type. (E) We evaluated the levels of BiP mRNA in homozygous cortex at 6, 12, and 18 months via qRT-PCR. BiP expression increases in mutant tissue in all the time points. The graph reports BiP expression normalized on RPL27 and β-actin at 6, 12, and 18 months, folded on corresponding wild type mean. Data are the means ± SEM; n 6M = 5; n 12M = 6; n 18M = 5; *, **, p<0.05, 0.01 vs. wild type.

To explore whether Parkin R275W directly causes UPR, we overexpressed either the wild type or the mutant protein in HEK293 cells. Consistent with our hypothesis, we

observed an increase of BiP mRNA also in this heterologous model upon acute Parkin R275W expression [Figure 28 A].

Additionally, to further confirm the specificity of this correlation, we noticed that only overexpression of mutant Parkin and not of NSF T645D, another protein known to aggregate in PD (Pischedda et al., 2021), triggers the increase of BiP mRNA level [Figure 28 B].

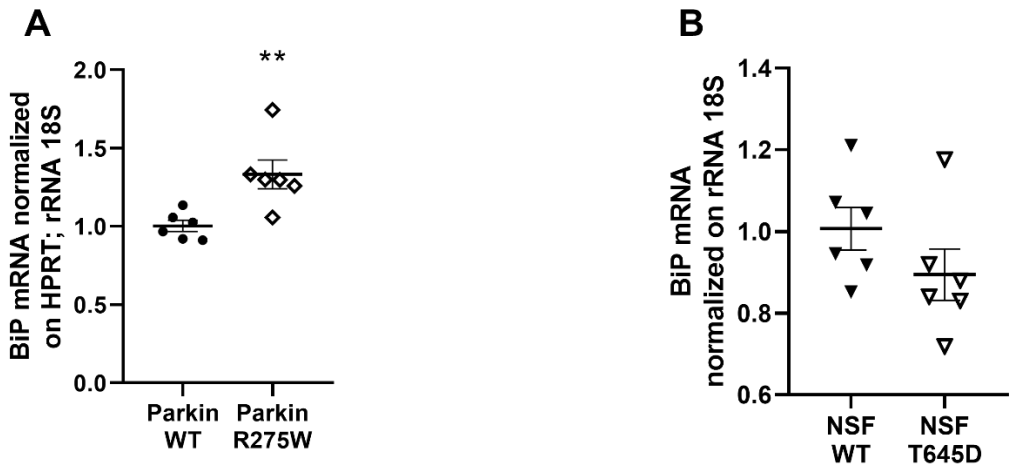

Figure 28: Activation of UPR is observed for Parkin R275W and not for aggregating-prone NSF T645D. We overexpressed (A) Parkin WT or R275W and (B) NSF WT or NSF T645D in HEK293 cells.
(A) Parkin R275W and not WT overexpression causes the activation of UPR through overexpression of BiP mRNA. (B) Increase in BiP mRNA expression was not observed in HEK293 cells overexpressing aggregating prone NSF T645D, compared to wild type. The graphs show BiP mRNA level normalized on rRNA 18S mRNA amount. Data are reported as means ±SEM; n = 6-6; ** $p<0.01$.

4 Alterations in AQP4 expression suggest impairment of the glymphatic system

As the involvement of the glymphatic system in neurodegenerative diseases is becoming more evident, we decided to explore whether glymphatic dysfunctions are present in our novel PD mouse model.

In brain specimens gathered from 18-months old mice, we observed the presence of GFAP-surrounded whole-shaped structures that were rarely found in wild type tissue. Interestingly, we noticed that these structures were also positive to CD31, a marker of endothelial cells [Figure 29 B] and AQP4 [Figure 29 C] staining. Hence, we concluded that these structures resemble the architecture of the glymphatic system [Figure 29 A], composed of blood vessels surrounded by astrocyte endfeet. These structures were not only increased in number, but also showed an enlarged diameter in homo- and heterozygous brain compared to wild type.

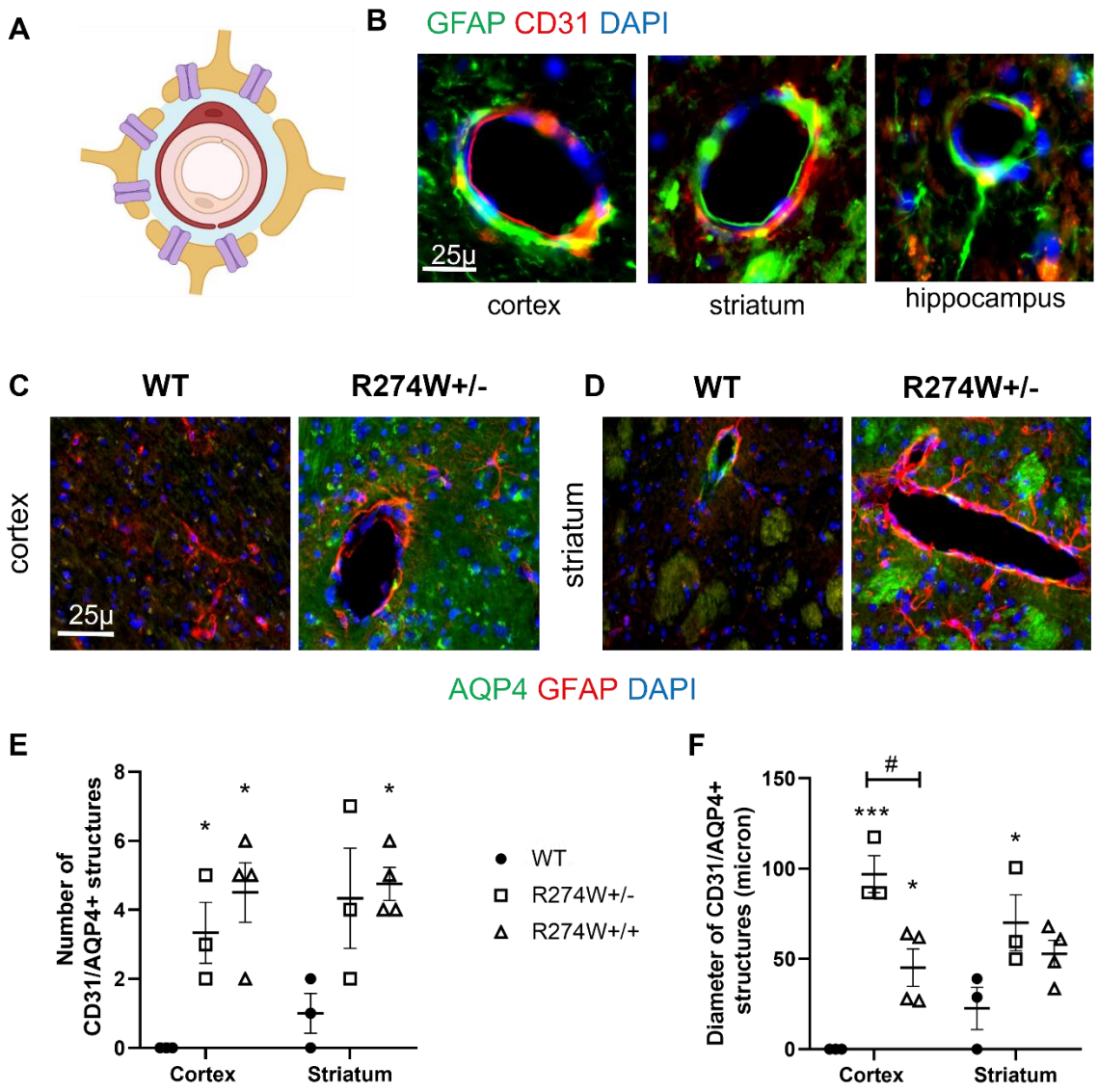

Figure 29: R274W mice show alterations of the glymphatic system architecture. (A) The cartoon indicates the principal components of the glymphatic astrocytes i.e., CD31+ blood vessels (red) and GFAP+ astrocyte endfeet (yellow) expressing high levels of polarized AQP4 (purple). PVS is presented in light blue. Created with BioRender.com. (B) Representative images of enlarged GFAP+(green)/CD31+(red) structures in the cortex, striatum, and hippocampus of 18-month-old homozygous mice. (C, D) Representative images of enlarged AQP4+(green)/GFAP+(red) structures in the cortex, striatum, and hippocampus of 18-month-old WT and heterozygous mice. Scale bar = 25 µm. The graphs show number (E) and maximum diameter (F) of such structures. Data are expressed as means ±SEM, n = 3-4; *, **, ***, p<0.05, 0.01, 0.001 versus wild type; #, p<0.05 R274W+/- versus R274W+/+.

AQP4 is a fundamental component of the glymphatic system. Accordingly, glymphatic dysfunctions are also characterized by the redistribution of AQP4 from endfeet to the astrocyte body (Kress et al., 2014). Strikingly, we noticed that in brain tissue from18-month-old homozygous mice AQP4 immunofluorescent signal was diffused into the

brain parenchyma, while in tissue from wild type mice of the same age it remained mostly confined to the perivascular space [Figure 30 A].

Glymphatic alterations are characterized by changes not only in the distribution of AQP4, but also in its expression levels. To verify this aspect, we analysed brain tissue derived from 6- and 18-month-old wild type and R274W+/+ mice. We observed that AQP4 levels are reduced in homozygous mice at 6 months compared to age-matched wild type, while the trend is inverted at 18 months [Figure 30 B, C].

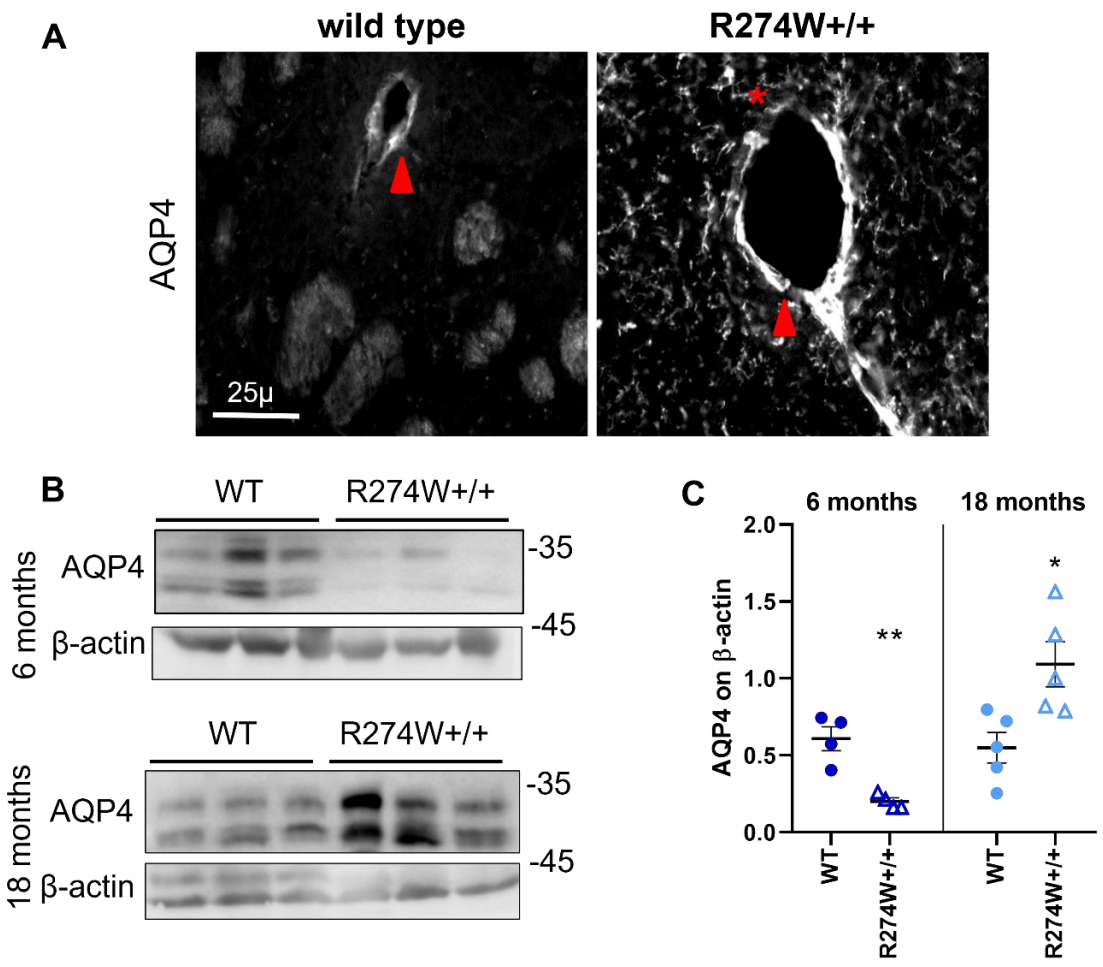

Figure 30: AQP4 expression is altered in homozygous mice brains. AQP4 mislocalization from astrocyte endfeet correlates with glymphatic dysfunctions. (A) We observed a diffuse AQP4 immunofluorescent signal in R274W+/+ brain tissue compared to wild type at 18 months of age. Correct perivascular localization is shown by red arrowhead, while red asterisk indicates mislocalization into the cell body. Scale bar = 25 µm. (B) We analysed by western blotting brain tissue from 6- and 18-month-old wild type and homozygous mice. We observed that AQP4 protein level is reduced compared to age-matched wild type at 6 months, while an increase is observed at 18 months. (C) The graph shows amount of AQP4 protein normalized on β-actin levels. Data are expressed as means ±SEM; n 6M = 4; n 18M = 5; two-sided t-test was performed comparing intra-age data vs. wild type; *, **, $p<0.05, 0.01$.

To better understand the link between Parkin and AQP4 expression, we overexpressed M23 AQP4-V5 in HEK293 cells together with wild type or R275W Parkin. Noteworthy, we observed that co-expression with WT but not with R275W Parkin correlates with a significant increase of AQP4 M23 protein levels [Figure 31 A, B].

AQP4 sub-cellular distribution is controlled by a complex code of post-translational modifications (PTMs), including phosphorylation and ubiquitination (Hsu et al., 2015; Vandebroek et al., 2020). For this reason, we investigated whether Parkin might influence AQP4 cellular localization. To this aim, we overexpressed in HEK293 cells M23 AQP4-V5 and WT or R275W Parkin and observed protein distribution by means of immunofluorescent assays. Interestingly, we observed that wild type but not R275W Parkin favours AQP4 membrane localization [Figure 31 C].

Strikingly, similar findings were obtained from astrocytes derived from WT and R274W+/+ mice. Indeed, endogenous AQP4 mostly decorates the periphery and the membrane of wild type astrocytes, whereas it aggregates in cytoplasmic puncta in homozygous cells [Figure 31 D].

Altogether, our data indicate that Parkin is important for the correct expression and organization of AQP4 in the architecture of the glymphatic system, that is instead altered in the presence of R274W substitution.

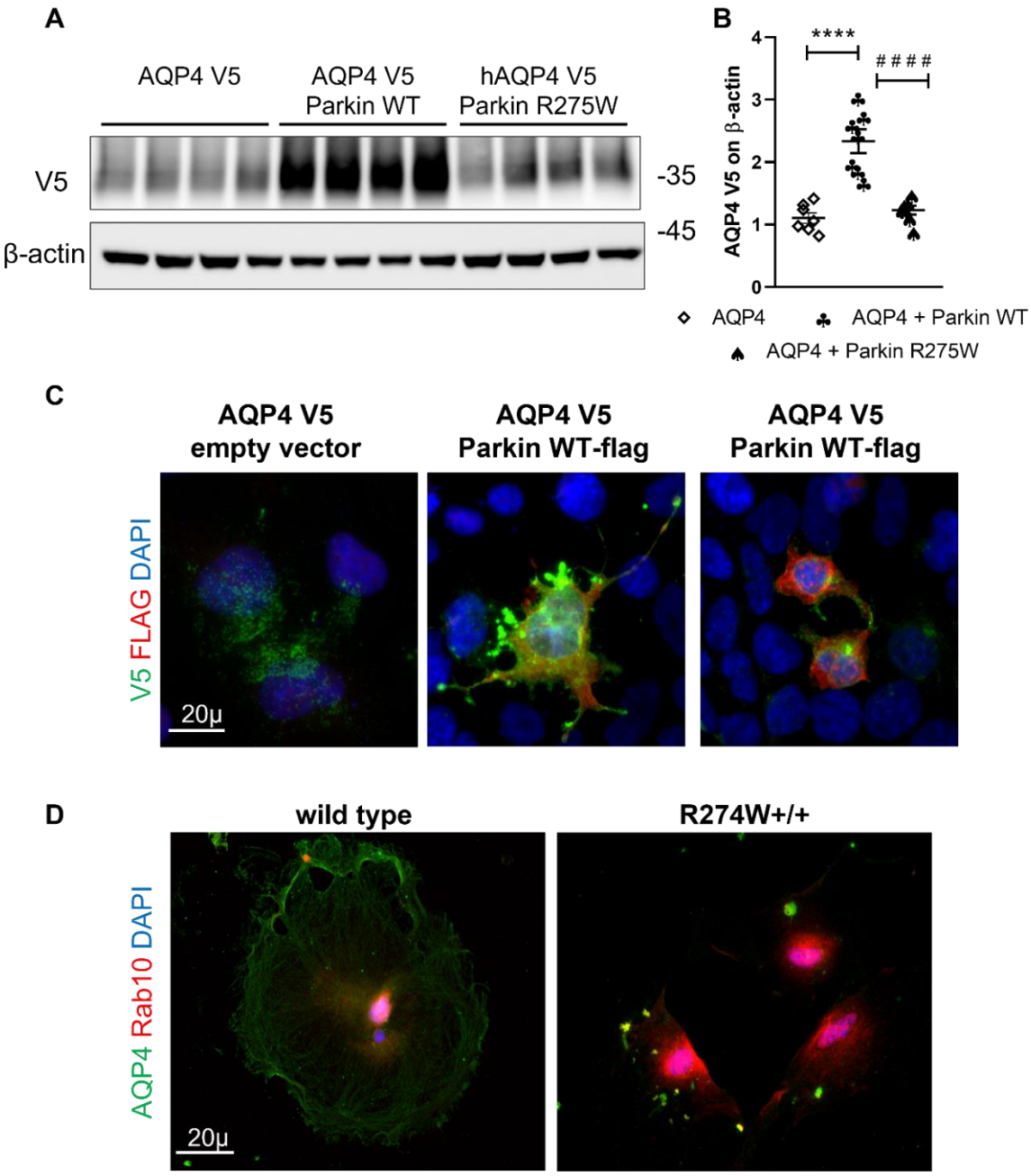

Figure 31: Parkin influences AQP4 expression and distribution. (A) Western blot analysis revealed that M23 AQP4-V5 levels increase when WT but not R275W Parkin is co-expressed in HEK293 cells. The graph (B) shows the level of M23 AQP4-V5 normalized on β-actin. Data are expressed as means ±SEM; n = 7; ****, p<0.0001 versus empty vector; ####, p<0.0001 R275W versus WT. (C) The co-expression of Parkin WT but not R275W (red) influences the localization of M23 AQP4-V5 (green) in HEK293 cells. Nuclei are visualized in blue. Scale bar = 20 µm (D) AQP4 localization is different in primary astrocytes derived from wild type and R274W+/+ mice. AQP4 is visualized in green, Rab10 decorating the endomembrane system is shown in red, nuclei in blue. Scale bar = 20 µm.

5 The impact of Parkin R274W on the skeletal muscle

The finding that R275W *Drosophila* model shows impairment in motor abilities linked to muscular strength (Wang et al., 2007) prompted us to verify whether skeletal muscle physiology may be affected in our mouse model as well. First, we detected by biochemical means a reduction in Parkin levels in 12-month-old homozygous tibialis anterior (TA) muscle compared to age-matched wild type [Figure 32], indicating that reduction in Parkin is not confined to the central nervous system but is also seen in the periphery.

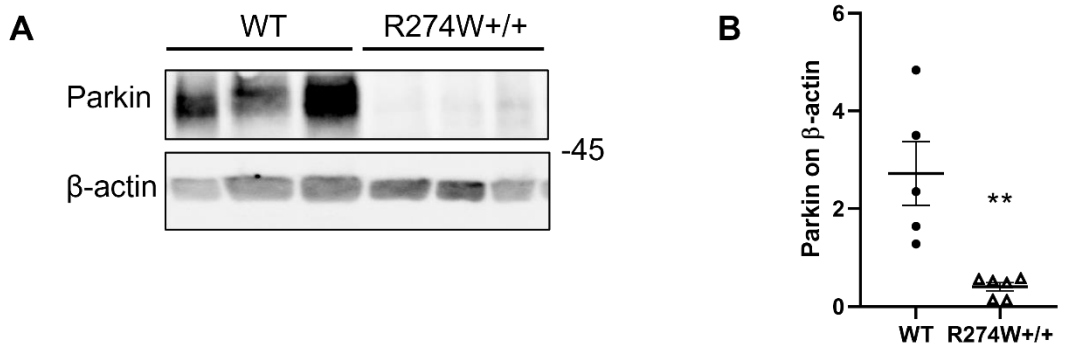

Figure 32: Parkin is decreased in homozygous skeletal muscle. (A) Parkin levels are reduced in 12-month-old homozygous mice compared to wild type in tibialis anteriore (TA). (B) The graph shows Parkin amount normalized on β-actin. Data are expressed as means ±SEM; n = 5-6; **, p<0.01 versus wild type.

5.1 Decreased muscular strength is observed in R274W mice

To analyse the phenotype of muscular fatigue we tested wild type, homo- and heterozygous mice at 6, 12, and 18 months on the rotarod at fixed acceleration (12 rpm), on the hanging wire and by the anterior limbs grip strength.

We observed a decreased muscular performance in homozygous mice at 12 months in the rotarod at fixed acceleration [Figure 33 D]. At 18 months, R274W+/+ mice performed poorly in all the tests performed [Figure 33 G, H, I].

In heterozygous mice, we observed a worse performance on the rotarod at fixed acceleration at 6, 12, and 18 months [Figure 34 A, D, G] and on the hanging wire at 12 and 18 months [Figure 34 E, H] compared to age-matched wild type.

Altogether, these data show that both R274W+/+ and R274W+/- mice display an age-dependent strength impairment starting at 12 months of age.

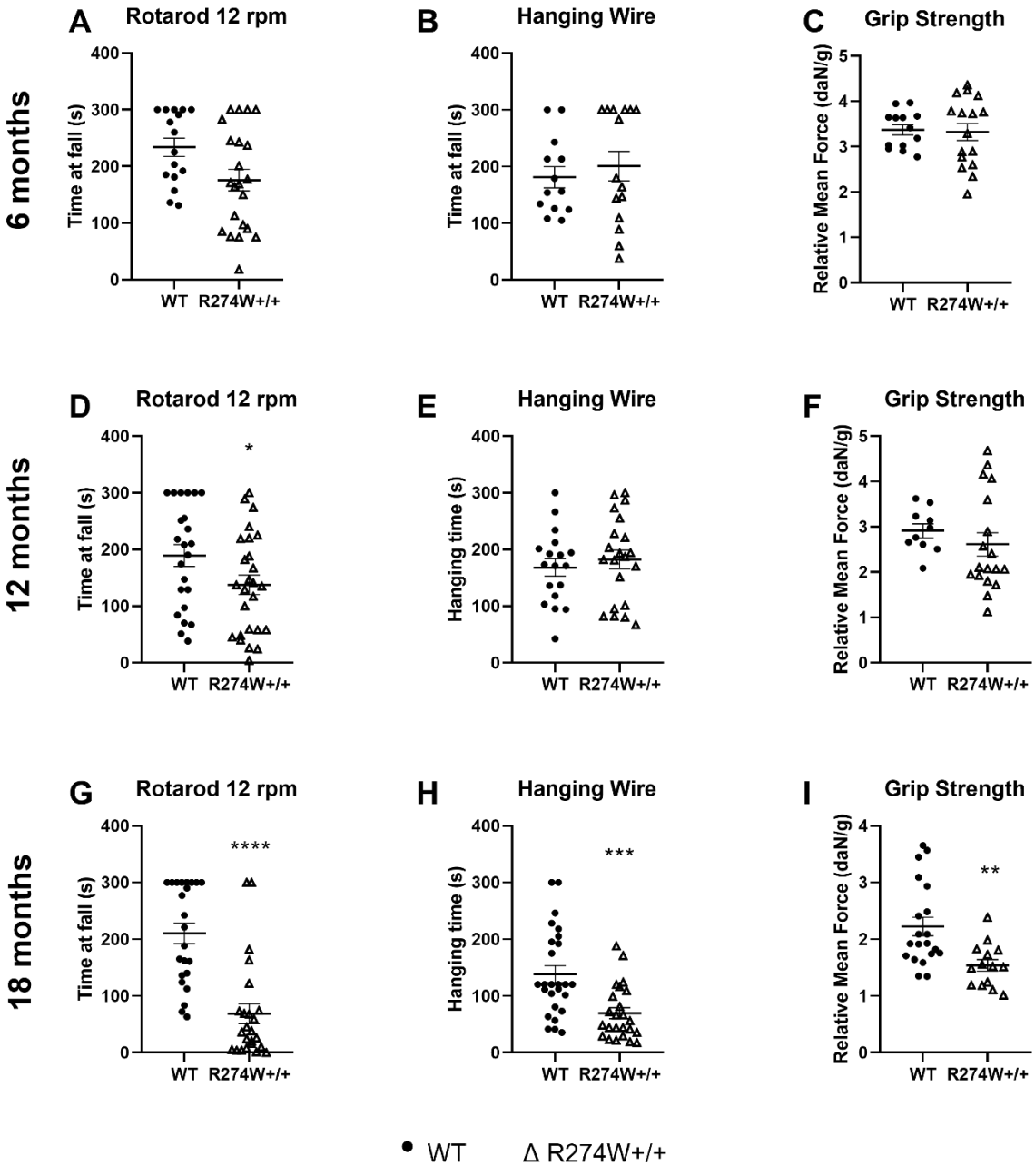

Figure 33: R274W+/+ mice show age-dependent impairment in muscular strength. We tested male and female mice at the indicated ages. We observed defects on the rotarod at fixed acceleration at 12 (D) and 18 months (G), and in the hanging wire and anterior limbs grip strength at 18 months (H, I). Data are the means ± SEM; n WT = 13-24, n R274W+/+ = 13-22; *, **, ***, ****, p<0.05, 0.01, 0.001, 0.0001 vs. wild type.

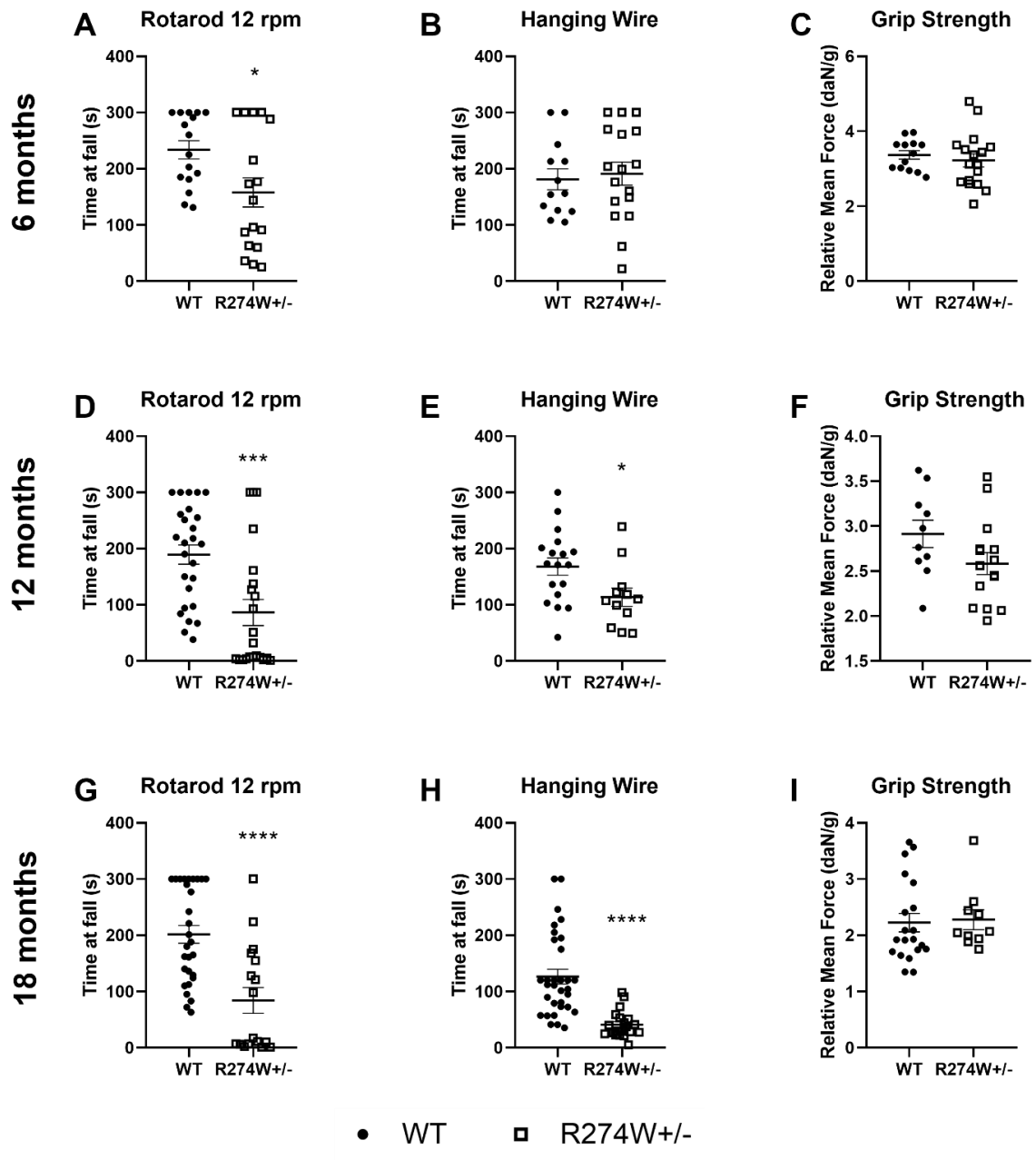

Figure 34: R274W+/- mice show age-dependent impairment in muscular strength. We tested male and female mice at the indicated ages. We observed defects on the rotarod at fixed acceleration at 6 (A), 12 (D), and 18 months (G), and in the hanging wire at 12 (E), and 18 months (H). Data are the means ± SEM; n WT = 10-26, n R274W+/- = 13-18; *, ***, ****, p<0.05, 0.001, 0.0001 vs. wild type.

5.2 Homozygous mice display alterations in the skeletal muscle

Having observed a phenotype of reduced muscular strength in mutant mice, we analysed skeletal muscle histology.

We focused our analysis on homozygous mice at 12 and 18 months, when muscular performance is overtly impaired. Histological experiments were conducted on soleus muscle, as it contains predominantly type I slow twitch fibres (Carroll et al., 2012), which are the most involved in efforts of long duration.

Haematoxylin and eosin staining on transversal sections of the soleus muscle revealed a 20% and 26% decrease in the fibres cross-sectional area (CSA) of mutant mice compared to wild type respectively at 12 and 18 months [Figure 35 A, B], with an increase in the interstitial tissue that surrounds the muscle units [Figure 35 C]. These findings suggest that homozygous mice present a degeneration in the skeletal muscle already at 12 months of age. The same phenotype was observed on heterozygous tissue derived from 12-month-old mice [Supplementary Figure S8].

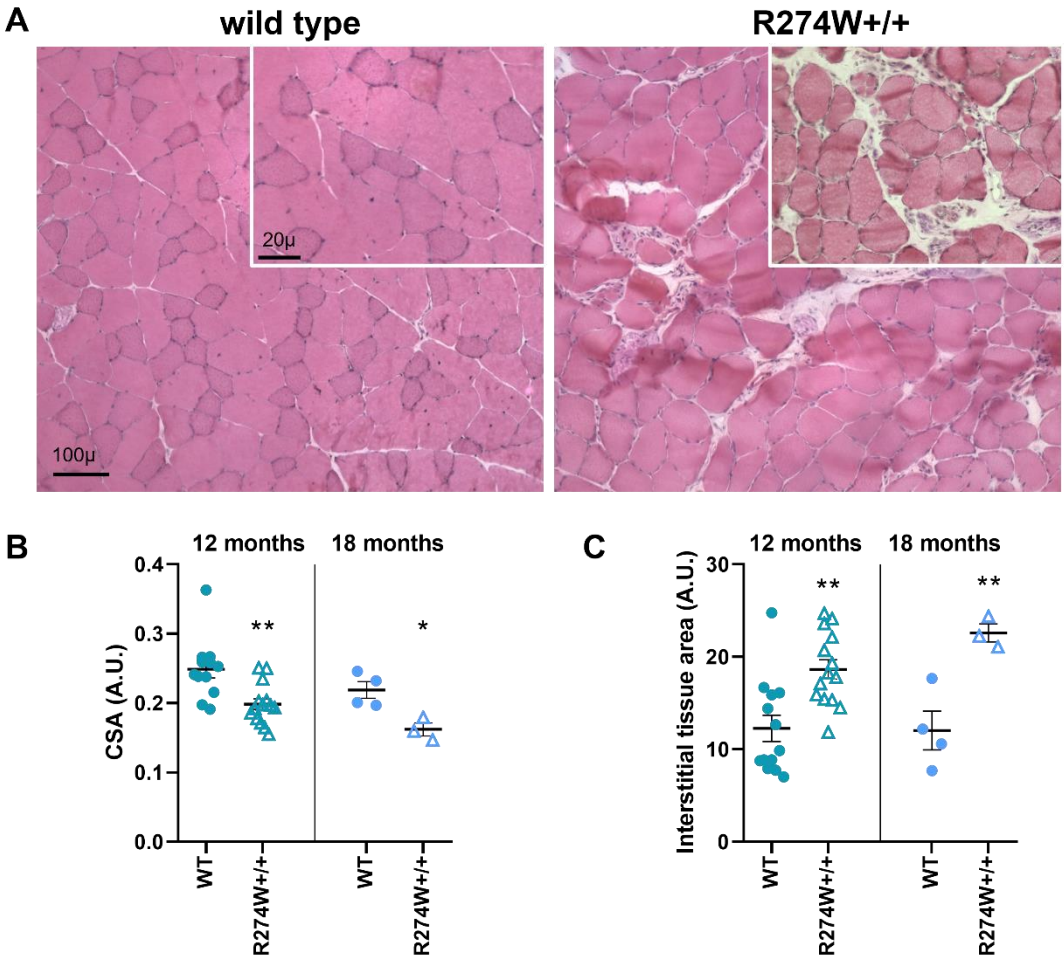

Figure 35: R274W mutation alters muscle tissue structure and organization in homozygous mice. (A) Representative images of haematoxylin and eosin staining on 14µ transversal sections of soleus muscle of 18-month-old wild type and homozygous mice. Decrease in muscle fibres size quantified as cross-sectional area (CSA) and increase in interstitial tissue are observed in homozygous tissue compared to wild type (B, C). Data are expressed as means ±SEM; n 12M = 12-13, n 18M = 4-3; two-sided t-test was performed comparing intra-age data vs. wild type, *, **, p<0.05, 0.01.

5.3 Homozygous muscle cells show alterations in the mitochondria, impaired fusion ability and reduced proliferation

At this point, we wanted to understand whether reduced strength and defects in muscle structure may follow mitochondrial impairment. To this aim we derived myoblasts from wild type and homozygous mice. Myoblasts are precursors of muscle cells that differentiate *in vitro* into myocytes which can fuse together to form multinucleated myotubes. Myotubes are terminally differentiated cells useful to study the characteristics of muscle fibres *in vitro* (Guo et al., 2020).

Transmitted electron microscopy (TEM) analysis of R274W+/+ myotubes revealed strong alterations in mitochondria, which appeared enlarged, vacuolated, with membrane and cristae degeneration compared to wild type [Figure 36 A]. Similarly to what we observed in neurons and fibroblasts, we also detected a reduction of Parkin level [Figure 32 B, D] and of mitochondrial mass in mutant myotubes compared to wild type, both using western blotting and qRT-PCR [Figure 36 C, E, F].

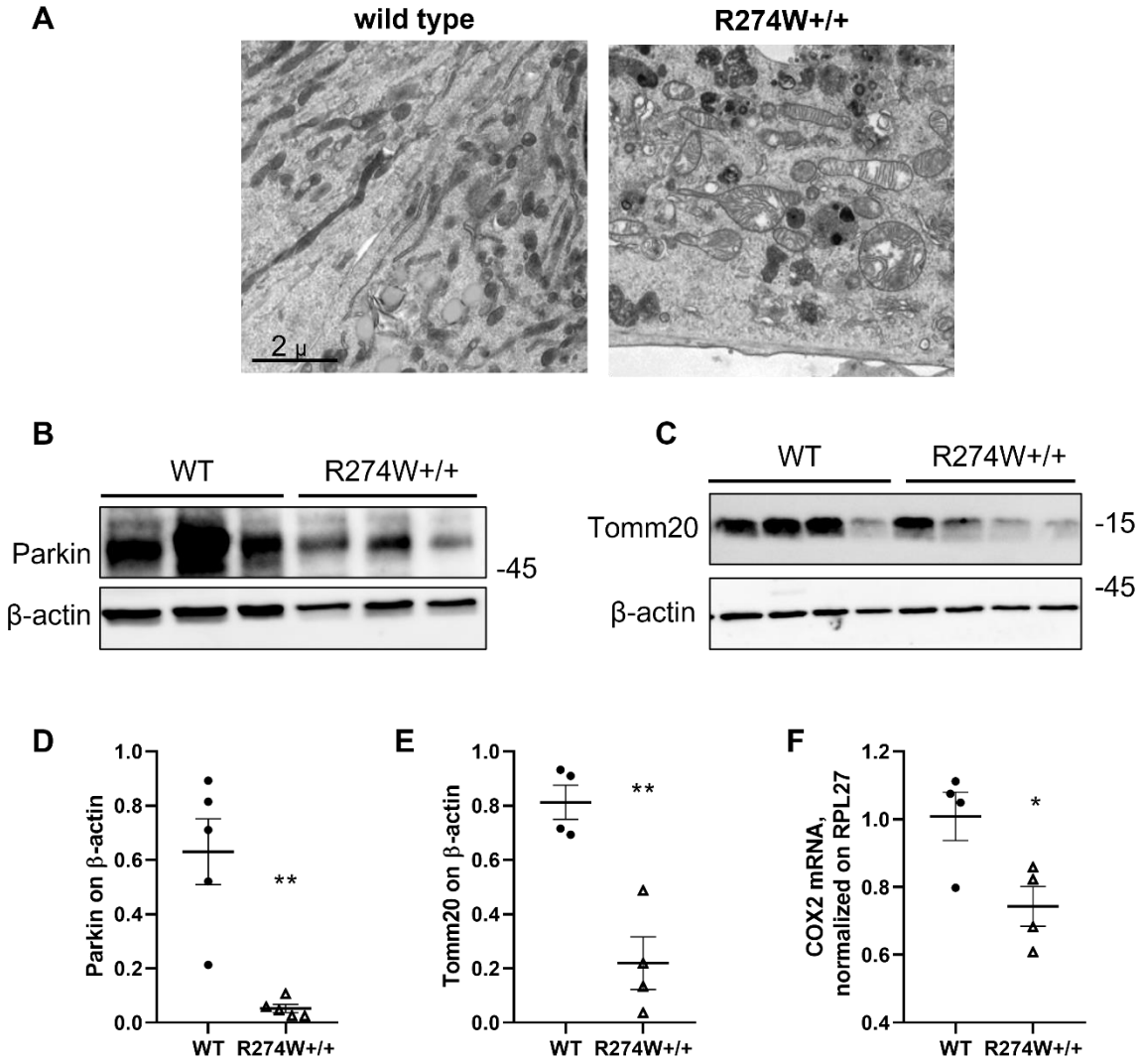

Figure 36: R274W+/+ myotubes show mitochondria defects. (A) Representative images of TEM analysis on wild type and homozygous myotubes. Scale bar = 2µ. In collaboration with Dr. Michael Hess. (B) We analysed wild type and R274W+/+ myotubes for Parkin content via western blot. The graph (D) shows Parkin level normalized on β-actin. Data are expressed as means ±SEM; n = 5; **, p<0.01 versus wild type.
(D) Biochemical analysis using Tomm20 antibody revealed a decrease in mitochondrial mass in homozygous myotubes compared to wild type. The graph (E) shows Tomm20 levels normalized on β-actin. Data are shown as means ±SEM; n = 4; **, p<0.01 versus wild type. (F) COX2 mRNA level is decreased in homozygous myotubes. The graph shows COX2 mRNA normalized on RPL27. Data are shown as means ±SEM; n = 4; *, p<0.05 vs WT.

Myoblasts differentiation and fusion processes strongly rely on ATP levels (O'Connor et al., 2008). Interestingly, myoblasts derived from homozygous mice showed a strong decrease in their fusion ability compared to wild type ones [Figure 37 A, B]. Additionally, myotubes generated from the fusion of homozygous myoblasts displayed a 25% reduction in their diameter compared to wild type [Figure 37 A, C], suggesting that R274W substitution in Parkin leads to altered formation of muscle fibres.

In addition, we observed that PARIS protein accumulates in R274W+/+ myotubes compared to wild type [Figure 37 D, E], while mRNA levels of PGC-1α and TFAM [Figure 37 F, G] are reduced, indicating that R274W mutation in Parkin impairs PARIS-PGC-1α pathway of mitochondria biogenesis not only in the CNS but also in the peripheral skeletal muscle.

Interestingly, it was observed by Bae group that the accumulation of PARIS in myoblasts causes their reduced proliferation, leading to cell senescence (Bae et al., 2020). Indeed, EdU analysis of myoblasts derived from wild type and homozygous mice showed that mutant cells are less proliferative, remaining mostly blocked in G1/G0 phase [Figure 38].

Altogether, our data imply that Parkin R274W-dependent disruption of PARIS-PGC-1α pathway impairs different features of muscle development.

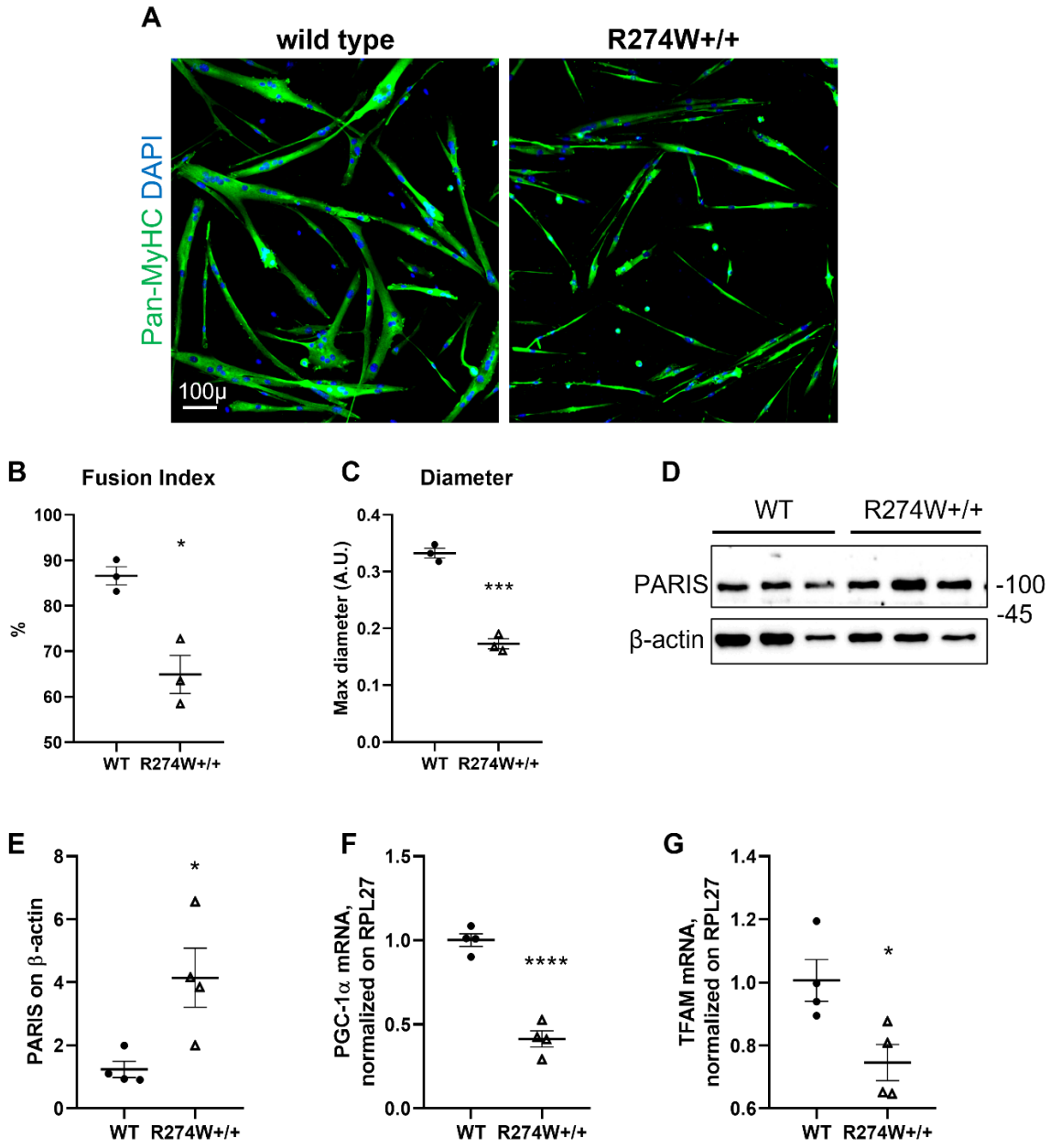

Figure 37: R274W Parkin impairs myotubes formation, as well as mitochondria biogenesis. (A) We differentiated myoblasts from wild type and R274W+/+ mice for 72 hours. Myogenic differentiation was evaluated by the expression of myosin heavy chain using Pan-MyHC antibodies (green). Nuclei are visualized by DAPI in blue. Scale bar = 100µ. Fusion index (B) was calculated as the number of multinucleated cells folded over total number of myosin-expressing differentiated cells (green). (C) The graphs show maximum diameter of wild type and homozygous myotubes, calculated with FIJI. For graphs (B, C) each point represents the mean of three technical replicates of a single cell line derived from a different mouse. Data are expressed as means ±SEM, n = 3; *, ***, p<0.05, 0.01, versus wild type.

PARIS-PGC-1α pathway is impaired in homozygous myotubes. (D) We selected a single line of wild type and homozygous myoblasts. After differentiation into myotubes for 72 hours we processed samples for biochemical characterization. (E) The graph shows PARIS levels in wild type and R274W+/+ myotubes normalized on β-actin. Data are represented as means ±SEM, n = 4; *, p<0.05 versus wild type. (F, G) The graphs show mRNA levels of

PGC-1α and TFAM normalized on RPL27 mRNA. Results are reported as means ±SEM, n = 4; *, ****, p<0.05, 0.0001, versus wild type.

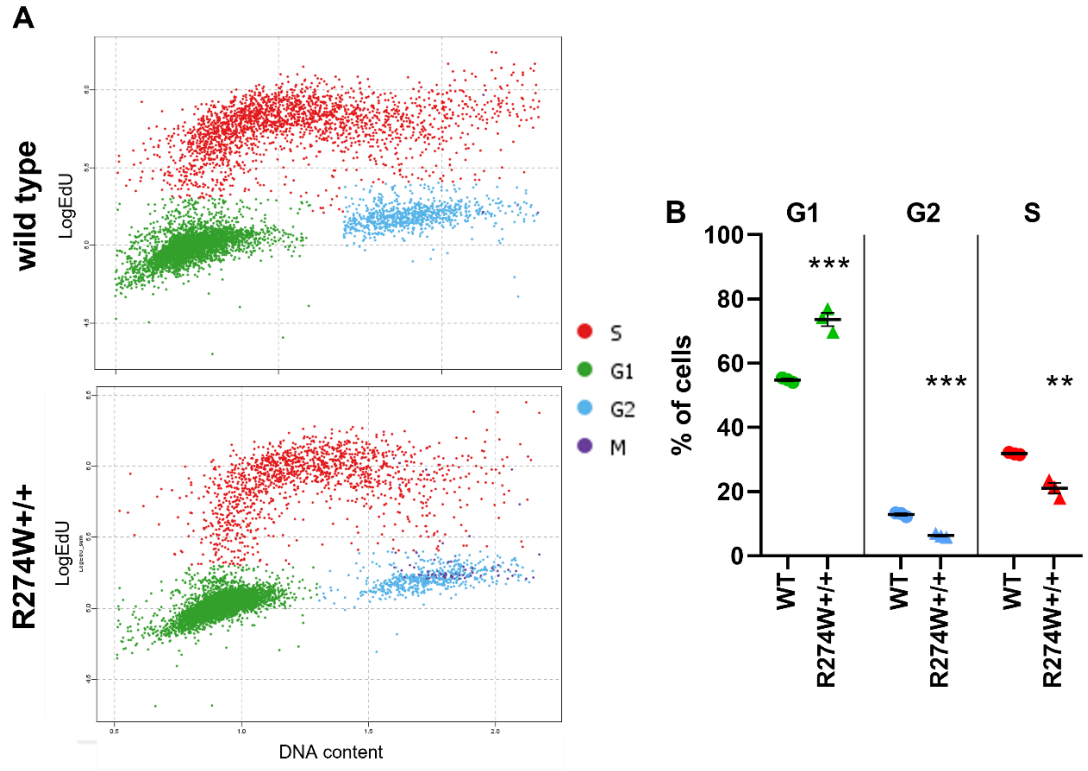

Figure 38: Parkin R274W+/+ myoblasts proliferate less than wild type ones. We analysed proliferative behaviour of wild type and homozygous myoblasts by means of a EdU assay. Only proliferative cells (G2, S phase) are able to incorporate fluorescently labelled EdU. Phospho-histone H3 (PH3) was used to specifically stain cells undergoing mitosis (M). DNA content (DAPI) was used to normalize the levels of fluorescent markers. Single cell analysis was performed in collaboration with HTS facility at CIBIO. (A) Each point of the graph represents a single cell and the relative position on x- (DNA content) and y-axis (LogEdU) was used to distinguish between different cell cycle phases. (B) The graph shows percentage of cells in G1/G0, G2, and M phase. Each point represents the mean values of all the single cells for each well analysed. Data are expressed as means ±SEM, n = 3; **, ***, p<0.01, 0.001, versus wild type.

DISCUSSION

1 Parkin R274W mouse is a robust model of PD, combining LOF and GOF effects

One of the most relevant setbacks in the study of PD pathogenesis and drug testing is the absence of animal models displaying the features typical of the disorder. Indeed, PD animal models should present late-onset, age-dependent, and progressive degeneration of DA neurons leading to motor symptoms responsive to L-DOPA treatment (McGonigle et al., 2013). Another key aspect would be the presence of Lewy pathology, even though PD cases without LBs have also been reported. Animal models should also be predictive of human response to drugs. However, to date no single animal model was able to show all the mentioned features (Jagmag et al., 2016).

Due to the easy possibility of genetic manipulation via transgene expression, knock-in and knock-out approaches, the rodent has become the mainly used system to model neurodegenerative diseases. However, despite different types of approaches in gene manipulation and different candidate genes, none of the current transgenic mouse lines can serve as a good model for PD (Dawson et al., 2012; Barker et al., 2020). Indeed, both α-synuclein and LRRK2 mice models fail to recapitulate DA neurodegeneration, despite showing some signs of alterations in the nigro-striatal system, presence of Lewy pathology only in rare cases, and minimal levels of motor impairment (Chesselet, 2007; Chesselet et al., 2008). Intoxication models of PD like non-human MPTP primate and 6-OHDA rodents are currently the most used for symptomatic drug testing, as they seem to be predictive enough of human response, even though they do not replicate the neurodegenerative nature of the disorder (Fox et al., 2010).

Among Parkin genetic models, Parkin KO mice display only slight defects in the balance beam at 18+ months (Goldberg et al., 2003), but these results could not be replicated (Perez et al., 2005). Subtle alterations of coordination were also observed in the Q311X Parkin mouse model (Lu et al., 2009).

Strikingly, motor tests on our R274W Parkin model revealed that coordination is impaired both in homo- and heterozygous mice starting from 6 months of age, with the strongest defects observed at 18 months, indicating that motor deficits are overt and progressive in our transgenic line. Motor performance was analysed both on male and female mice, but no significant sex-related variations were reported.

No differences were detected in the anxiety phenotype nor in the weight of mutant animals compared to age-matched wild type, suggesting that the alterations observed are strictly confined to the motor area.

Decreased coordination is classified as one of the major motor symptoms for the diagnosis of PD and has been put in relation to the death of dopaminergic neurons in the SN pc. Accordingly, our *ex vivo* characterization of mouse midbrain tissue showed that dopaminergic neurons are lost and TH expression is reduced at 6, 12 and 18 months both in homo- and heterozygous mice compared to wild type. A stereological count in heterozygous tissue is still needed to confirm this result. However, this finding is important because age-dependent TH loss was never observed before in Parkin-null mice (Goldberg et al., 2003), and a reduction of dopaminergic neurons was only reported in the Q311X Parkin mouse at 16 months (Lu et al., 2009; Regoni et al., 2021).

Moreover, we observed that loss of dopaminergic neurons is accompanied by increased astrogliosis in the mutant striatum and cortex at all time points, while the increase of astrocytes in the substantia nigra was more heterogeneous. Complementary assays are still necessary to validate these data. Finally, whether the increase in astrocytes represents a cause or is just a consequence of neurodegeneration is still to be addressed. Nevertheless, these results suggest that diffuse neuroinflammation is an early histological marker of both hetero- and homozygous brains.

Altogether, these data show that the R274W Parkin mouse line we generated is among the few genetic models which show age-dependent coordination impairments, degeneration of dopaminergic neurons and astrogliosis, making it relevant not only for further investigation into PD pathogenesis but also for testing therapeutic drugs.

Parkin R274W behaves as a LOF mutant on the mitochondria

Defects in mitochondria structure and functionality have been deeply connected with the pathogenesis of PD, especially since the discovery of PD-linked mutations in PINK1 and Parkin, which coordinate the removal of damaged mitochondria through mitophagy. Several studies have shown that loss of PINK1 or Parkin in different cell types including DA neurons leads to defects in mitophagy and increased cell death (Cummins et al., 2018). These findings generated the idea that impaired mitophagy may account for neurodegeneration in PD.

However, despite much evidence coming from *in vitro* studies, there is little indication that PINK1 and Parkin actually mediate mitophagy *in vivo*. Additionally, it has been severely debated whether degeneration of dopaminergic neurons could be caused by defective mitophagy (Whitworth et al., 2017).

Anyhow, defects in mitochondria structure and decreased respiratory capacity are often observed in brain specimens derived from PD patients and animal models of disease,

indicating that alterations in these organelles play a role in PD pathogenesis. Interestingly, Parkin substrate PARIS was observed to accumulate in the brain of sporadic PD patients (Shin et al., 2011). PARIS accumulation leads to the downregulation of PGC-1α, a key regulator of mitochondrial biogenesis. The PARIS-PGC-1α pathway is controlled by the activity of Parkin, which is responsible for PARIS proteasomal degradation and subsequent increased PGC-1α expression. Accordingly, Parkin-null mice show PARIS accumulation in brain tissue, a diminished number of mitochondria and degeneration of dopaminergic neurons (Lee et al., 2017; Siddiqui et al., 2015), leading to the hypothesis that decreased mitochondria biogenesis may be involved in the neurodegeneration process.

To gain insight into the mechanisms of R274W substitution in Parkin, we decided to explore its effect on the PARIS-PGC-1α pathway of mitochondrial biogenesis. Remarkably, we observed a net reduction in mitochondrial mass by western blot analysis in DIV14 cortical neurons derived from homozygous mice. Similar results were obtained in mutant fibroblasts, which showed a decrease in mitochondria quantity and defects in the PARIS-PGC-1α pathway, with an increase in PARIS protein level and a decrease in PGC-1α mRNA. Interestingly, PGC-1α overexpression was able to restore mitochondria levels in Parkin R274W+/+ fibroblasts, suggesting that this could be a good therapeutic strategy to deal with mitochondria defects.

This result is coherent with recent work published by Kumar group, in which they observed that PARIS knockdown in Parkin-null human DA neurons was enough to restore mitochondrial function, and this could not be obtained by solely rescuing the mitophagy pathway (Kumar et al., 2020). Despite experiments addressing the role of mitophagy in our mouse model have yet to be performed, these data suggest that Parkin R274W mutation behaves as a LOF on the PARIS-PGC-1α axis, leading to decreased mitochondria biogenesis in neurons and fibroblasts.

As several pieces of evidence indicate that PGC-1α reduction is deeply involved in PD pathogenesis, the modulation of its expression has been proposed as a possible therapeutic strategy in the early phase of the disease. However, it should be noted that the neuroprotective effect of PGC-1α in the SN is controversial. Indeed, some works showed that the transgenic expression of PGC-1α exerts a protective effect on dopaminergic neurons in the MPTP mouse model of PD (Schintu et al., 2009; Carta et al., 2011; Mudò et al., 2012), while other groups observed that PGC-1α overexpression in the acute MPTP rat model sensitized dopaminergic neurons to MPTP toxicity (Clark et al., 2012), and the same strategy was proven ineffective in the 6-OHDA rat model of PD (Laloux et al., 2012).

Finally, we also observed that homozygous fibroblasts displayed a reduced mitochondria functionality at different levels of the respiratory chain, indicating that Parkin R274W not only impairs mitochondria biogenesis through the PARIS-PGC-1α axis, but also their functionality.

Parkin R274W behaves as a dominant GOF mutant in the CNS

The observation that heterozygous mice display a phenotype that mirrors the one of homozygous animals both at the motor and the histological level supports the idea that R274W Parkin is not a simple LOF mutant.

Coherent with this hypothesis we observed that total Parkin levels are reduced in a similar manner in homozygous and heterozygous brain tissue at 6, 12, and 18 months of age. It was reported in literature that R275W substitution destabilizes Parkin structure leading to its degradation (Yi et al., 2019), but the comparable reduction of protein level in both genotypes suggests that wild type protein is affected as well.

Given that mutant Parkin forms aggresomes *in vitro* (Cookson et al., 2003), and that half of the patients with R275W Parkin-PD displays Lewy pathology (Madsen et al., 2021), we decided to deepen our knowledge of protein aggregation in our mouse model. Unluckily, we were not able to verify whether Parkin forms proper aggregates in the brain of hetero- and homozygous mice, because of the absence of commercially available KO-validated antibodies for specific immunodetection of Parkin/Parkin mutants. However, we plan to perform immunostaining experiments using recently released antibodies by BioLegend® which produced promising results in the midbrain of mice and human PD patients (Tokarew et al., 2021).

In this work, we analysed signs of Parkin altered solubility by western blotting. Noteworthy, we found that Parkin accumulates in Triton-X100 insoluble fraction both in R274W+/+ and R274W+/- mouse lines. These observations suggest not only that R274W substitution alters Parkin structure and folding, but also that mutant Parkin affects the wild type protein. Therefore, our data suggest that Parkin R274W acts as a dominant-negative mutation on the protein solubility.

To better understand the effect of R274W substitution on protein aggregation, we analysed the distribution of other proteins known to accumulate and decorate aggresomes in the brains of PD patients, such as ubiquitin and p62 (Liu et al., 2016). For the moment, we have focused our analysis on tissue derived from 18-month-old animals, as aged mice should present a phenotype that is closer to the clinical situation of symptomatic PD patients. In the future, we intend to repeat our analysis also on tissues gathered from 6- and 12-month-old mice.

We observed that ubiquitin and p62 staining is more pronounced in the midbrain of transgenic homo- and heterozygous mice compared to WT. Intriguingly, no difference between genotypes was observed in other brain areas analysed, suggesting that protein aggregation may happen primarily in the midbrain and SN, similarly to what is observed in sporadic PD patients. Protein aggregation points towards a gain of toxic function for R274W Parkin mutant.

α-synuclein phosphorylated on serine 129 was identified as the main component of LBs in human patients (Samuel et al., 2015). Strikingly, we noticed an accumulation of α-synuclein pS129 in the midbrain of 18-month-old heterozygous mice, both in cell bodies and neurites, replicating Lewy pathology that is observed in most sporadic PD patients. This finding was remarkable, as none of the genetic PARK2 knock-out models exhibits LBs (Goldberg et al., 2003; Itier et al., 2003), which are only observed in mouse models of α-synuclein mutation/overexpression (Masliah et al., 2000; Giasson et al., 2003) and in the Q311X Parkin mouse (Lu et al., 2009).

In line with Parkin-deficient mouse models, homozygous mice do not show α-synuclein pS129 aggregates in the midbrain at 18 months of age. This observation is coherent with literature data showing that correct lysine 63-linked poly-ubiquitination by Parkin is required for the sequestration of misfolded proteins into aggresomes and their subsequent elimination through degradation pathways (Olzmann et al., 2007; Chin et al., 2010). The complete absence of wild type protein could thus impair this mechanism. Biochemical analysis of α-synuclein solubility supports this idea, as increased insolubility was observed only in heterozygous and not in homozygous brains. However, additional experiments are needed to validate these data.

Taken together, biochemical and histological findings indicate that R274W Parkin mutation triggers protein aggregation and could thus be classified as a GOF substitution.

Protein aggregates can activate the UPR, an elaborate pathway which turns on to defend the cell from stress. BiP, one of the best-characterized chaperons of the UPR, is indeed increased in homo- and heterozygous brains at 12 months, and augmented BiP mRNA expression was observed in homozygous cortexes already at 6 months of age, suggesting that protein stress is an early factor in PD pathogenesis.

In vitro characterization of R275W mutant brings support to the hypothesis that protein stress is generated through a dominant GOF mechanism. Indeed, once overexpressed in HEK293 cells, R275W protein forms aggregates that colocalize with ubiquitin. Additionally, cells that overexpress mutant but not WT protein show enhanced BiP mRNA expression. Interestingly, increased BiP was observed only after overexpression of R275W Parkin, and not of NSF T645D, a PD-linked protein prone to aggregation

(Pischedda et al., 2021), suggesting that UPR activation is selectively linked to specific types of aggregates.

Finally, coherent with the idea of a dominant-negative mechanism, overexpression of Parkin R275W mutant in HEK293 cells increased the insolubility of wild type protein, suggesting that mutant Parkin may bind and sequester wild type form. This result is in agreement with the work of Wang group, which observed that R275W overexpression in Parkin-null *Drosophila* aggravates motor impairment even if it does not accelerate neurodegeneration, suggesting that mutant protein may affect the functionality of surviving neurons (Wang et al., 2007).

Altogether, these data imply that the effect of Parkin R275W mutation is more complex than the one derived from a simple loss of Parkin activity. A mechanism of dominant gain of toxic function for R275W substitution offers an explanation not only for the phenotype observed in our heterozygous mice but also in heterozygous and compound heterozygous PD patients.

Additionally, a gain of toxic function for the mutation explains why we observe overt phenotype of motor impairment, neurodegeneration and neuroinflammation in our transgenic mice, while almost no PD-linked hallmarks are observed in Parkin-null mouse models (Perez et al., 2005). Moreover, Parkin deficient mice may benefit from compensatory mechanisms (He et al., 2018), which may not be put in place if the protein function is not completely ablated.

It is of particular interest to notice that the only other mouse model that displays some degree of motor deficits, mitochondria abnormalities, dopaminergic loss and α-synuclein aggregation is the Q311X Parkin mouse (Lu et al., 2009; Regoni et al., 2021), in which mutant Parkin is introduced as a bacterial artificial chromosome (BAC) thus replicating heterozygous condition. Q311X and R275W substitutions both impair the RING1 domain of Parkin and behave as dominant GOF mutations in mice and *Drosophila* models, suggesting that the RING1 domain is critical for the correct functionality of the protein and its mutation can be related to Parkin-linked dominant toxicity.

2 Parkin R274W impairs the architecture of the glymphatic system, which may serve for the clearance of phosphorylated α-synuclein

In the last decade, many neurodegenerative disorders have been put in relation by the presence of protein aggregates in the brain tissue. For this reason, the proposal of the glymphatic system as the main brain clearance route is particularly appealing in this field.

Alterations in the glymphatic system have especially been linked to Alzheimer's disease, with the observation that human patients' brains display enlarged perivascular spaces compared to healthy individuals [Supplementary Figure S9].

Strikingly, we observed that our mouse model shows similar alterations, with the presence of enlarged CD31+/GFAP+/AQP4+ structures especially localized in the cortex and striatum of homo- and heterozygous mice at 18 months of age. A clear distinction of the space between the blood vessel and the astrocyte endfeet was not possible in our working condition, as perfusion and paraformaldehyde fixation eliminate blood pressure causing the collapse of the PVS. For this reason, we talk about a general enlargement of the glymphatic structures in mutant tissue, which should *bona fide* reflect what happens in the perivascular space. However, *in vivo* studies using MRI approach with fluorescent brain tracers will be needed in the future to assess the functioning of the system in our mouse model.

The loss of AQP4 endfeet localization is another key feature of glymphatic dysfunction that was observed in different mouse models of AD, ageing, and brain injury. Accordingly, we noticed that in Parkin R274W+/+ brain tissue the immunofluorescent signal of AQP4 is more dispersed and less localized around vessels compared to wild type, suggesting that R274W substitution is linked to the mislocalization of AQP4.

This observation led to the idea that Parkin activity is necessary for the correct expression and localization of AQP4 in the membrane of the astrocytes. Coherent with this hypothesis, we observed that AQP4 is not correctly localized in homozygous astrocytes compared to wild type.

Such findings are supported by *in vitro* experiments on HEK293 cells, in which we noticed that AQP4 is located to the membrane when wild type Parkin is overexpressed, while such localization is lost when R275W Parkin is present. To date, our experiments have been performed using M23 isoform of AQP4, but they need to be replicated both using M1 isoform and M1:M23 combination.

Recent evidence from proteomic studies proposes AQP3, another member of the aquaporins family, as a putative Parkin substrate (Zittlau et al., 2022). AQP3 and AQP4 share a common peptide, K**K**GKDQS, harbouring the putative ubiquitin acceptor site (in bold). It is thus intriguing to speculate that Parkin could ubiquitinate AQP4 and promote its correct membrane insertion.

However, Parkin could also act indirectly by ubiquitinating other proteins involved in the control of AQP4 trafficking. For example, α-syntrophin is part of the protein complex that is needed to maintain AQP4 proper position in the membrane. Interestingly, α-syntrophin present a PDZ (PSD-95/Discs-large/Zona Occludens-1) domain which was proven necessary for the correct sarcolemmal insertion of AQP4 (Adams et al., 2001).

Literature data have shown that PDZ element is present in several Parkin substrates, and that monoubiquitination at this level is not connected with proteasomal degradation (Joch et al., 2007), suggesting that PDZ ubiquitination is linked with the regulation of substrate function.

At the moment, preliminary data produced in our laboratory by *in vitro* ubiquitination seem to exclude a direct interaction between Parkin and AQP4 (data not shown), but a deeper analysis is needed to confirm this hypothesis. However, whether it occurs directly or indirectly, it is fascinating to think that incorrect ubiquitination by Parkin mutants may alter AQP4 localization and expression, possibly hampering glymphatic system functionality.

This idea is coherent with the observation that AQP4 levels are increased in the presence of wild type and not R275W Parkin in HEK293 cells. A reduction in AQP4 levels is also observed in homozygous mice brains at 6 months of age, suggesting that R274W substitution may behave as a loss of function in this context. The increased AQP4 signal that we observed in the brains of 18-month-old R274W+/+ mice may be the result of a compensatory mechanism that leads to augmented non-polarized expression of the protein, a condition that was also seen in aged brains, during brain inflammation but also in neurodegenerative disorders like Alzheimer's disease (Simon et al. 2022; Salman et al., 2022).

The correlation between glymphatic system dysfunctions and AD is becoming clearer and clearer, as it turned out to be evident that this route is important for the removal of β amyloids and that it is often altered in the brains of humans and animal models of disease. Whether this could be applied also to Parkinson's disease is appealing but still under discussion. Undoubtedly, PD and AD present many similarities, among which we can list neurodegeneration, inflammation, cognitive deficits, prodromal sleep disturbances and protein aggregation.

An important step to validate the link between glymphatic dysfunctions and Parkinson's disease pathology would be to show that this route is implied in the clearance of phosphorylated α-synuclein, the major component of Lewy bodies. Interestingly, we produced some preliminary data that show how pS129 α-synuclein signal decorates the glymphatic structures in our mouse model at 18 months of age. Remarkably, we observed that in the midbrain of the heterozygous mice, the only genotype in which we detected proper α-synuclein aggregates, cells positive to pS129 α-synuclein accumulate in close proximity to the enlarged glymphatic structures [Supplementary Figure S10], suggesting that glymphatic system may actually play a role in the elimination of α-synuclein aggresomes in PD. However, many other experiments are needed to confirm this data. Additionally, it is still not clear whether alterations in the

glymphatic system architecture can be considered as a part of the pathological cascade or a simple consequence of the disease progression. It is interesting however to speculate that our mouse line displays such an overt Parkinsonian phenotype because it combines Parkin LOF and GOF, which may be exacerbated by impairments in the glymphatic system route of brain waste removal.

Interestingly, the activity of the glymphatic system clearance pathway can clarify why protein aggregation observed in homo- and heterozygous brains was restricted to the midbrain region, while neuroinflammation, protein stress and UPR are observed also in other brain areas. Indeed, according to Braak theory, extracellular waste products can spread throughout the brain and outside the CNS (and *vice versa*) with a specific pattern in time and space (Rietdijk et al., 2017). It is possible that such distribution may follow the route of the glymphatic system inside the CNS and of the lymphatic system in the periphery. In accordance with this, dysfunctions of AQP4 polarization in the brain of human AD patients have been proven to be predictive of both amyloid β deposition levels and Braak staging (Zeppenfeld et al., 2017). However, these are just preliminary findings that need to be further validated both in humans and animal models of AD and other neurodegenerative disorders.

In any case, a link between PD and dysfunction of the glymphatic system may offer a novel strategy to improve the removal of brain aggregates.

In conclusion, our mouse model might represent an important tool to model glymphatic system alterations linked to PD, a potential new target for PD pharmacology.

3 Parkin R274W impairs the skeletal muscle at different levels by disrupting the PARIS-PGC-1α pathway of mitochondrial biogenesis

PD in humans is also characterized by motor symptoms that are not strictly correlated with dopamine depletion in the extrapyramidal system. For example, bilateral muscle weakness and fatigue are often present in PD patients with unilateral parkinsonism (Cano-de-la-Cuerda et al., 2010). It is still not clear whether impairments in the muscle are caused by central deficits due to lack of dopamine (Frazzitta et al., 2015), incorrect muscular stimulation and stiffness, or other peripheral causes secondarily linked to PD like ATP depletion, mitochondrial degeneration, and inflammation (Kostić et al., 2016). It is important to recognize the causes of muscular deficits in order to select the best treatments and ameliorate PD patients' quality of life.

Parkin R274W homozygous and heterozygous mice display defects in muscular strength and increased fatigue compared to wild type starting from 12 months of age.

Accordingly, our *ex vivo* analysis of muscle tissue revealed alterations in the structure and organization of the fibres, with decreased diameter and enlargement of interstitial

tissue, similarly to R275W *Drosophila*. Alterations in muscle functionality were recently observed also in the 6-OHDA rat model of PD (Albarracìn et al., 2022), while they were never investigated in mice. Although histological data on muscle tissues need to be expanded, these findings suggest that R274W Parkin correlates with muscle issues in 12- and 18-month-old hetero- and homozygous mice.

In 2007 Wang group demonstrated that both Parkin-null and R275W *Drosophila* displayed mitochondrial alterations in the indirect flight muscles. Coherent with these observations, TEM analysis of myotubes derived from our R274W+/+ mice showed seriously damaged mitochondria. Additionally, muscle cells derived from R274W+/+ mice also displayed alterations in their ability to replicate and fuse, processes that deeply rely on the correct functionality of the mitochondrial respiratory chain. Considering that histological analysis on muscle tissue offered similar results for both mutant genotypes, we expect that experiments on R274W+/- myotubes will reveal comparable defects.

To obtain insight into the mechanisms that link Parkin R274W substitution, impaired mitochondria, and defects in muscle tissue we again explored the PARIS-PGC-1α pathway of mitochondrial biogenesis, which is activated by Parkin (Shin et al., 2011).

Interestingly, we observed that this pathway is impaired in presence of R274W mutation not only in homozygous neurons and fibroblasts, but also in the skeletal muscle. Indeed, we noticed that PARIS accumulates in homozygous muscle cells. PARIS accumulation has been put in relation to ROS production that may damage mitochondria and at the same time reduce cell proliferation (Bae et al., 2020). On the other hand, the downregulation of PGC-1α and its downstream target genes may lead to the reduction in mitochondrial mass that we observed in homozygous myotubes both by qRT-PCR and biochemical assays.

Altogether, these data show that Parkin R274W causes different alterations in the mitochondria which mirror the ones observed in the CNS and in mutant fibroblasts. This indicates that the correct functionality of Parkin is important for mitochondrial biogenesis and tissue functionality not only in the CNS but also in the periphery.

The modulation of the PARIS-PGC-1α axis represents a therapeutic target also in the skeletal muscle. In accordance with this, several groups have shown that overexpression of PGC-1α in the muscle of aged mice leads to decreased oxidative stress, increased energy metabolism, muscle integrity and regeneration (Garcia et al., 2018; Southern et al., 2019). In the future, we intend to evaluate whether PGC-1α overexpression can rescue myoblasts' phenotype of fusion and replication and can restore mitochondrial content in mutant cells.

4 Significance and innovation of our mouse model

Consistent with our results, we believe that our project has provided several key findings:

1) R274W Parkin acts as a LOF on the PARIS-PGC-1α pathway leading to decreased mitochondria biogenesis both in the CNS and in skeletal muscle.
2) R274W Parkin acts as a dominant GOF in the CNS leading to protein accumulation and α-synuclein deposition in the midbrain.
3) R274W Parkin impairs the structure of the glymphatic system.
4) R274W Parkin mouse line is a new model of genetic PD: to date no genetic mouse model was able to recapitulate all the features of human Parkinson's disease. Parkin R274W mice instead present age-dependent motor impairment and neurodegeneration, decreased striatal dopamine, mitochondrial aberrations and decreased respiratory capacity, neuroinflammation, α-synuclein positive aggregates, protein stress, muscle alterations and glymphatic architecture deficits. Our transgenic mouse model configures itself as a key tool to clarify pathological mechanisms of PD and to design and test therapeutic strategies with a good predictive index.
5) R274W Parkin mouse line is a new model of glymphatic dysfunction: currently, the studies focusing on glymphatic alterations are based on AQP4-null mice (Cui et al., 2021) or on the mechanical blockage of the lymphatic system (Zou et al., 2019; Ding et al., 2021). These animal models are far from the conditions happening during ageing and are not suitable for the assessment of pharmacological interventions. Parkin R274W mice represent a new opportunity to model and treat glymphatic dysfunction.

5 Future directions

In the future, we plan to plan to complete our characterization of the R274W model with the time point and genotypes missing for some experiments. Additionally, we would like to better explore the role of neuroinflammation in our mice: in particular, we will investigate whether astrogliosis is present before the presentation of motor symptoms (i.e., 3 months). We will also explore the interaction between astrocytes and neurons, exploiting co-cultures of different combinations of WT/mutant cells to understand whether the effect of R274W substitution primarily affects glial or neuronal cells.

Further analysis will also be performed to understand when protein aggregation in the midbrain begins, and the mechanism underlying it. We will also try to identify the process through which R274W Parkin triggers the deposition of pS129-α-

synuclein. As a therapeutic strategy, we would like to test drugs known to stimulate the removal of aggregates (i.e., trehalose as in Assoni et al., 2021; Pischedda et al., 2021) and verify whether this strategy can ameliorate the motor impairment observed in our mouse line.

We also plan to deepen our analysis on mitochondria alterations, performing TEM experiments on mutant neurons, brains and muscle tissue. We will also explore possible alterations in mitophagy using mitochondria-targeted probes of membrane polarization (i.e., mt-Keima). Additionally, rescue experiments with overexpression of PGC-1α/downregulation of PARIS will also be performed both on fibroblasts and myoblasts, to assess whether improvement of mitochondria biogenesis may positively affect the phenotype of mutant mice.

Our analysis of the glymphatic system will be expanded both *ex vivo* and *in vivo*. Ongoing experiments in our laboratory are aiming to disclose the link between Parkin and AQP4. In particular, we are evaluating whether Parkin directly ubiquitinates AQP4 by means of biochemical *in vitro* assays.

Finally, we plan to assess the functionality of the glymphatic system by combining the use of MRI and *cisterna magna* infusion of fluorescent tracers as described in the work of Mestre group (Mestre et al., 2018). Modulation of the glymphatic system activity will also be taken into consideration for future experiments.

MATERIALS AND METHODS

EXPERIMENTAL MODELS DETAILS

Animals

The University of Trento and National Ministry of Health approved all animals protocol (authorization #162/2022-PR). Experiments were designed to limit the number of mice to be sacrificed respecting the 3Rs rule and according to national guidelines. All the experiments were done in compliance with EU Directive 2010/63 and national law D.L. 26/2014.

Parkin R274W+/+ mice were generated via CRISPR/Cas9 technology by Taconic Biosciences. Transgenic animals were crossed with C57BL/6N mice for more than 10 generations to produce R274W+/- and WT littermates. Transgenic animals are viable and fertile. Animals were kept in a normal light/dark cycle (12 hours light, 12 hours dark) with food and water *ad libitum*. At 6-, 12- and 18-months Parkin R274W+/+, R274W+/- and WT mice were evaluated for behavioural performance. Male and female mice were used in the same ratio. After motor assessment, mice were sacrificed according to guidelines with CO_2 or anaesthetic overdose followed by transcardial perfusion to gather the skeletal muscle tissue (TA, soleus) and brain.

Primary cell cultures: neurons

Primary cortical neurons were derived from embryonic day 17.5-18.5 wild type and Parkin R274W+/+ mouse embryos through dissection procedure. Neurons were plated at a 150 cells/mm^{2}density on 12-well culture plates coated with poly-d-lysine 50 µg/ml and grown in Neurobasal (Gibco) supplemented with B27, L-glutamine 0.5 mM and 10 µg/mL gentamicin. Cells were incubated at 37°C in a humified 5% CO_2 incubator.

Fibroblasts

Mouse fibroblasts were collected from female and male wild type and Parkin R274W mouse ears. Tissue was incubated with 70% ethanol for 5 minutes. After air-drying, the ears were cut into small pieces and incubated for 60 minutes at 37°C with a 1:1 mixture of collagenase II (Worthington) and dispase II (Gibco). Smashed tissue was put in a 70 µM cell strainer and ground using a syringe plunger. Cell suspension was centrifuged twice for 7 minutes at 580g at 4°C. Surnatant was discarded, and pellet was resuspended and grown in DMEM with 20% FBS, 1% L-glutamine and 1% Pen-Strep. A complete medium change was performed after 48 hours, and after that was replaced every third day. Cells were incubated at 37°C in a humified 5% CO_2 incubator. Cells were split 1:10 every 4 days with 0.25% trypsin and cryopreserved at need in 90% FBS – 10% DMSO.

Myoblasts and myotubes

Female and male wild type and R274W+/+ mice were sacrificed at 3 months of age, and all the hind-limbs muscles were collected and minced. Disaggregated tissue was incubated in Muscle Dissociation Buffer (MDB, 490 U/mL collagenase II in HamF10, 1% Pen-Strep, and 1% L-glutamine) for 40 minutes at 37°C under 70 rpm agitation. A wash was performed in ice cold Wash Media (WM, 1% Pen-Strep, 1% L-glutamine, 10% Horse Serum in HamF10) followed by centrifugation at 1600 rpm for 5 minutes at 4°C. After supernatant removal, dispase II (11 U/mL in PBS) and collagenase II (1960 U/mL in PBS) were added to the pellet and incubation was performed at 37°C under 70 rpm agitation for 20 minutes. Supernatant was further dissociated using 18'' and 20'' syringe needles and 70 µm Nylon strainer. After each step, a wash in WM was performed followed by centrifugation at 1600 rpm for 10 minutes at 4°C.

Muscle satellite cells were isolated from the resulting pellet using MACS® (magnetic cells separation) technology by Miltenyi Biotec. Isolated cells were plated in 60mm collagen-coated (Collagen Sigma C3867) Petri dishes and growth in Growth Medium (GM, 2% Pen-Strep, 1% L-glutamine, 20% FBS, 2.5 ng/mL FGFβ in HamF10). Medium was changed every second day. Cells were incubated at 37°C in a humified 5% CO_2 incubator. Cells were split at around 70% of confluency with 0.25% trypsin and cryopreserved at need in 90% FBS – 10% DMSO.

To induce differentiation, cells were plated at 20000 cells/cm^2 onto matrigel-coated plates in GM. After 24 hours, cells were placed in Differentiation Medium (DM, 2% Pen-Strep, 1% L-glutamine, 2% Horse Serum in DMEM) for 72 hours.

METHODS DETAILS

Behavioural tests

Before proceeding to motor tests, mice were habituated to the presence of the operator for 5 consecutive days.

Rotarod

Balance and coordination were measured using the rotarod apparatus from Ugo Basile (Biological Research Apparatus). The rotarod was set with increasing speed from 4 to 32 rpm with a ramp-rate of 120 seconds or with fixed acceleration of 12 rpm, and the time needed to fall off the rotarod was recorded. Mice were habituated to the task for four consecutive days. The fourth trial of the last test day was evaluated for statistical analysis. A cut-off of 300 seconds was imposed.

Balance beam walking

The beam apparatus consists of 1-meter beams with a flat surface of 12 mm or 6 mm located 60 cm above the table, with a black box filled with nesting material at the end (endpoint). On the other side of the beam (start), a halogen lamp was placed as an aversive stimulus.

Time required to reach the endpoint from the start was recorded. The stopwatch was stopped when the anterior limbs of the animal reached the endpoint. Three trial tests were performed with one minute of rest in between. The result of the fourth trial was considered for statistical analysis. The beams were cleaned with 70% ethanol followed by water before placing the next mouse on the apparatus. A cut-off of 30 seconds was imposed.

Pole Test

In the vertical pole task, mice were placed on a 50 cm vertical pole with a diameter of 1.2 cm with the head facing upwards. Mice were habituated to the task in three trials for two consecutive days. On test day, mice were subjected to three trials: the total time taken to turn the body completely and descend (latency) was recorded. A cut-off of 20 seconds was imposed. Data are shown as a mean of three trials performed during test day.

Hanging Wire Test (four limbs)

Mice were placed on a metal grid. The grid was kept upside down and total hanging time was recorded. The stopwatch was stopped when the animals had lost grip with all four limbs. Three trials were performed for each mouse, and the best performance was used for statistical analysis. A cut-off of 300 seconds was imposed.

Grip Strength Test (anterior limbs)

Strength in the anterior limbs was measured using the grip strength apparatus from Ugo Basile (Biological Research Apparatus). The maximum strength was set to 500g/f at a rate of 30gf/s. Mice were placed so that their anterior limbs could grasp a horizontal bar, and gently pulled by the tail with a direction parallel to the ground. Mean peak force of three consecutive trials with one minute rest in between was measured using the Ugo Basile DCA software. Mean peak force was then normalized on the animal weight, measured on the same day of the test.

Novel Object Recognition (NOR)

The NOR test was performed in an open arena (60x50x30cm). Habituation was achieved over three consecutive days. On test day, mice were exposed to habituation, familiarization, and novel object recognition. During familiarization, each mouse was placed in the centre of the arena for 5 minutes with two identical objects. Objects were removed, and after 5 minutes pause a familiar object (old) and a new one were

introduced in the arena for 5 minutes. Object recognition was scored when the mouse nose was within 0.5 cm of an object. Data represent the percentage of time spent exploring the novel object compared to total exploration. The role (familiar or new) of the objects and their relative position were randomly permuted from mouse to mouse. The objects consisted of wooden cylinders, cubes, and pyramids. Arena was cleaned with 70% ethanol between trials. Data were analyzed using EthoVision XT software.

Open Field

In the open field test, an open arena of 60x50x30cm was used. Time of exploration in the central zone was recorded and compared to the borders of the arena. Total time of exploration was set at 300 seconds.

Light Dark

The light dark test was performed in a brightly illuminated arena with a dark insert. Mice were placed in the dark side of the arena. The total time spent in the bright side of the arena was recorded and used as an index of anxiety, as more anxious animals will spend less time in the bright compartment. Total time of exploration was set at 600 seconds.

Animal Sacrifice

Mice were euthanized with carbon dioxide (CO_2) inhalation according to AVMA Guidelines for the Euthanasia of Animals. After sacrifice mice were decapitated, and brains and hindlimb muscle tissue were collected. Brain hemispheres and TA muscle were stored at -20°C for subsequent biochemical preparations. Gastrocnemius and soleus muscle were frozen in isopentane placed on liquid nitrogen and kept at -80°C for immunostaining experiments.

Transcardial Perfusion and Brain Freezing

Anaesthetic administration was performed via intraperitoneal injection. Complete unconscious stage was checked by loss of pain reflex in the paw/tail. Mice were placed on perfusion stage and after exposure of the abdominal wall and heart cavity, a needle attached to a peristaltic pump was inserted in the left ventricle. PBS perfusion was followed by perfusion with paraformaldehyde (PFA) 4% in PBS for 5-10 minutes. Mice were decapitated and brains were kept in 4% PFA-PBS solution overnight at 4°C. Fixed brains were then put in ice-cold sucrose 30% solution overnight at 4°C until complete sinking.

Tissues were washed in PBS and covered in O.C.T. (compound embedding medium for cryostat, Killik) for 20 minutes before inclusion. Brains were put in polystyrene

boxes filled with O.C.T. and placed on an ethanol freezing bath until complete solidification. Frozen samples were stored at -80°C until cryostat sectioning.

Cryostat Sectioning

Frozen brains and soleus muscles were cut using Thermo Scientific HM525 NX cryostat at a temperature of -21°C. 14 µm transversal sections were cut and placed on Polysine™ Adhesion Microscope Slides (Epredia). Slides were stored at -20°C until further analysis.

Immunostaining

The list of antibodies used is displayed in Supplementary Table S1.

Immunofluorescence

For cell cultures, cells were seeded at low density on ø12mm Cover Glasses (Thermo Fisher Scientific). Cells were fixed with PFA 4% for 10 minutes and washed with PBS. Brain sections were defrosted at RT and washed in PBS. Antigen retrieval was performed when needed using Citrate Buffer (Sodium citrate 10 mM in dH_2O, Tween 0.05%, pH 6) for 20 minutes at 100°C.

After washing with PBS, samples were incubated for 1 hour in saturation buffer (2.5% BSA, 10% goat serum, 0.2% Triton). Subsequent washes were all performed with PBS-Triton 0.2%. Samples were incubated with primary antibodies in incubation buffer (2.5% BSA in PBS-Triton 0.2%) overnight at 4°C. After three washes of 10 minutes each, specimens were incubated with fluorescent secondary antibodies in incubation buffer for 1 hour. DAPI was used to visualize nuclei. After three washes of 10 minutes each, slides were mounted using FluorSave™ Reagent (Millipore).

Images were acquired using optical microscope Zeiss Axio Imager M2 and analysed for signal intensity using FIJI software.

DAB Immunohistochemical Staining

Slices were treated as described above for antigen retrieval and saturation. After incubation with primary antibodies, slices were washed three times for 5 minutes in PBS-Triton 0.2% and then incubated with peroxidase blocking reagent (H_2O_2 3% in PBS) for 15 minutes. Samples were incubated with biotinylated secondary antibodies in incubation buffer for 45 minutes. After three washes of 5 minutes in PBS-Triton 0.2% slices were incubated for 30 minutes with ABC(avidin-biotin complex)-HRP kit (Vectastain®) for signal amplification. Specimens were washed three times for 5 minutes in PBS-Triton 0.2% followed by a PBS wash. Slices were incubated with DAB Chromogen Solution (Biotium) for 30 seconds to 1 minute maximum depending on the antibody. The intensity of tissue staining visualized by brown precipitate was monitored under a light microscope.

Samples were then rinsed in PBS and deionized water. Hematoxylin counterstain was performed to visualize the nuclei. Specimens were mounted using DPX mounting medium (Sigma).

Slices were visualized in brightfield illumination using optical microscope Zeiss Axio Imager M2 equipped with a colour camera and analysed for signal intensity using FIJI software.

Hematoxylin & Eosin Staining (H&E)

Sections were defrosted and washed in deionized water. Glass slices were covered with Mayer's Hematoxylin (abcam) for 4 minutes. After 2 minutes wash in distilled water, bluing was achieved by dipping slices into a Differentiation Solution (70% EtOH; 0.3% HCl) and Scott's Solution. Slides were washed in water for 2 minutes, then in 70%, and 90% alcohol. Eosin Y solution (abcam) was applied for about 30 seconds. Samples were washed in absolute alcohol for 1 minute. After being washed in xylene for 3 minutes, slices were mounted using DPX mounting medium (Sigma). Samples were visualized in brightfield illumination using optical microscope Zeiss Axio Imager M2 equipped with a colour camera and analysed for signal intensity using FIJI software.

Plasmids and Transfection

WT Parkin-Flag pcDNA 3.1+ vector was a kind gift of Dr. Jenny Sassone. R275W Parkin-flag construct was generated by site-directed mutagenesis to introduce C>T single point mutation within the coding sequence at position 823. *E. coli* DH5alpha were transformed to amplify the plasmid. Primers used for cloning and sequencing are shown in Supplementary Table S2.

The pcDNA 3.1-c-Myc-Parkin plasmid was purchased through GeneScript (OHu26139C).

The pcDNA 3.1-Flag-PGC-1α plasmid was purchased through Addgene (#45501). Empty pcDNA 3.1+ vector was used as transfection control.

HEK293 cells were transfected with Jet-PEI (Polyethylenimine, Polysciences) with a ratio DNA:PEI of 0.8:100. Desired micrograms of DNA were dissolved in PEI and vortexed for 10 seconds. The DNA-PEI mix was then incubated at room temperature for 10 minutes and added to cell medium.

Mouse primary fibroblasts were transfected with Lipofectamine 2000 (Life Technologies) following manufacturer's instructions. Medium was changed after 24 hours. Cells were processed after 48 hours.

Soluble-Insoluble Assay, Western Blotting and Antibodies

For Soluble-Insoluble assay, cells were lysed in cold Lysis Buffer (150 mM NaCl, 50 mM HEPES, 1% Triton) completed with protease inhibitors (Calbiochem) for 30 minutes at 4°C. After 10 minutes of 16000 g centrifugation at 4°C, the supernatant was collected and used as soluble fraction, while the pellet was used as Triton-X100 insoluble fraction. Laemmli Buffer was added to the samples, followed by 10 minutes boiling at 95°C.

For total amount of protein analysis, cells were lysed in cold RIPA Buffer (150 mM NaCl, 2mM EDTA, 50mM Tris-HCl, 1% NP40, 0.25% sodium deoxycholate, pH 7.4) completed with protease inhibitors (Calbiochem) for 30 minutes at 4°C. After 10 minutes of 10000 g centrifugation at 4°C, Laemmli Buffer was added to the supernatant and samples were boiled for 10 minutes at 95°C.

Brain hemispheres from WT or R274W mice were processed in the same way after being lysed in Lysis or RIPA buffer using a 7 ml glass dounce tissue grinder (Wheaton). Samples were then loaded onto 10% or 15% handcast polyacrylamide gels for protein identification by Western blotting.

Proteins were transferred onto nitrocellulose membrane (Sigma-Aldrich) at 25V for 10 minutes using Trans-Blot Turbo Transfer (BioRad). After 1 hour saturation in blocking buffer (5% non-fat dry milk in 20 mM Tris, 150 mM NaCl, 0.1% Tween20, pH 7.4) primary antibodies were left overnight in blocking buffer at 4°C. Three washes of 10 minutes in TBS-Tween 0.1% were performed before 1 hour incubation with HRP-conjugated secondary antibodies in blocking buffer. The list of antibodies employed is presented in Supplementary Table S3.

ECL prime or select detection systems (Cynagen) were used to detect proteins and images were acquired with ChemiDoc Touch imaging system (BioRad).

To obtain protein quantification, FIJI software was used to measure the optical density of the bands.

For total protein analysis, β-actin was used as a housekeeping to normalize protein content. For soluble-insoluble assay, protein levels in the soluble fraction were normalized on total protein level normalized on β-actin.

RNA extraction and quantitative real-time PCR (qRT-PCR)

Total RNA was isolated from cells and cortexes using Total RNA Purification Kit (Norgen) and Animal Tissue RNA Purification Kit (Norgen) respectively, according to manufacturer's protocol. After extraction, RNA concentration was quantified with NanoDrop 2000C spectrophotometer (Thermo Fisher Scientific). After DNAse treatment (Thermo Fisher Scientific, according to manufacturer's instructions),

complementary DNA (cDNA) was generated using qRT SuperMix (Bimake). The cDNAs were used for quantitative PCR (qPCR) exploiting iTaq Universal SYBR® Green Supermix and CFX96 RealTime System (BioRad) for 40 cycles. Primers utilized are shown in Supplementary Table S4.
All samples were triplicated, and transcripts levels normalized for housekeeping genes relative abundance (β-actin, RPL27, HPRT, rRNA18S). Data shown were produced using Bio-Rad CFX Manager software and analyzed according to ddCt algorithm.

Transmitted Electron Microscopy (in collaboration with Prof. Michael Hess)
Myoblasts were plated onto Thermanox plastic cell culture coverslips (Thermo Fisher Scientific) at 20000 cells/cm^2 and differentiated into myotubes as already described. Samples were fixed using glutaraldehyde solution (Sigma) in 0.1 M phosphate buffer for 12 hours. Specimens were analysed by Transmitted Electron Microscopy (TEM) in the laboratory of Prof. Michael Hess to look at mitochondria structure.

HPLC measure of Striatal Dopamine (in collaboration with Prof. Michele Morari)
Endogenous dopamine levels in striatal tissue were measured by HPLC, as described in Marti et al., 2003. After o-phthaldialdehyde/mercaptoethanol addition, tissue homogenate was loaded onto 5-C18 Chromosep columns. The column was perfused (0.48 mL/min) with a mobile phase composed of 10% methanol, 2.5% tetrahydrofuran (pH 6.5), and 0.1 M sodium acetate. A Beckam pump was used to obtain a two-step gradient of methanol in aqueous buffer. The levels of dopamine were normalized on the weight of starting tissue.

Analysis of Mitochondrial Activity (in collaboration with Dr. Irene Pichler)
High-resolution respirometer (Oxygraph-2k; Oroboros Instruments) was used to measure mitochondrial respiration in primary mouse fibroblasts.
First, cells were permeabilized with digitonin (8 µg/mL) in MiRo5 medium (10 mM KH2PO4, 60 mM lactobionic acid, 20 mM HEPES, 3 mM MgCl2, 0.5 mM EGTA, 20 mM taurine, 110 mM D-Sucrose and 1 mg/ml BSA fatty acid free). To characterize mitochondrial respiration the following aspects were assessed: physiological respiration with endogenous substrates (routine respiration), complex I- and complex II-dependent respiration, maximal capacity of the electron transfer system after uncoupler addition, respiration after complex I inhibition with Rotenone (Rot). Residual oxygen consumption (ROX) was measured after addition of antimycin A (2.5 µM). Spare capacity was determined as the difference between maximal respiration and routine respiration. Absolute respiration values were normalized for the total number of cells

($1x10^6$) and total activity of citrate synthase (nmol ml^{-1} min^{-1}). All reagents were purchased from Sigma Aldrich.

Statistical analysis

For quantification analysis of brain slices, three fields for each brain region were acquired. The mean of the three fields was considered as one value for each animal. For myoblasts and myotubes experiments, three replicates have been performed for three different cell lines obtained from distinct mice. Each point in the graph is the mean of the three technical replicates.

For experiments including live animals, sample sizes were determined with the software G*power (3.1 version).

All data are expressed as the mean ± standard error of the mean (SEM). GraphPad PRISM was used to perform data analysis through unpaired Student's T-test (two classes), or ANOVA *post hoc* test (Bonferroni correction) (more than two classes with one degree of freedom). For the analysis of more than two classes with 2 or more degrees of freedom, two-sided ANOVA was used. Normality distribution was always tested prior to apply a parametric or non-parametric test. The level of significance (P, F) is indicated throughout the text.

SUPPLEMENTARY

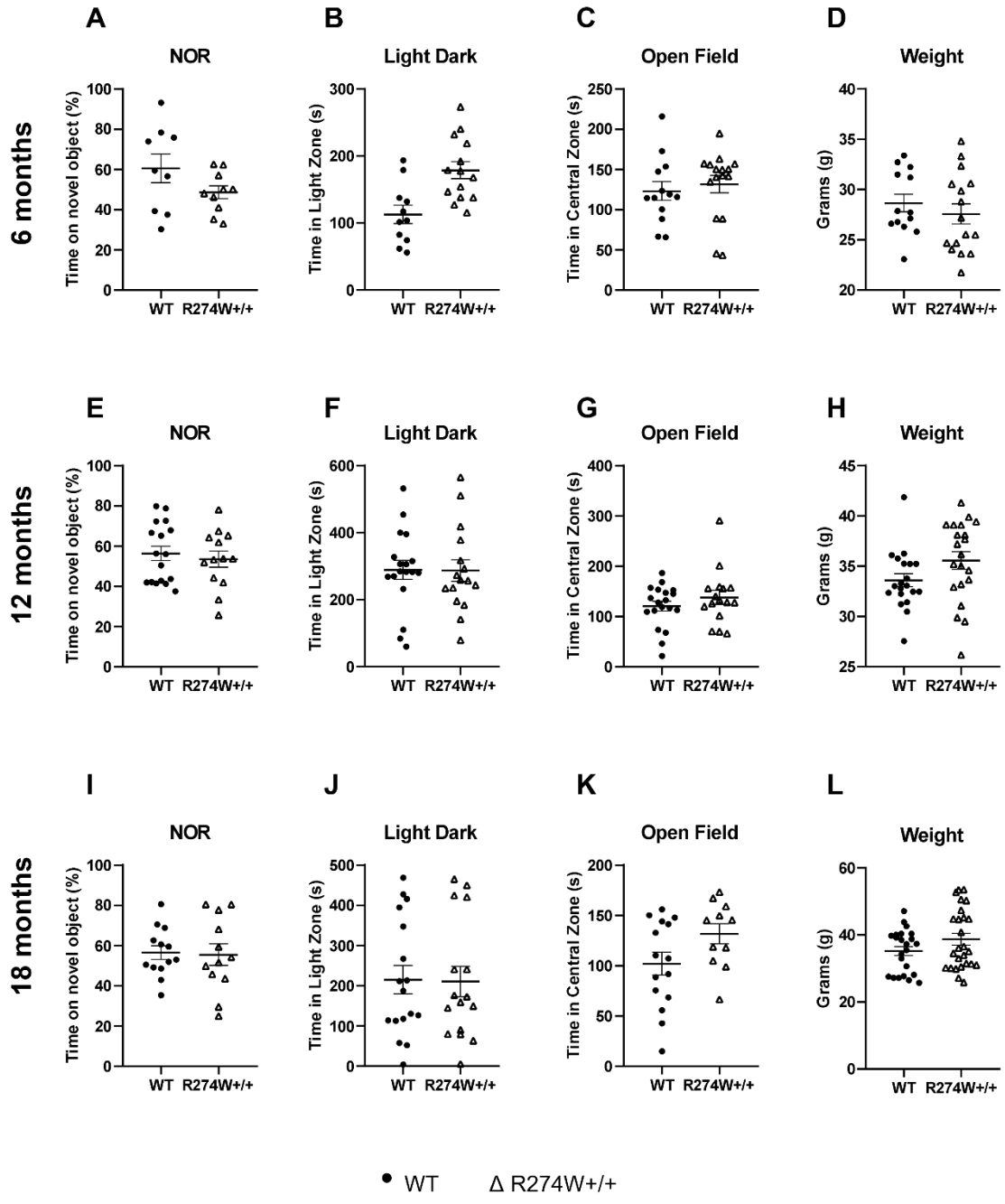

Supplementary Figure S1: R274W+/+ mice do not show non-motor differences compared to wild type. We tested male and female mice at the indicated ages. We did not observe differences in the cognitive performance (A, E, I), nor in the anxiety (B, C, F, G, J, K) compared to age-matched wild type. Differences in weight (D, H, L) were not significant between genotypes. Data are the means ± SEM; n WT = 10-16; n R274W+/+ = 11-20.

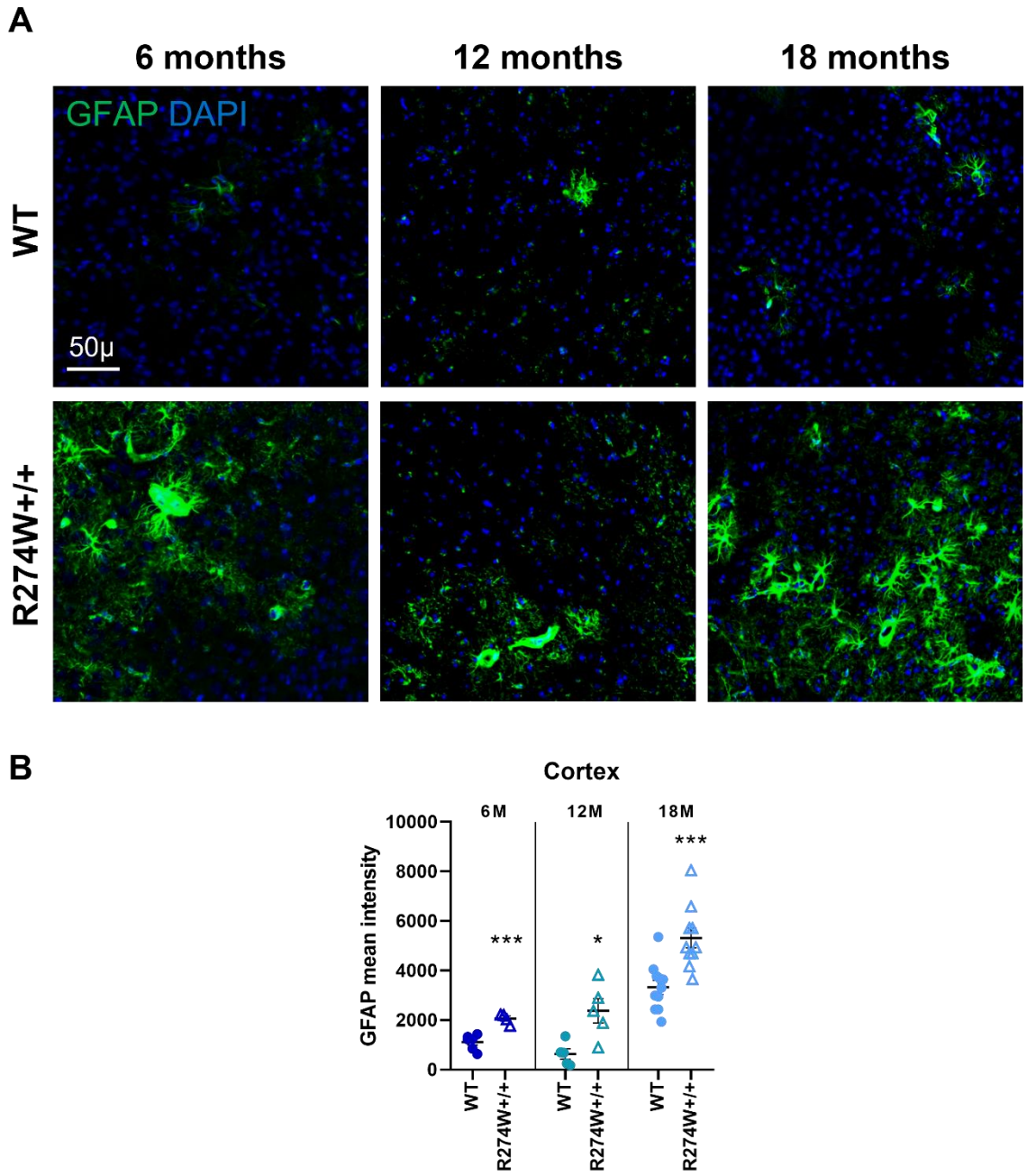

Supplementary Figure S2: R274W+/+ mice cortex displays age-dependent astrogliosis. (A) Representative images of cortex sections from 6-, 12-, and 18-month-old wild type and Parkin R274W+/+ mice stained with anti-GFAP antibody (green) and DAPI to visualize nuclei (blue). Scale bar = 50 µm. (B) The graph reports the GFAP mean intensity for each time-point folded on wild type mean. Data are shown as the means ±SEM; n 6M = 4; n 12M = 5; n 18M = 10; two-sided t-test was performed comparing intra-age data vs. wild type; *, **, ***, p<0.05, 0.01, 0.001. One-way ANOVA (Bonferroni *post hoc*) showed that GFAP signal is increased in WT at 18 months compared to 12 months (p<0.0001, ****) and 6 months (p<0.0001, ****).

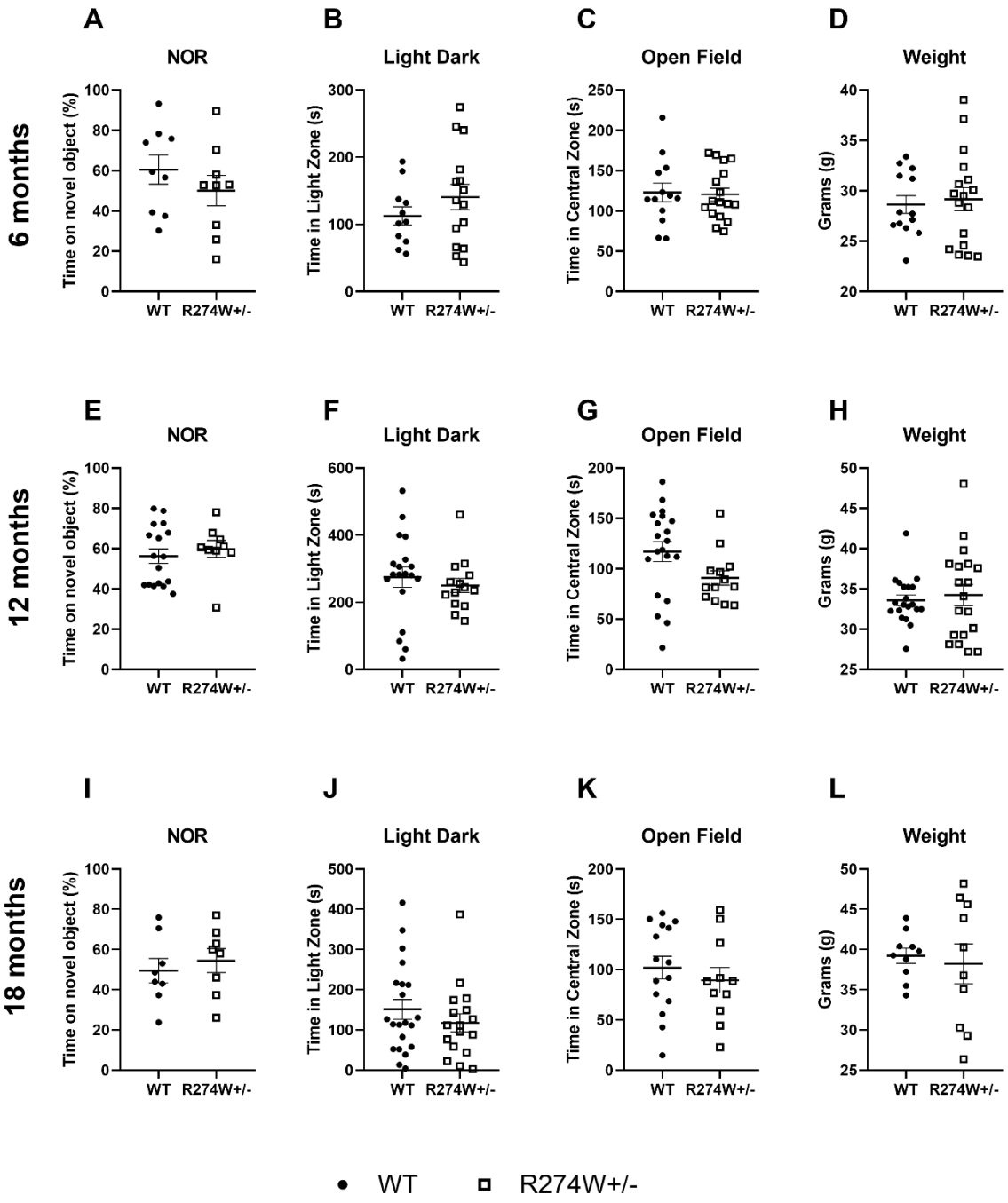

Supplementary Figure S3: R274W+/- mice do not show non-motor differences compared to wild type. We tested male and female mice at the indicated ages. We did not observe differences in the cognitive performance (A, E, I), nor in the anxiety (B, C, F, G, J, K) compared to age-matched wild type. Differences in weight (D, H, L) were not significant between genotypes. Data are the means ± SEM; n WT = 9-21; n R274W+/- = 9-19.

.

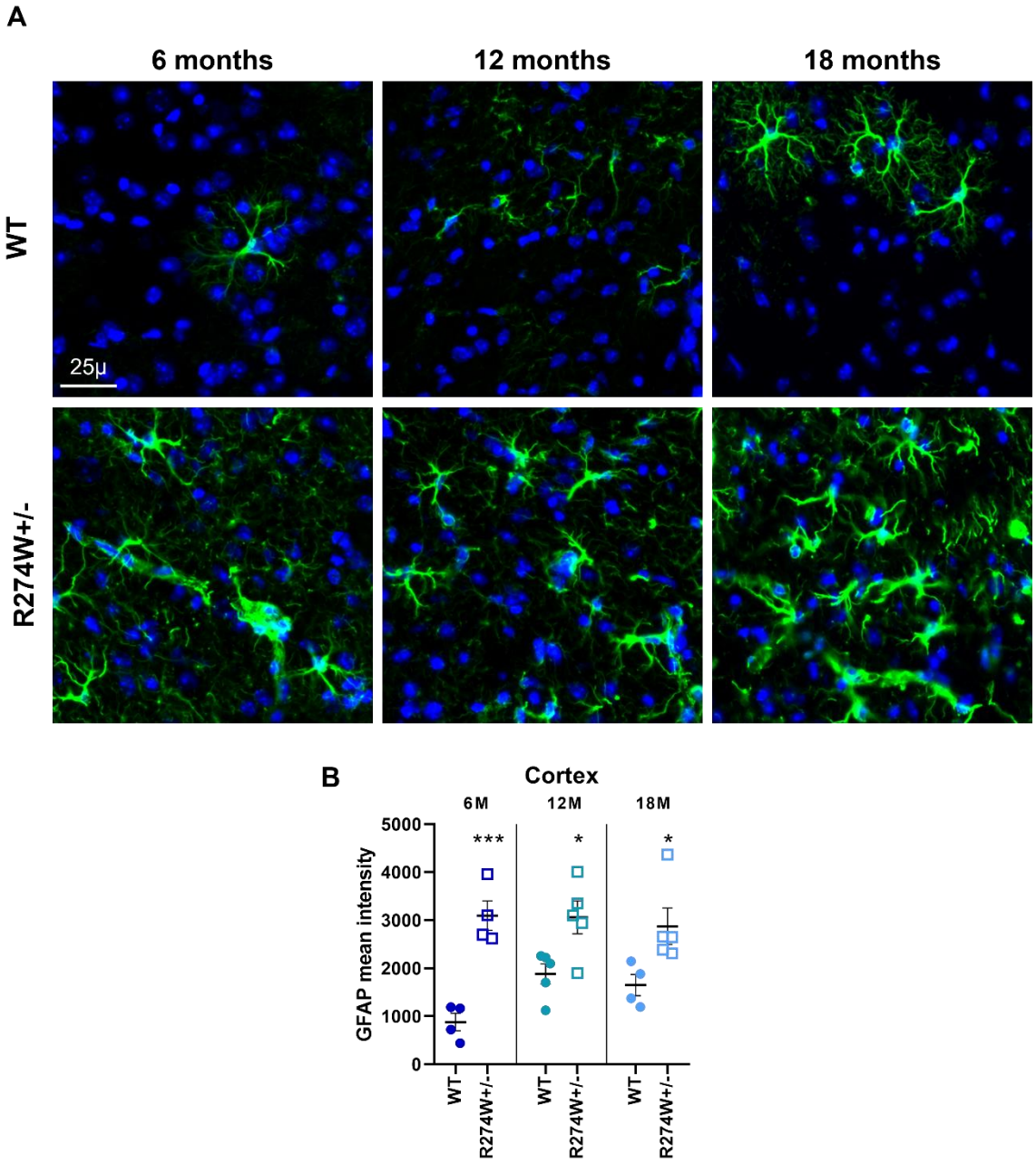

Supplementary Figure S4: R274W+/- mice cortex displays age-dependent astrogliosis. (A) Representative images of cortex sections from 6-, 12-, and 18-month-old wild type and Parkin R274W+/- mice stained with anti-GFAP antibody (green) and DAPI to visualize nuclei (blue). Scale bar = 50 µm. (B) The graph reports the GFAP mean intensity for each time-point folded on wild type mean. Data are shown as means ±SEM; n 6M = 4; n 12M = 5; n 18M = 4-5; two-sided t-test was performed comparing intra-age data vs. wild type; *, **, ***, p<0.05, 0.01, 0.001. One-way ANOVA (Bonferroni *post hoc*) showed that GFAP signal is increased in WT at 12 months compared to 6 months (p = 0.0191, *).

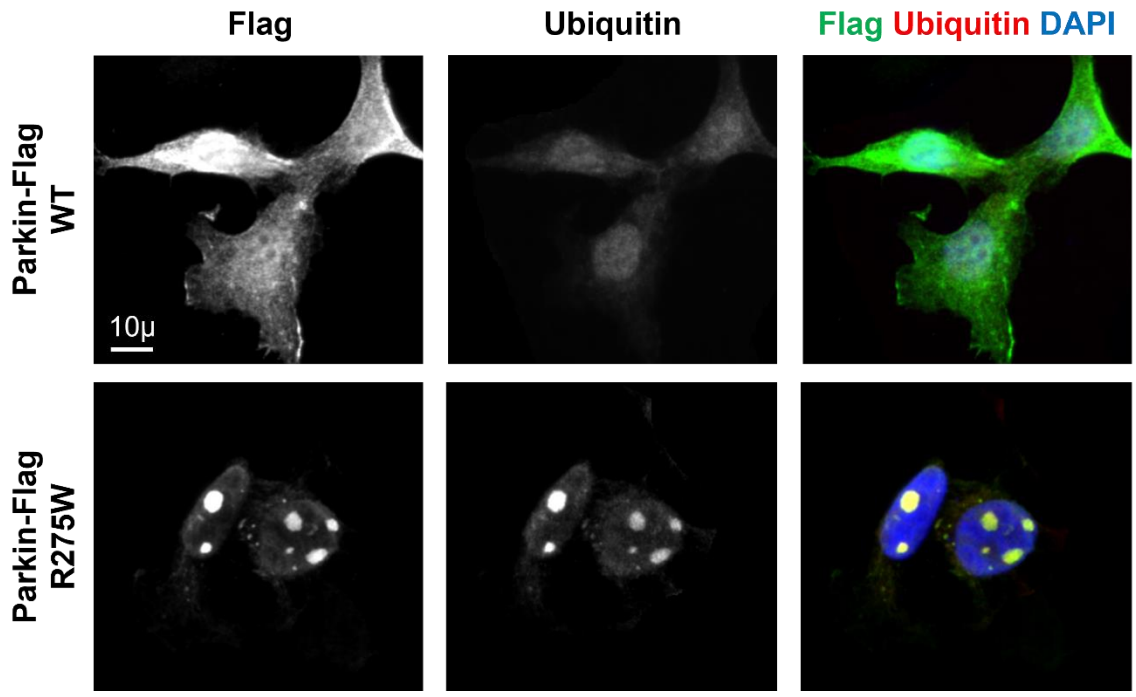

Supplementary Figure S5: R275W Parkin forms ubiquitin-positive aggregates in HEK293 cells. Parkin R275W forms aggregates that colocalize with ubiquitin. We processed HEK293 cells transfected with Parkin-Flag WT or R275W for imaging purpose. Cells were stained with anti-Flag (green) and anti-Ubiquitin (red) antibodies and DAPI to visualize the nuclei. Parkin-ubiquitin colocalization is detected in yellow. Scale bar = 10 µm.

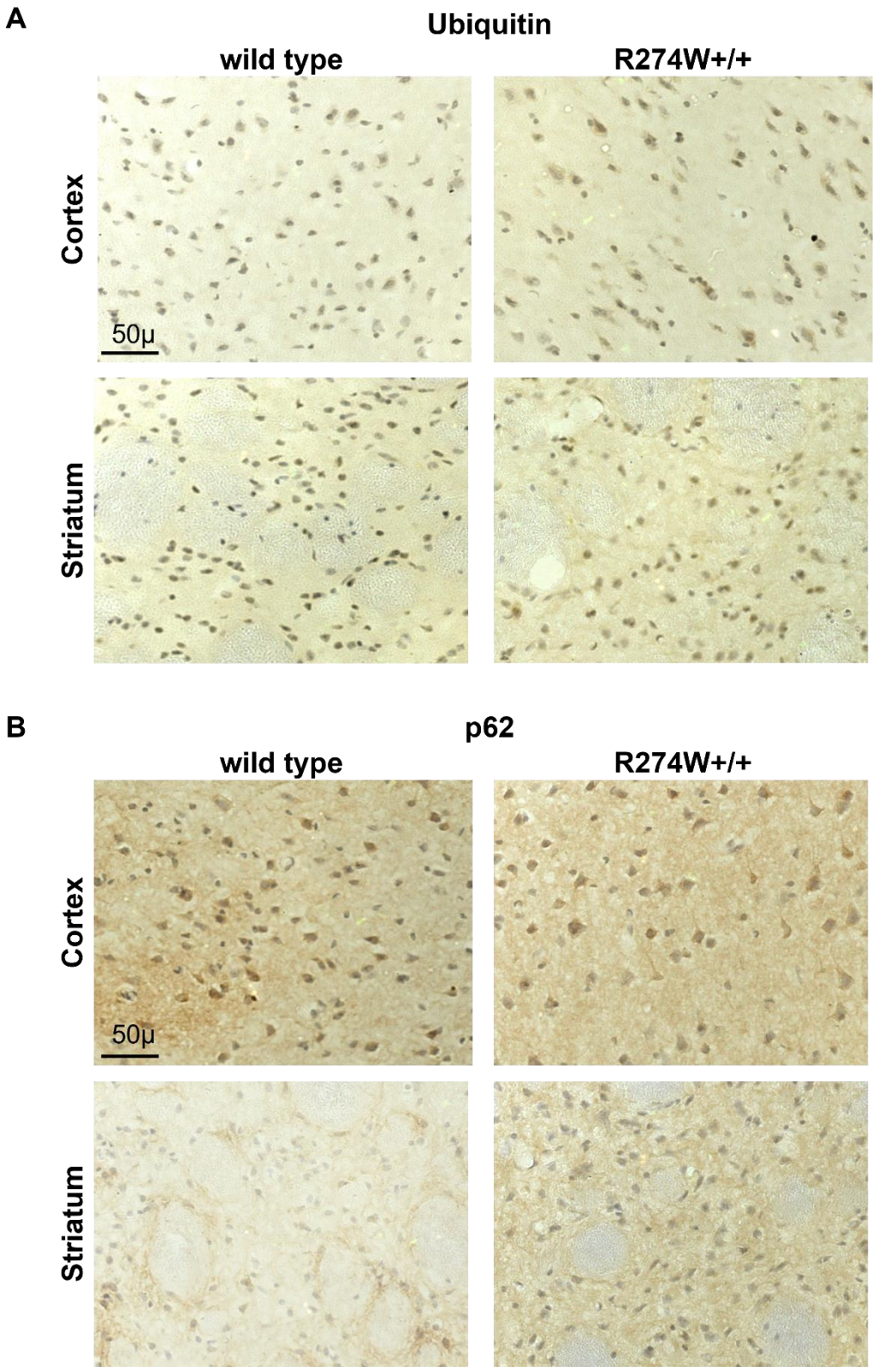

Supplementary Figure S6: Ubiquitin and p62 do not change in the cortex and striatum of homozygous mice at 18 months. (A) Immunoperoxidase labelling for ubiquitin (A) or p62 (B) (brown) in the cortex and striatum of 18-month-old wild type or R274W+/+ mice. Nuclei are seen in blue. No differences were observed between genotypes. N = 4-3.

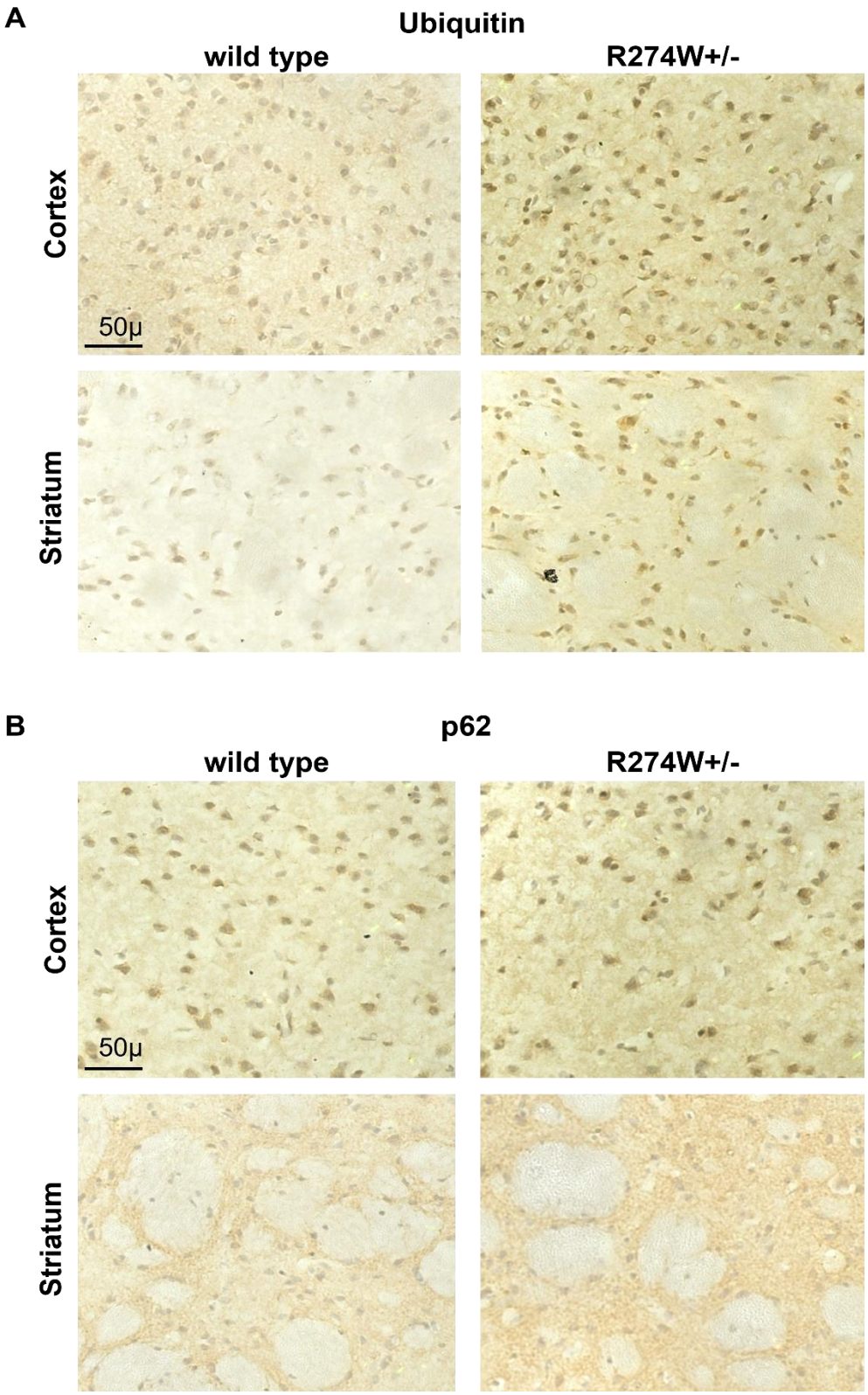

Supplementary Figure S7: Ubiquitin and p62 do not change in the cortex and striatum of heterozygous mice at 18 months. (A) Immunoperoxidase labelling for ubiquitin (A) or p62 (B) (brown) in the cortex and striatum of 18-month-old wild type or R274W+/- mice. Nuclei are seen in blue. No differences were observed between genotypes. N = 4-3.

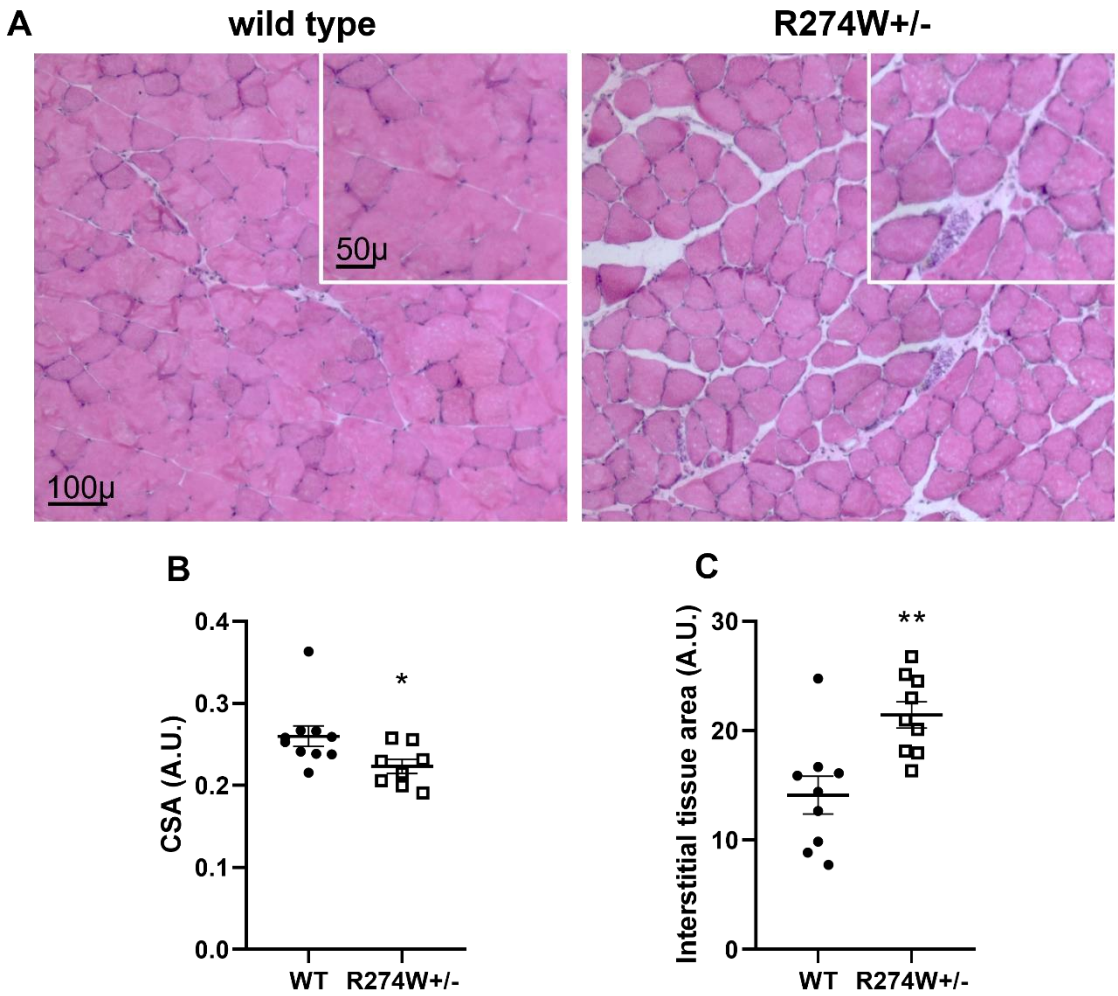

Supplementary Figure S8: R274W mutation alters muscle tissue structure and organization in heterozygous mice. (A) Representative images of haematoxylin and eosin staining on 14µ transversal sections of soleo muscle of 12-month-old wild type and heterozygous mice. Decrease in muscle fibres size quantified as cross-sectional area (CSA) and increase in interstitial tissue are observed in mutant tissue compared to wild type (B, C). Data are expressed as means ±SEM; n= 9; *, **, p<0.05, 0.01 versus wild type.

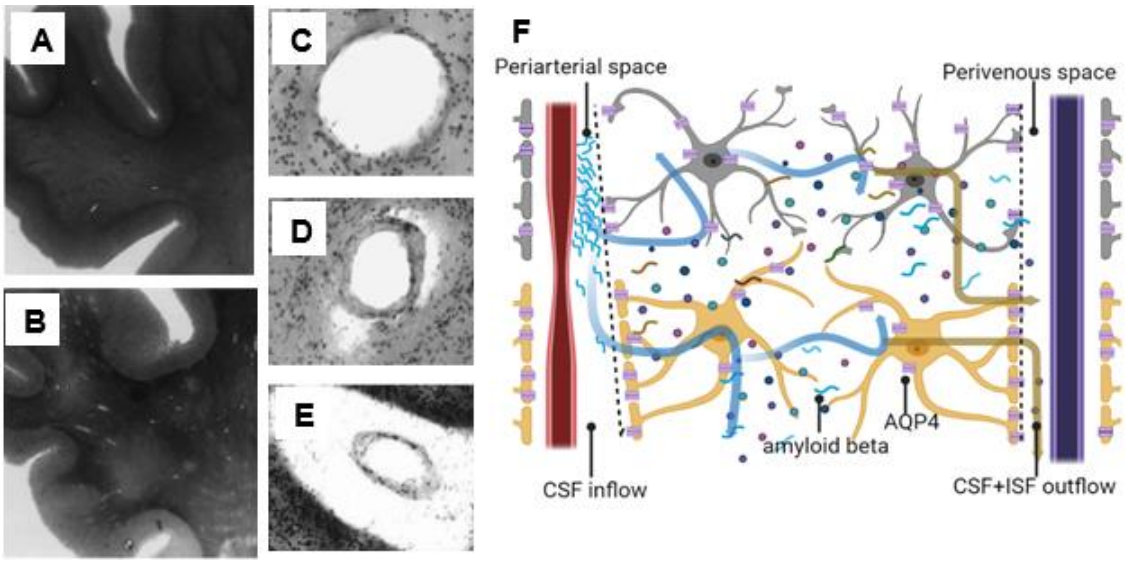

Supplementary Figure S9: **Alterations in AD brains suggest an impairment in the glymphatic system.** The white matter of an AD patient (B) stained with haematoxylin and eosin shows many enlarged perivascular spaces compared to a healthy age-matched control (A). (C) shows normal, (D) slightly enlarged, (E) severely dilated perivascular space. Adapted from Roher et al., 2003. (F) In addition to decrease in the glymphatic system activity that occurs with age (due to stiffening of arteries, astrogliosis, and AQP4 mislocalization), in Alzheimer's disease amyloid beta accumulate in the periarterial spaces, causing their enlargement and further impairment of glymphatic clearance. Created with BioRender.com.

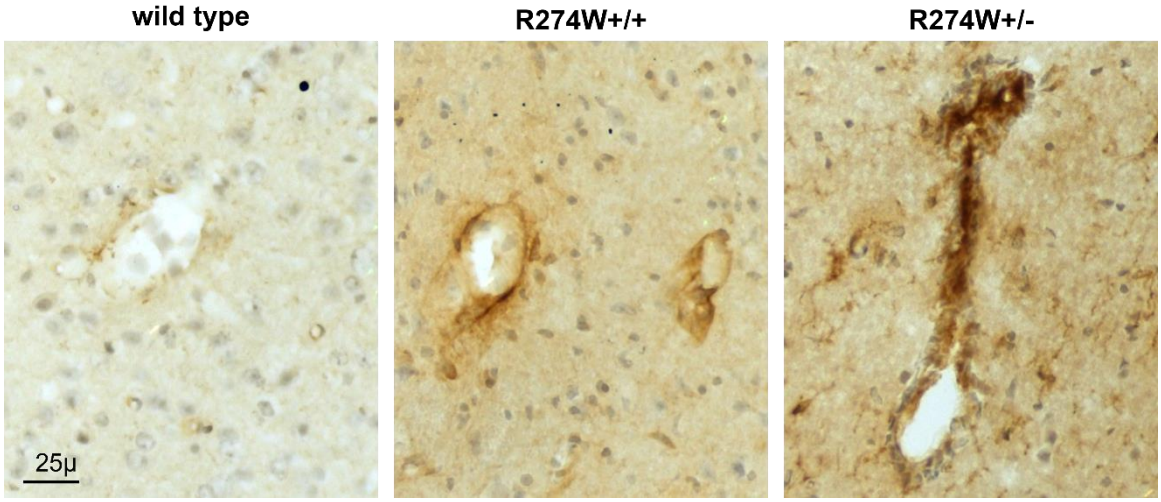

Supplementary Figure S10: α-synuclein pS129 colocalizes with putative glymphatic structures in mutant mice brain. (A) Representative images of immunoperoxidase labelling for S129 phosphorylated α-synuclein (pS129 α-Syn) (brown) in the midbrain of 18-month-old wild type, R274W+/- or R274W+/+ mice. Increased immunoreactivity around the structures of glymphatic system is observed in homozygous and especially heterozygous mice compared to wild type. N = 6. Scale bar = 25µm.

Type	Antigen	Host	Dilution	AR	Code
Primary	TH	Rabbit	1:1000	No	AB152 Sigma
Primary	TH	Chicken	1:400	Yes	AB76442 Abcam
Primary	GFAP	Rabbit	1:800/1:1000	No	#12389 Cell Signaling
Primary	GFAP	Mouse	1:500	Yes	60190 Proteintech
Primary	Tomm20	Rabbit	1:250	No	HPA011562 Sigma
Primary	FLAG	Rabbit	1:500	No	F7425 Sigma
Primary	FLAG	Mouse	1:500	No	SC-166355 Santa Cruz
Primary	p62	Rabbit	1:800	No	AB109012 Abcam
Primary	Ubiquitin	Rabbit	1:100/1:250	Yes	ABB7780 Abcam
Primary	pS129 α-synuclein	Mouse	1:500	No	AB184674 Abcam
Primary	CD31	Rabbit	1:400	Yes	AB9498 Abcam
Primary	AQP4	Mouse	1:500	Yes	SC-32739 Santa Cruz
Primary	V5	Mouse	1:500	No	#13202 Cell signaling
Primary	Rab10	Rabbit	1:500	No	AB237703 Abcam
Primary	Pan-MyHC	Mouse	1:33	No	MF 20 DSHB
Secondary	Anti-Rabbit 488	Goat	1:500	-	111-545-144 Jackson Laboratory
Secondary	Anti-Mouse 488	Goat	1:500	-	115-545-144 Jackson Laboratory
Secondary	Anti-Chicken 488	Goat	1:300	-	AB150169 Abcam
Secondary	Anti-Rabbit 568	Goat	1:500	-	A11011 Invitrogen
Secondary	Anti-Mouse 568	Goat	1:500	-	A11004 Invitrogen
Secondary	Biotinylated anti-Mouse HRP	Horse	1:500	-	BA-2000 Vector
Secondary	Biotinylated anti-Rabbit HRP	Goat	1:500	-	BA-1000 Vector

Supplementary Table S1: Antibodies used for immunostaining. For each antibody the type (primary/secondary), the antigen, the host, the dilution, the necessity of antigen retrieval (AR), and the code are reported.

R275W cloning	FW	TGTGTGACAAGACTCAATGAT**T**GGCAGTTTGTTCACGACCCTC
R275W cloning	Rev	GAGGGTCGTGAACAAACTGCCAATCATTGAGTCTTGTCACACA
Parkin sequencing	FW	GAAACATCAGTAGCTTTGCAC

Supplementary Table S2: Primers used for R275W Parkin mutagenesis and sequencing. C>T substitution introduced at position 823 is in bold. Primers are reported with 5'-3' orientation. FW: forward, Rev: reverse.

Type	Antigen	Host	Dilution	MW (kDa)	Code
Primary	Tomm20	Rabbit	1:500	16	HPA011562 Sigma
Primary	PARIS	Rabbit	1:500	100/70	AB130867 Abcam
Primary	Parkin	Mouse	1:500	55	P6248 Sigma
Primary	β-actin	Mouse	1:1000	42	SC-811178 Santa Cruz
Primary	FLAG	Mouse	1:1000	-	SC-166355 Santa Cruz
Primary	MYC	Mouse	1:800	-	SC-40 Santa Cruz
Primary	α-synuclein	Mouse	1:500	15	610787 BD biosciences
Primary	BiP/GRP78	Rabbit	1:500	78	SPA-826 Stressgen
Primary	AQP4	Mouse	1:200	35	SC-32739 Santa Cruz
Primary	V5	Mouse	1:1000	-	#13202 Cell signaling
Secondary	Anti-Rabbit	Goat	1:5000	-	#7074 Cell signaling
Secondary	Anti-Mouse	Donkey	1:5000	-	715-039-191 ThermoFisher

Supplementary Table S3: Antibodies used for western blotting. For each antibody the type (primary/secondary), the antigen, the host, the dilution, the predicted molecular weight (MW), and the code are reported.

	Forward	Reverse
PGC-1α	AGCCGTGACCACTGACAACGAG	GCTGCATGGTTCTGAGTGCTAAG
BiP	TGTCTTCTCAGCATCAAG CAAGG	CCAACACTTCCTGGACAGGCT
BiP	CTGTCCAGGCTGGTGTGCTCT	CTTGGTAGGCACCACTGTGTTC
COX2	ACGAAATCAACAACCCCGTA	GCAGAACGACTCGGTTATC
TFAM	CCAAAAAGACCTCGTTCAGC	CTGCTTTTCCTCAGGAGACA
β-actin	CAACGGCTCCGGCATGTG	CTCTTGCTCTGGGCCTCG
RPL27	AAGCCGTCATCGTGAAGAACA	CTTGATCTTGGATCGCTTGGC
HPRT	CATTATGCTGAGGATTTGGAAAGG	CTTGAGCACACAGAGGGCTACA
rRNA18S	GCAGAATCCACGCCAGTACAAG	GCTTGTTGTCCAGACCATTGGC

Supplementary Table S4: Primers used for qRT-PCR. Primers designed on human sequences are indicated in bold. Primers are reported with 5'-3' orientation.

REFERENCES

A. Siddiqui, D. Bhaumik, S.J. Chinta, A. Rane, S. Rajagopalan, C.A. Lieu, G.J. Lithgow, J.K. Andersen. itochondrial quality control via the PGC1alpha-TFEB signaling pathway is compromised by PARKIN Q311X mutation but independently restored by rapamycin. J. Neurosci., 35 (2015), pp. 12833-12844

Abou-Sleiman PM, Muqit MM, McDonald NQ, Yang YX, Gandhi S, Healy DG, Harvey K, Harvey RJ, Deas E, Bhatia K, Quinn N, Lees A, Latchman DS, Wood NW. A heterozygous effect for PINK1 mutations in Parkinson's disease? Ann Neurol. 2006 Oct;60(4):414-9. doi: 10.1002/ana.20960. PMID: 16969854.

Absinta M, Ha SK, Nair G, Sati P, Luciano NJ, Palisoc M, Louveau A, Zaghloul KA, Pittaluga S, Kipnis J, Reich DS. Human and nonhuman primate meninges harbor lymphatic vessels that can be visualized noninvasively by MRI. Elife. 2017 Oct 3;6:e29738. doi: 10.7554/eLife.29738. PMID: 28971799; PMCID: PMC5626482.

Adams ME, Mueller HA, Froehner SC. In vivo requirement of the alpha-syntrophin PDZ domain for the sarcolemmal localization of nNOS and aquaporin-4. J Cell Biol. 2001 Oct 1;155(1):113-22. doi: 10.1083/jcb.200106158. Epub 2001 Sep 24. PMID: 11571312; PMCID: PMC2150783.

Alexander J Whitworth, Leo J Pallanck. PINK1/Parkin mitophagy and neurodegeneration—what do we really know in vivo?,Current Opinion in Genetics & Development, Volume 44, 2017, Pages 47-53, ISSN 0959-437X, https://doi.org/10.1016/j.gde.2017.01.016.

Ana L. Albarracín, Fernando D. Farfán, Muscle function alterations in a Parkinson's disease animal model: Electromyographic recordings dataset, Data in Brief, Volume 40, 2022, 107712, ISSN 2352-3409, https://doi.org/10.1016/j.dib.2021.107712.

Andersen PH, Gingrich JA, Bates MD, Dearry A, Falardeau P, Senogles SE, Caron MG. Dopamine receptor subtypes: beyond the D1/D2 classification. Trends Pharmacol Sci. 1990 Jun;11(6):231-6. doi: 10.1016/0165-6147(90)90249-8. PMID: 2200181.

Anglade P, Vyas S, Javoy-Agid F, Herrero MT, Michel PP, Marquez J, Mouatt-Prigent A, Ruberg M, Hirsch EC, Agid Y. Apoptosis and autophagy in nigral neurons of patients with Parkinson's disease. Histol Histopathol. 1997 Jan;12(1):25-31. PMID: 9046040.

Antony PM, Diederich NJ, Krüger R, Balling R. The hallmarks of Parkinson's disease. FEBS J. 2013 Dec;280(23):5981-93. doi: 10.1111/febs.12335. Epub 2013 Jun 10. PMID: 23663200.

Antony PM, Diederich NJ, Krüger R, Balling R. The hallmarks of Parkinson's disease. FEBS J. 2013 Dec;280(23):5981-93. doi: 10.1111/febs.12335. Epub 2013 Jun 10. PMID: 23663200.

Appel-Cresswell S, Vilarino-Guell C, Encarnacion M, Sherman H, Yu I, Shah B, Weir D, Thompson C, Szu-Tu C, Trinh J, Aasly JO, Rajput A, Rajput AH, Jon Stoessl A, Farrer MJ. Alpha-synuclein p.H50Q, a novel pathogenic mutation for Parkinson's disease. Mov Disord. 2013 Jun;28(6):811-3. doi: 10.1002/mds.25421. Epub 2013 Mar 1. PMID: 23457019.

Aspelund A, Antila S, Proulx ST, Karlsen TV, Karaman S, Detmar M, Wiig H, Alitalo K. A dural lymphatic vascular system that drains brain interstitial fluid and macromolecules. J Exp Med. 2015 Jun 29;212(7):991-9. doi: 10.1084/jem.20142290. Epub 2015 Jun 15. PMID: 26077718; PMCID: PMC4493418.

Assoni, G.; Frapporti, G.; Colombo, E.; Gornati, D.; Perez-Carrion, M.D.; Polito, L.; Seneci, P.; Piccoli, G.; Arosio, D. Trehalosebased neuroprotective autophagy inducers. Bioorg. Med. Chem. Lett. 2021, 40, 127929.

Baba Y, Markopoulou K, Putzke JD, et al. Phenotypic Commonalities in Familial and Sporadic Parkinson Disease. Arch Neurol. 2006;63(4):579–583. doi:10.1001/archneur.63.4.579

Bae, JH., Jeong, HJ., Kim, H. et al. ZNF746/PARIS overexpression induces cellular senescence through FoxO1/p21 axis activation in myoblasts. Cell Death Dis 11, 359 (2020). https://doi.org/10.1038/s41419-020-2552-7

Barker RA, Björklund A. Animal Models of Parkinson's Disease: Are They Useful or Not? J Parkinsons Dis. 2020;10(4):1335-1342. doi: 10.3233/JPD-202200. PMID: 32716322.

Beach TG, Adler CH, Sue LI, Vedders L, Lue L, White Iii CL, Akiyama H, Caviness JN, Shill HA, Sabbagh MN, Walker DG; Arizona Parkinson's Disease Consortium. Multi-organ distribution of phosphorylated alpha-synuclein histopathology in subjects with Lewy body disorders. Acta Neuropathol. 2010 Jun;119(6):689-702. doi: 10.1007/s00401-010-0664-3. Epub 2010 Mar 21. PMID: 20306269; PMCID: PMC2866090.

Beasley SA, Hristova VA, Shaw GS. Structure of the Parkin in-between-ring domain provides insights for E3-ligase dysfunction in autosomal recessive Parkinson's disease. Proc Natl Acad Sci U S A. 2007 Feb 27;104(9):3095-100. doi: 10.1073/pnas.0610548104. PMID: 17360614; PMCID: PMC1805599.

Bedussi B, Naessens DMP, de Vos J, Olde Engberink R, Wilhelmus MMM, Richard E, Ten Hove M, vanBavel E, Bakker ENTP. Enhanced interstitial fluid drainage in the hippocampus of spontaneously hypertensive rats. Sci Rep. 2017 Apr 7;7(1):744. doi: 10.1038/s41598-017-00861-x. PMID: 28389645; PMCID: PMC5429689.

Bellucci A, Navarria L, Zaltieri M, Falarti E, Bodei S, Sigala S, Battistin L, Spillantini M, Missale C, Spano P. Induction of the unfolded protein response by α-synuclein in experimental models of Parkinson's disease. J Neurochem. 2011 Feb;116(4):588-605. doi: 10.1111/j.1471-4159.2010.07143.x. Epub 2011 Jan 19. PMID: 21166675.

Bender A, Krishnan KJ, Morris CM, Taylor GA, Reeve AK, Perry RH, Jaros E, Hersheson JS, Betts J, Klopstock T, Taylor RW, Turnbull DM. High levels of mitochondrial DNA deletions in substantia nigra neurons in aging and Parkinson disease. Nat Genet. 2006 May;38(5):515-7. doi: 10.1038/ng1769. Epub 2006 Apr 9. PMID: 16604074.

Berg D, Schweitzer KJ, Leitner P, Zimprich A, Lichtner P, Belcredi P, Brüssel T, Schulte C, Maass S, Nägele T, Wszolek ZK, Gasser T. Type and frequency of mutations in the LRRK2 gene in familial and sporadic Parkinson's disease*. Brain. 2005 Dec;128(Pt 12):3000-11. doi: 10.1093/brain/awh666. PMID: 16251215.

Bernardi G, Cecchetti L, Siclari F, Buchmann A, Yu X, Handjaras G, Bellesi M, Ricciardi E, Kecskemeti SR, Riedner BA, Alexander AL, Benca RM, Ghilardi MF, Pietrini P, Cirelli C, Tononi G. Sleep reverts changes in human gray and white matter caused by wake-dependent training. Neuroimage. 2016 Apr 1;129:367-377. doi: 10.1016/j.neuroimage.2016.01.020. Epub 2016 Jan 23. PMID: 26812659; PMCID: PMC4803519.

Berndsen CE, Wolberger C. New insights into ubiquitin E3 ligase mechanism. Nat Struct Mol Biol. 2014 Apr;21(4):301-7. doi: 10.1038/nsmb.2780. PMID: 24699078.

Blesa J, Trigo-Damas I, Quiroga-Varela A, Jackson-Lewis VR. Oxidative stress and Parkinson's disease. Front Neuroanat. 2015 Jul 8;9:91. doi: 10.3389/fnana.2015.00091. PMID: 26217195; PMCID: PMC4495335.

Bohnen NI, Hu MTM. Sleep Disturbance as Potential Risk and Progression Factor for Parkinson's Disease. J Parkinsons Dis. 2019;9(3):603-614. doi: 10.3233/JPD-191627. PMID: 31227656; PMCID: PMC6700634.

Braak, H., Rüb, U., Gai, W. P., and Del Tredici, K. (2003). Idiopathic Parkinson's disease: possible routes by which vulnerable neuronal types may be subject to neuroinvasion by an unknown pathogen. J. Neural Transm. (Vienna) 110, 517–536. doi: 10.1007/s00702-002-0808-2

Breen DP, Vuono R, Nawarathna U, Fisher K, Shneerson JM, Reddy AB, Barker RA. Sleep and circadian rhythm regulation in early Parkinson disease. JAMA Neurol. 2014 May;71(5):589-595. doi: 10.1001/jamaneurol.2014.65. PMID: 24687146; PMCID: PMC4119609.

Buerge C, Steiger G, Kneifel S, Wetzel S, Wollmer MA, Probst A, Baumann TP. Lobar Dementia due to Extreme Widening of Virchow-Robin Spaces in One Hemisphere. Case Rep Neurol. 2011 May;3(2):136-40. doi: 10.1159/000329267. Epub 2011 Jun 10. PMID: 21734888; PMCID: PMC3128129.

Cano-de-la-Cuerda R, Pérez-de-Heredia M, Miangolarra-Page JC, Muñoz-Hellín E, Fernández-de-Las-Peñas C. Is there muscular weakness in Parkinson's disease? Am J Phys Med Rehabil. 2010 Jan;89(1):70-6. doi: 10.1097/PHM.0b013e3181a9ed9b. PMID: 19487924.

Carnemolla A, Fossale E, Agostoni E, Michelazzi S, Calligaris R, De Maso L, Del Sal G, MacDonald ME, Persichetti F. Rrs1 is involved in endoplasmic reticulum stress response in Huntington disease. J Biol Chem. 2009 Jul 3;284(27):18167-73. doi: 10.1074/jbc.M109.018325. Epub 2009 May 11. PMID: 19433866; PMCID: PMC2709382.

Carroll AM, Palmer AA, Lionikas A. QTL Analysis of Type I and Type IIA Fibers in Soleus Muscle in a Cross between LG/J and SM/J Mouse Strains. Front Genet. 2012 Jan 6;2:99. doi: 10.3389/fgene.2011.00099. PMID: 22303393; PMCID: PMC3262224.

Carta AR, Frau L, Pisanu A, Wardas J, Spiga S, Carboni E. Rosiglitazone decreases peroxisome proliferator receptor-γ levels in microglia and inhibits TNF-α production: new evidences on neuroprotection in a progressive Parkinson's disease model. Neuroscience. 2011 Oct 27;194:250-61. doi: 10.1016/j.neuroscience.2011.07.046. Epub 2011 Jul 27. PMID: 21839812.

Castelo Rueda MP, Raftopoulou A, Gögele M, Borsche M, Emmert D, Fuchsberger C, Hantikainen EM, Vukovic V, Klein C, Pramstaller PP, Pichler I, Hicks AA. Frequency of Heterozygous Parkin (PRKN) Variants and Penetrance of Parkinson's Disease Risk Markers in the Population-Based CHRIS Cohort. Front Neurol. 2021 Aug 9;12:706145. doi: 10.3389/fneur.2021.706145. PMID: 34434164; PMCID: PMC8382284.

Chahine LM, Amara AW, Videnovic A. A systematic review of the literature on disorders of sleep and wakefulness in Parkinson's disease from 2005 to 2015. Sleep Med Rev. 2017 Oct;35:33-50. doi: 10.1016/j.smrv.2016.08.001. Epub 2016 Aug 31. PMID: 27863901; PMCID: PMC5332351.

Chaugule VK, Burchell L, Barber KR, Sidhu A, Leslie SJ, Shaw GS, Walden H. Autoregulation of Parkin activity through its ubiquitin-like domain. EMBO J. 2011 Jun

21;30(14):2853-67. doi: 10.1038/emboj.2011.204. PMID: 21694720; PMCID: PMC3160258.

Chesselet MF, Fleming S, Mortazavi F, Meurers B. Strengths and limitations of genetic mouse models of Parkinson's disease. Parkinsonism Relat Disord. 2008;14 Suppl 2(Suppl 2):S84-7. doi: 10.1016/j.parkreldis.2008.04.004. Epub 2008 Jun 27. PMID: 18585084; PMCID: PMC2577895.

Chesselet MF. In vivo alpha-synuclein overexpression in rodents: a useful model of Parkinson's disease? Exp Neurol. 2008 Jan;209(1):22-7. doi: 10.1016/j.expneurol.2007.08.006. Epub 2007 Aug 23. PMID: 17949715; PMCID: PMC2262051.

Chin LS, Olzmann JA, Li L. Parkin-mediated ubiquitin signalling in aggresome formation and autophagy. Biochem Soc Trans. 2010 Feb;38(Pt 1):144-9. doi: 10.1042/BST0380144. PMID: 20074049; PMCID: PMC2846638.

Cho, Y., Jang, YS., Jang, YM. et al. Induction of unfolded protein response during neuronal induction of rat bone marrow stromal cells and mouse embryonic stem cells. Exp Mol Med 41, 440–452 (2009). https://doi.org/10.3858/emm.2009.41.6.049

Christoph Köhler, Maja Dinekov, Jürgen Götz, Granulovacuolar degeneration and unfolded protein response in mouse models of tauopathy and Aβ amyloidosis, Neurobiology of Disease,Volume 71, 2014, Pages 169-179, ISSN 0969-9961, https://doi.org/10.1016/j.nbd.2014.07.006.

Chung KK, Thomas B, Li X, Pletnikova O, Troncoso JC, Marsh L, Dawson VL, Dawson TM. S-nitrosylation of parkin regulates ubiquitination and compromises parkin's protective function. Science. 2004 May 28;304(5675):1328-31. doi: 10.1126/science.1093891. Epub 2004 Apr 22. PMID: 15105460.

Clark J, Silvaggi JM, Kiselak T, Zheng K, Clore EL, Dai Y, Bass CE, Simon DK. Pgc-1α overexpression downregulates Pitx3 and increases susceptibility to MPTP toxicity associated with decreased Bdnf. PLoS One. 2012;7(11):e48925. doi: 10.1371/journal.pone.0048925. Epub 2012 Nov 7. PMID: 23145024; PMCID: PMC3492133.

Clark LN, Afridi S, Mejia-Santana H, Harris J, Louis ED, Cote LJ, Andrews H, Singleton A, Wavrant De-Vrieze F, Hardy J, Mayeux R, Fahn S, Waters C, Ford B, Frucht S, Ottman R, Marder K. Analysis of an early-onset Parkinson's disease cohort for DJ-1 mutations. Mov Disord. 2004 Jul;19(7):796-800. doi: 10.1002/mds.20131. PMID: 15254937.

Colla E, Jensen PH, Pletnikova O, Troncoso JC, Glabe C, Lee MK. Accumulation of toxic α-synuclein oligomer within endoplasmic reticulum occurs in α-synucleinopathy in vivo. J Neurosci. 2012 Mar 7;32(10):3301-5. doi: 10.1523/JNEUROSCI.5368-11.2012. PMID: 22399752; PMCID: PMC3548448.

Cookson MR, Lockhart PJ, McLendon C, O'Farrell C, Schlossmacher M, Farrer MJ. RING finger 1 mutations in Parkin produce altered localization of the protein. Hum Mol Genet. 2003 Nov 15;12(22):2957-65. doi: 10.1093/hmg/ddg328. Epub 2003 Sep 30. PMID: 14519684.

Cooper AA, Gitler AD, Cashikar A, Haynes CM, Hill KJ, Bhullar B, Liu K, Xu K, Strathearn KE, Liu F, Cao S, Caldwell KA, Caldwell GA, Marsischky G, Kolodner RD, Labaer J, Rochet JC, Bonini NM, Lindquist S. Alpha-synuclein blocks ER-Golgi traffic and Rab1

rescues neuron loss in Parkinson's models. Science. 2006 Jul 21;313(5785):324-8. doi: 10.1126/science.1129462. Epub 2006 Jun 22. PMID: 16794039; PMCID: PMC1983366.

Corti O, Lesage S, Brice A. What genetics tells us about the causes and mechanisms of Parkinson's disease. Physiol Rev. 2011 Oct;91(4):1161-218. doi: 10.1152/physrev.00022.2010. PMID: 22013209.

Crane JM, Van Hoek AN, Skach WR, Verkman AS. Aquaporin-4 dynamics in orthogonal arrays in live cells visualized by quantum dot single particle tracking. Mol Biol Cell. 2008 Aug;19(8):3369-78. doi: 10.1091/mbc.e08-03-0322. Epub 2008 May 21. PMID: 18495865; PMCID: PMC2488293.

Cui H, Wang W, Zheng X, Xia D, Liu H, Qin C, Tian H, Teng J. Decreased AQP4 Expression Aggravates α-Synuclein Pathology in Parkinson's Disease Mice, Possibly via Impaired Glymphatic Clearance. J Mol Neurosci. 2021 Dec;71(12):2500-2513. doi: 10.1007/s12031-021-01836-4. Epub 2021 Mar 26. PMID: 33772424.

D.M. Zeppenfeld, M. Simon, J.D. Haswell, D. D'abreo, C. Murchison, J.F. Quinn, et al. Association of perivascular localization of aquaporin-4 with cognition and Alzheimer disease in aging brains. JAMA Neurol., 74 (1) (2017), pp. 91-99

da Costa CA, Sunyach C, Giaime E, West A, Corti O, Brice A, Safe S, Abou-Sleiman PM, Wood NW, Takahashi H, Goldberg MS, Shen J, Checler F. Transcriptional repression of p53 by parkin and impairment by mutations associated with autosomal recessive juvenile Parkinson's disease. Nat Cell Biol. 2009 Nov;11(11):1370-5. doi: 10.1038/ncb1981. Epub 2009 Oct 4. PMID: 19801972; PMCID: PMC2952934.

Da Mesquita S, Louveau A, Vaccari A, Smirnov I, Cornelison RC, Kingsmore KM, Contarino C, Onengut-Gumuscu S, Farber E, Raper D, Viar KE, Powell RD, Baker W, Dabhi N, Bai R, Cao R, Hu S, Rich SS, Munson JM, Lopes MB, Overall CC, Acton ST, Kipnis J. Functional aspects of meningeal lymphatics in ageing and Alzheimer's disease. Nature. 2018 Aug;560(7717):185-191. doi: 10.1038/s41586-018-0368-8. Epub 2018 Jul 25. Erratum in: Nature. 2018 Nov 5;: PMID: 30046111; PMCID: PMC6085146.

Dawson TM, Ko HS, Dawson VL. Genetic animal models of Parkinson's disease. Neuron. 2010 Jun 10;66(5):646-61. doi: 10.1016/j.neuron.2010.04.034. PMID: 20547124; PMCID: PMC2917798.

Ding XB, Wang XX, Xia DH, Liu H, Tian HY, Fu Y, Chen YK, Qin C, Wang JQ, Xiang Z, Zhang ZX, Cao QC, Wang W, Li JY, Wu E, Tang BS, Ma MM, Teng JF, Wang XJ. Impaired meningeal lymphatic drainage in patients with idiopathic Parkinson's disease. Nat Med. 2021 Mar;27(3):411-418. doi: 10.1038/s41591-020-01198-1. Epub 2021 Jan 18. PMID: 33462448.

Dorsey ER, Constantinescu R, Thompson JP, Biglan KM, Holloway RG, Kieburtz K, Marshall FJ, Ravina BM, Schifitto G, Siderowf A, Tanner CM. Projected number of people with Parkinson disease in the most populous nations, 2005 through 2030. Neurology. 2007 Jan 30;68(5):384-6. doi: 10.1212/01.wnl.0000247740.47667.03. Epub 2006 Nov 2. PMID: 17082464.

Driver JA, Logroscino G, Gaziano JM, Kurth T. Incidence and remaining lifetime risk of Parkinson disease in advanced age. Neurology. 2009 Feb 3;72(5):432-8. doi: 10.1212/01.wnl.0000341769.50075.bb. PMID: 19188574; PMCID: PMC2676726.

Duennwald ML, Lindquist S. Impaired ERAD and ER stress are early and specific events in polyglutamine toxicity. Genes Dev. 2008 Dec 1;22(23):3308-19. doi: 10.1101/gad.1673408. Epub 2008 Nov 17. PMID: 19015277; PMCID: PMC2600758.

Eriksen JL, Przedborski S, Petrucelli L. Gene dosage and pathogenesis of Parkinson's disease. Trends Mol Med. 2005 Mar;11(3):91-6. doi: 10.1016/j.molmed.2005.01.001. PMID: 15760766.

Fantini ML, Gagnon JF, Petit D, Rompré S, Décary A, Carrier J, Montplaisir J. Slowing of electroencephalogram in rapid eye movement sleep behavior disorder. Ann Neurol. 2003 Jun;53(6):774-80. doi: 10.1002/ana.10547. PMID: 12783424.

Farrer M, Chan P, Chen R, Tan L, Lincoln S, Hernandez D, Forno L, Gwinn-Hardy K, Petrucelli L, Hussey J, Singleton A, Tanner C, Hardy J, Langston JW. Lewy bodies and parkinsonism in families with parkin mutations. Ann Neurol. 2001 Sep;50(3):293-300. doi: 10.1002/ana.1132. PMID: 11558785.

Fox SH, Brotchie JM. The MPTP-lesioned non-human primate models of Parkinson's disease. Past, present, and future. Prog Brain Res. 2010;184:133-57. doi: 10.1016/S0079-6123(10)84007-5. PMID: 20887873.

Frazzitta G, Ferrazzoli D, Maestri R, Rovescala R, Guaglio G, Bera R, Volpe D, Pezzoli G. Differences in muscle strength in parkinsonian patients affected on the right and left side. PLoS One. 2015 Mar 25;10(3):e0121251. doi: 10.1371/journal.pone.0121251. PMID: 25806509; PMCID: PMC4373899.

Frost B, Jacks RL, Diamond MI. Propagation of tau misfolding from the outside to the inside of a cell. J Biol Chem. 2009 May 8;284(19):12845-52. doi: 10.1074/jbc.M808759200. Epub 2009 Mar 11. PMID: 19282288; PMCID: PMC2676015.

Fuchs J, Tichopad A, Golub Y, Munz M, Schweitzer KJ, Wolf B, Berg D, Mueller JC, Gasser T. Genetic variability in the SNCA gene influences alpha-synuclein levels in the blood and brain. FASEB J. 2008 May;22(5):1327-34. doi: 10.1096/fj.07-9348com. Epub 2007 Dec 27. PMID: 18162487.

Gan-Or Z, Giladi N, Rozovski U, Shifrin C, Rosner S, Gurevich T, Bar-Shira A, Orr-Urtreger A. Genotype-phenotype correlations between GBA mutations and Parkinson disease risk and onset. Neurology. 2008 Jun 10;70(24):2277-83. doi: 10.1212/01.wnl.0000304039.11891.29. Epub 2008 Apr 23. PMID: 18434642.

Gao L, Tang H, Nie K, Wang L, Zhao J, Gan R, Huang J, Zhu R, Feng S, Duan Z, Zhang Y, Wang L. Cerebrospinal fluid alpha-synuclein as a biomarker for Parkinson's disease diagnosis: a systematic review and meta-analysis. Int J Neurosci. 2015;125(9):645-54. doi: 10.3109/00207454.2014.961454. Epub 2014 Oct 2. PMID: 25202803.

Garcia S, Nissanka N, Mareco EA, Rossi S, Peralta S, Diaz F, Rotundo RL, Carvalho RF, Moraes CT. Overexpression of PGC-1α in aging muscle enhances a subset of young-like molecular patterns. Aging Cell. 2018 Apr;17(2):e12707. doi: 10.1111/acel.12707. Epub 2018 Feb 10. PMID: 29427317; PMCID: PMC5847875.

Gardner BM, Pincus D, Gotthardt K, Gallagher CM, Walter P. Endoplasmic reticulum stress sensing in the unfolded protein response. Cold Spring Harb Perspect Biol. 2013 Mar 1;5(3):a013169. doi: 10.1101/cshperspect.a013169. PMID: 23388626; PMCID: PMC3578356.

George JM. The synucleins. Genome Biol. 2002;3(1):REVIEWS3002. doi: 10.1186/gb-2001-3-1-reviews3002. Epub 2001 Dec 20. PMID: 11806835; PMCID: PMC150459.

Giasson BI, Forman MS, Higuchi M, Golbe LI, Graves CL, Kotzbauer PT, Trojanowski JQ, Lee VM. Initiation and synergistic fibrillization of tau and alpha-synuclein. Science. 2003 Apr 25;300(5619):636-40. doi: 10.1126/science.1082324. PMID: 12714745.

Gjerstad MD, Boeve B, Wentzel-Larsen T, Aarsland D, Larsen JP. Occurrence and clinical correlates of REM sleep behaviour disorder in patients with Parkinson's disease over time. J Neurol Neurosurg Psychiatry. 2008 Apr;79(4):387-91. doi: 10.1136/jnnp.2007.116830. Epub 2007 Jun 8. PMID: 17557796.

Glass CK, Saijo K, Winner B, Marchetto MC, Gage FH. Mechanisms underlying inflammation in neurodegeneration. Cell. 2010 Mar 19;140(6):918-34. doi: 10.1016/j.cell.2010.02.016. PMID: 20303880; PMCID: PMC2873093.

Goetz CG, Ouyang B, Negron A, Stebbins GT. Hallucinations and sleep disorders in PD: ten-year prospective longitudinal study. Neurology. 2010 Nov 16;75(20):1773-9. doi: 10.1212/WNL.0b013e3181fd6158. Epub 2010 Oct 20. PMID: 20962287; PMCID: PMC2995381.

Goetz CG. The history of Parkinson's disease: early clinical descriptions and neurological therapies. Cold Spring Harb Perspect Med. 2011 Sep;1(1):a008862. doi: 10.1101/cshperspect.a008862. PMID: 22229124; PMCID: PMC3234454.

Goldberg MS, Fleming SM, Palacino JJ, Cepeda C, Lam HA, Bhatnagar A, Meloni EG, Wu N, Ackerson LC, Klapstein GJ, Gajendiran M, Roth BL, Chesselet MF, Maidment NT, Levine MS, Shen J. Parkin-deficient mice exhibit nigrostriatal deficits but not loss of dopaminergic neurons. J Biol Chem. 2003 Oct 31;278(44):43628-35. doi: 10.1074/jbc.M308947200. Epub 2003 Aug 20. PMID: 12930822.

Grad LI, Yerbury JJ, Turner BJ, Guest WC, Pokrishevsky E, O'Neill MA, Yanai A, Silverman JM, Zeineddine R, Corcoran L, Kumita JR, Luheshi LM, Yousefi M, Coleman BM, Hill AF, Plotkin SS, Mackenzie IR, Cashman NR. Intercellular propagated misfolding of wild-type Cu/Zn superoxide dismutase occurs via exosome-dependent and -independent mechanisms. Proc Natl Acad Sci U S A. 2014 Mar 4;111(9):3620-5. doi: 10.1073/pnas.1312245111. Epub 2014 Feb 18. PMID: 24550511; PMCID: PMC3948312.

Greene JC, Whitworth AJ, Kuo I, Andrews LA, Feany MB, Pallanck LJ. Mitochondrial pathology and apoptotic muscle degeneration in Drosophila parkin mutants. Proc Natl Acad Sci U S A. 2003 Apr 1;100(7):4078-83. doi: 10.1073/pnas.0737556100. Epub 2003 Mar 17. PMID: 12642658; PMCID: PMC153051.

Grenier K, McLelland GL, Fon EA. Parkin- and PINK1-Dependent Mitophagy in Neurons: Will the Real Pathway Please Stand Up? Front Neurol. 2013 Jul 19;4:100. doi: 10.3389/fneur.2013.00100. PMID: 23882257; PMCID: PMC3715719.

Groeschel, S., Chong, W.K., Surtees, R. et al. Virchow-Robin spaces on magnetic resonance images: normative data, their dilatation, and a review of the literature. Neuroradiology 48, 745–754 (2006). https://doi.org/10.1007/s00234-006-0112-1

Grünewald A, Kasten M, Ziegler A, Klein C. Next-generation phenotyping using the parkin example: time to catch up with genetics. JAMA Neurol. 2013 Sep 1;70(9):1186-91. doi: 10.1001/jamaneurol.2013.488. PMID: 23835509.

Guo X, Badu-Mensah A, Thomas MC, McAleer CW, Hickman JJ. Characterization of Functional Human Skeletal Myotubes and Neuromuscular Junction Derived-From the Same Induced Pluripotent Stem Cell Source. Bioengineering (Basel). 2020 Oct 22;7(4):133. doi: 10.3390/bioengineering7040133. PMID: 33105732; PMCID: PMC7712960.

Gupta RK, Kanungo M. Glial molecular alterations with mouse brain development and aging: up-regulation of the Kir4.1 and aquaporin-4. Age (Dordr). 2013 Feb;35(1):59-67. doi: 10.1007/s11357-011-9330-5. Epub 2011 Nov 6. PMID: 22057895; PMCID: PMC3543735.

Hablitz LM, Vinitsky HS, Sun Q, Stæger FF, Sigurdsson B, Mortensen KN, Lilius TO, Nedergaard M. Increased glymphatic influx is correlated with high EEG delta power and low heart rate in mice under anesthesia. Sci Adv. 2019 Feb 27;5(2):eaav5447. doi: 10.1126/sciadv.aav5447. PMID: 30820460; PMCID: PMC6392807.

Hachinski V; World Stroke Organization. Stroke and Potentially Preventable Dementias Proclamation: Updated World Stroke Day Proclamation. Stroke. 2015 Nov;46(11):3039-40. doi: 10.1161/STROKEAHA.115.011237. Erratum in: Stroke. 2016 Jan;47(1):e18. Erratum in: Stroke. 2016 Feb;47(2):e37. PMID: 26504189.

Halsey AM, Conner AC, Bill RM, Logan A, Ahmed Z. Aquaporins and Their Regulation after Spinal Cord Injury. Cells. 2018 Oct 18;7(10):174. doi: 10.3390/cells7100174. PMID: 30340399; PMCID: PMC6210264.

Hampe C, Ardila-Osorio H, Fournier M, Brice A, Corti O. Biochemical analysis of Parkinson's disease-causing variants of Parkin, an E3 ubiquitin-protein ligase with monoubiquitylation capacity. Hum Mol Genet. 2006 Jul 1;15(13):2059-75. doi: 10.1093/hmg/ddl131. Epub 2006 May 19. PMID: 16714300.

Hanson JE, Orr AL, Madison DV. Altered hippocampal synaptic physiology in aged parkin-deficient mice. Neuromolecular Med. 2010 Sep;12(3):270-6. doi: 10.1007/s12017-010-8113-y. Epub 2010 Mar 16. PMID: 20232175; PMCID: PMC4326226.

Hara T, Nakamura K, Matsui M, Yamamoto A, Nakahara Y, Suzuki-Migishima R, Yokoyama M, Mishima K, Saito I, Okano H, Mizushima N. Suppression of basal autophagy in neural cells causes neurodegenerative disease in mice. Nature. 2006 Jun 15;441(7095):885-9. doi: 10.1038/nature04724. Epub 2006 Apr 19. PMID: 16625204.

Harper JW, Ordureau A, Heo JM. Building and decoding ubiquitin chains for mitophagy. Nat Rev Mol Cell Biol. 2018 Jan 23;19(2):93-108. doi: 10.1038/nrm.2017.129. PMID: 29358684.

Harvey BK, Wang Y, Hoffer BJ. Transgenic rodent models of Parkinson's disease. Acta Neurochir Suppl. 2008;101:89-92. doi: 10.1007/978-3-211-78205-7_15. PMID: 18642640; PMCID: PMC2613245.

Hawkes CH, Del Tredici K, Braak H. A timeline for Parkinson's disease. Parkinsonism Relat Disord. 2010 Feb;16(2):79-84. doi: 10.1016/j.parkreldis.2009.08.007. Epub 2009 Oct 28. PMID: 19846332.

He J, Xia M, Yeung PKK, Li J, Li Z, Chung KK, Chung SK, Xia J. PICK1 inhibits the E3 ubiquitin ligase activity of Parkin and reduces its neuronal protective effect. Proc Natl Acad Sci U S A. 2018 Jul 24;115(30):E7193-E7201. doi: 10.1073/pnas.1716506115. Epub 2018 Jul 9. PMID: 29987020; PMCID: PMC6064985.

Hetz C, Mollereau B. Disturbance of endoplasmic reticulum proteostasis in neurodegenerative diseases. Nat Rev Neurosci. 2014 Apr;15(4):233-49. doi: 10.1038/nrn3689. Epub 2014 Mar 12. PMID: 24619348.

Hoozemans JJ, van Haastert ES, Eikelenboom P, de Vos RA, Rozemuller JM, Scheper W. Activation of the unfolded protein response in Parkinson's disease. Biochem Biophys Res Commun. 2007 Mar 16;354(3):707-11. doi: 10.1016/j.bbrc.2007.01.043. Epub 2007 Jan 17. PMID: 17254549.

Hoozemans JJ, van Haastert ES, Nijholt DA, Rozemuller AJ, Eikelenboom P, Scheper W. The unfolded protein response is activated in pretangle neurons in Alzheimer's disease hippocampus. Am J Pathol. 2009 Apr;174(4):1241-51. doi: 10.2353/ajpath.2009.080814. Epub 2009 Mar 5. PMID: 19264902; PMCID: PMC2671357.

Hristova VA, Beasley SA, Rylett RJ, Shaw GS. Identification of a novel Zn2+-binding domain in the autosomal recessive juvenile Parkinson-related E3 ligase parkin. J Biol Chem. 2009 May 29;284(22):14978-86. doi: 10.1074/jbc.M808700200. Epub 2009 Apr 1. PMID: 19339245; PMCID: PMC2685680.

Hsu Y, Tran M, Linninger AA. Dynamic regulation of aquaporin-4 water channels in neurological disorders. Croat Med J. 2015 Oct;56(5):401-21. doi: 10.3325/cmj.2015.56.401. PMID: 26526878; PMCID: PMC4655926.

Hwang S, Kim D, Choi G, An SW, Hong YK, Suh YS, Lee MJ, Cho KS. Parkin suppresses c-Jun N-terminal kinase-induced cell death via transcriptional regulation in Drosophila. Mol Cells. 2010 Jun;29(6):575-80. doi: 10.1007/s10059-010-0068-1. Epub 2010 May 22. PMID: 20496123.

Ichimura T, Fraser PA, Cserr HF. Distribution of extracellular tracers in perivascular spaces of the rat brain. Brain Res. 1991 Apr 5;545(1-2):103-13. doi: 10.1016/0006-8993(91)91275-6. PMID: 1713524.

Iliff JJ, Lee H, Yu M, Feng T, Logan J, Nedergaard M, Benveniste H. Brain-wide pathway for waste clearance captured by contrast-enhanced MRI. J Clin Invest. 2013 Mar;123(3):1299-309. doi: 10.1172/JCI67677. Epub 2013 Feb 22. PMID: 23434588; PMCID: PMC3582150.

Iliff JJ, Wang M, Liao Y, Plogg BA, Peng W, Gundersen GA, Benveniste H, Vates GE, Deane R, Goldman SA, Nagelhus EA, Nedergaard M. A paravascular pathway facilitates CSF flow through the brain parenchyma and the clearance of interstitial solutes, including amyloid β. Sci Transl Med. 2012 Aug 15;4(147):147ra111. doi: 10.1126/scitranslmed.3003748. PMID: 22896675; PMCID: PMC3551275.

Irwin MR, Opp MR. Sleep Health: Reciprocal Regulation of Sleep and Innate Immunity. Neuropsychopharmacology. 2017 Jan;42(1):129-155. doi: 10.1038/npp.2016.148. Epub 2016 Aug 11. PMID: 27510422; PMCID: PMC5143488.

Ishihara L, Warren L, Gibson R, Amouri R, Lesage S, Dürr A, Tazir M, Wszolek ZK, Uitti RJ, Nichols WC, Griffith A, Hattori N, Leppert D, Watts R, Zabetian CP, Foroud TM, Farrer MJ, Brice A, Middleton L, Hentati F. Clinical features of Parkinson disease patients with homozygous leucine-rich repeat kinase 2 G2019S mutations. Arch Neurol. 2006 Sep;63(9):1250-4. doi: 10.1001/archneur.63.9.1250. PMID: 16966502.

Itier JM, Ibanez P, Mena MA, Abbas N, Cohen-Salmon C, Bohme GA, Laville M, Pratt J, Corti O, Pradier L, Ret G, Joubert C, Periquet M, Araujo F, Negroni J, Casarejos MJ, Canals S, Solano R, Serrano A, Gallego E, Sanchez M, Denefle P, Benavides J, Tremp G,

Rooney TA, Brice A, Garcia de Yebenes J. Parkin gene inactivation alters behaviour and dopamine neurotransmission in the mouse. Hum Mol Genet. 2003 Sep 15;12(18):2277-91. doi: 10.1093/hmg/ddg239. Epub 2003 Jul 22. PMID: 12915482.

Jagmag SA, Tripathi N, Shukla SD, Maiti S, Khurana S. Evaluation of Models of Parkinson's Disease. Front Neurosci. 2016 Jan 19;9:503. doi: 10.3389/fnins.2015.00503. PMID: 26834536; PMCID: PMC4718050.

Jessen NA, Munk AS, Lundgaard I, Nedergaard M. The Glymphatic System: A Beginner's Guide. Neurochem Res. 2015 Dec;40(12):2583-99. doi: 10.1007/s11064-015-1581-6. Epub 2015 May 7. PMID: 25947369; PMCID: PMC4636982.

Joch M, Ase AR, Chen CX, MacDonald PA, Kontogiannea M, Corera AT, Brice A, Séguéla P, Fon EA. Parkin-mediated monoubiquitination of the PDZ protein PICK1 regulates the activity of acid-sensing ion channels. Mol Biol Cell. 2007 Aug;18(8):3105-18. doi: 10.1091/mbc.e05-11-1027. Epub 2007 Jun 6. PMID: 17553932; PMCID: PMC1949385.

Johanson, C.E., Duncan, J.A., Klinge, P.M. et al. Multiplicity of cerebrospinal fluid functions: New challenges in health and disease. Fluids Barriers CNS 5, 10 (2008). https://doi.org/10.1186/1743-8454-5-10

Johnston JA, Ward CL, Kopito RR. Aggresomes: a cellular response to misfolded proteins. J Cell Biol. 1998 Dec 28;143(7):1883-98. doi: 10.1083/jcb.143.7.1883. PMID: 9864362; PMCID: PMC2175217.

Ju YS, Ooms SJ, Sutphen C, Macauley SL, Zangrilli MA, Jerome G, Fagan AM, Mignot E, Zempel JM, Claassen JAHR, Holtzman DM. Slow wave sleep disruption increases cerebrospinal fluid amyloid-β levels. Brain. 2017 Aug 1;140(8):2104-2111. doi: 10.1093/brain/awx148. PMID: 28899014; PMCID: PMC5790144.

Jucker M, Walker LC. Pathogenic protein seeding in Alzheimer disease and other neurodegenerative disorders. Ann Neurol. 2011 Oct;70(4):532-40. doi: 10.1002/ana.22615. PMID: 22028219; PMCID: PMC3203752.

Kalaitzakis ME, Gentleman SM, Pearce RKB, 2013. Disturbed sleep in Parkinson's disease: Anatomical and pathological correlates. Neuropathol. Appl. Neurobiol 39, 644–653. 10.1111/nan.12024

Kalia LV, Lang AE. Parkinson's disease. Lancet. 2015 Aug 29;386(9996):896-912. doi: 10.1016/S0140-6736(14)61393-3. Epub 2015 Apr 19. PMID: 25904081.

Kang DW, Lee CU, Lim HK. Role of Sleep Disturbance in the Trajectory of Alzheimer's Disease. Clin Psychopharmacol Neurosci. 2017 May 31;15(2):89-99. doi: 10.9758/cpn.2017.15.2.89. PMID: 28449556; PMCID: PMC5426492.

Katja K. Dove, Rachel E. Klevit, Structural Biology: Parkin's Serpentine Shape Revealed in the year of the Snake, Current Biology, Volume 23, Issue 16, 2013, Pages R691-R693, ISSN 0960-9822, https://doi.org/10.1016/j.cub.2013.07.039.

Kazlauskaite A, Kondapalli C, Gourlay R, Campbell DG, Ritorto MS, Hofmann K, Alessi DR, Knebel A, Trost M, Muqit MM. Parkin is activated by PINK1-dependent phosphorylation of ubiquitin at Ser65. Biochem J. 2014 May 15;460(1):127-39. doi: 10.1042/BJ20140334. PMID: 24660806; PMCID: PMC4000136.

Kitada T, Asakawa S, Hattori N, Matsumine H, Yamamura Y, Minoshima S, Yokochi M, Mizuno Y, Shimizu N. Mutations in the parkin gene cause autosomal recessive juvenile parkinsonism. Nature. 1998 Apr 9;392(6676):605-8. doi: 10.1038/33416. PMID: 9560156.

Klein C, Westenberger A. Genetics of Parkinson's disease. Cold Spring Harb Perspect Med. 2012 Jan;2(1):a008888. doi: 10.1101/cshperspect.a008888. PMID: 22315721; PMCID: PMC3253033.

Komander D, Rape M. The ubiquitin code. Annu Rev Biochem. 2012;81:203-29. doi: 10.1146/annurev-biochem-060310-170328. Epub 2012 Apr 10. PMID: 22524316.

Kordower JH, Chu Y, Hauser RA, Freeman TB, Olanow CW. Lewy body-like pathology in long-term embryonic nigral transplants in Parkinson's disease. Nat Med. 2008 May;14(5):504-6. doi: 10.1038/nm1747. Epub 2008 Apr 6. PMID: 18391962.

Kostić VS, Tomić A, Ječmenica-Lukić M. The Pathophysiology of Fatigue in Parkinson's Disease and its Pragmatic Management. Mov Disord Clin Pract. 2016 Mar 11;3(4):323-330. doi: 10.1002/mdc3.12343. PMID: 30363584; PMCID: PMC6178705.

Koyano F, Okatsu K, Kosako H, Tamura Y, Go E, Kimura M, Kimura Y, Tsuchiya H, Yoshihara H, Hirokawa T, Endo T, Fon EA, Trempe JF, Saeki Y, Tanaka K, Matsuda N. Ubiquitin is phosphorylated by PINK1 to activate parkin. Nature. 2014 Jun 5;510(7503):162-6. doi: 10.1038/nature13392. Epub 2014 Jun 4. PMID: 24784582.

Kress BT, Iliff JJ, Xia M, Wang M, Wei HS, Zeppenfeld D, Xie L, Kang H, Xu Q, Liew JA, Plog BA, Ding F, Deane R, Nedergaard M. Impairment of paravascular clearance pathways in the aging brain. Ann Neurol. 2014 Dec;76(6):845-61. doi: 10.1002/ana.24271. Epub 2014 Sep 26. PMID: 25204284; PMCID: PMC4245362.

Krüger R, Kuhn W, Müller T, Woitalla D, Graeber M, Kösel S, Przuntek H, Epplen JT, Schöls L, Riess O. Ala30Pro mutation in the gene encoding alpha-synuclein in Parkinson's disease. Nat Genet. 1998 Feb;18(2):106-8. doi: 10.1038/ng0298-106. PMID: 9462735.

Krüger R, Kuhn W, Müller T, Woitalla D, Graeber M, Kösel S, Przuntek H, Epplen JT, Schöls L, Riess O. Ala30Pro mutation in the gene encoding alpha-synuclein in Parkinson's disease. Nat Genet. 1998 Feb;18(2):106-8. doi: 10.1038/ng0298-106. PMID: 9462735.

Kruppa AJ, Kishi-Itakura C, Masters TA, Rorbach JE, Grice GL, Kendrick-Jones J, Nathan JA, Minczuk M, Buss F. Myosin VI-Dependent Actin Cages Encapsulate Parkin-Positive Damaged Mitochondria. Dev Cell. 2018 Feb 26;44(4):484-499.e6. doi: 10.1016/j.devcel.2018.01.007. Epub 2018 Feb 1. PMID: 29398621; PMCID: PMC5932465.

Laloux C, Petrault M, Lecointe C, Devos D, Bordet R. Differential susceptibility to the PPAR-γ agonist pioglitazone in 1-methyl-4-phenyl-1,2,3,6-tetrahydropyridine and 6-hydroxydopamine rodent models of Parkinson's disease. Pharmacol Res. 2012 May;65(5):514-22. doi: 10.1016/j.phrs.2012.02.008. Epub 2012 Mar 3. PMID: 22391246.

Langston JW, Ballard P, Tetrud JW, Irwin I. Chronic Parkinsonism in humans due to a product of meperidine-analog synthesis. Science. 1983 Feb 25;219(4587):979-80. doi: 10.1126/science.6823561. PMID: 6823561.

Lee H, Xie L, Yu M, Kang H, Feng T, Deane R, Logan J, Nedergaard M, Benveniste H. The Effect of Body Posture on Brain Glymphatic Transport. J Neurosci. 2015 Aug 5;35(31):11034-44. doi: 10.1523/JNEUROSCI.1625-15.2015. PMID: 26245965; PMCID: PMC4524974.

Lee JY, Nagano Y, Taylor JP, Lim KL, Yao TP. Disease-causing mutations in parkin impair mitochondrial ubiquitination, aggregation, and HDAC6-dependent mitophagy. J Cell Biol. 2010 May 17;189(4):671-9. doi: 10.1083/jcb.201001039. Epub 2010 May 10. PMID: 20457763; PMCID: PMC2872903.

Lee VM, Trojanowski JQ. Mechanisms of Parkinson's disease linked to pathological alpha-synuclein: new targets for drug discovery. Neuron. 2006 Oct 5;52(1):33-8. doi: 10.1016/j.neuron.2006.09.026. PMID: 17015225.

Leitman, J., Ulrich Hartl, F. & Lederkremer, G. Soluble forms of polyQ-expanded huntingtin rather than large aggregates cause endoplasmic reticulum stress. Nat Commun 4, 2753 (2013). https://doi.org/10.1038/ncomms3753

Lesage S, Anheim M, Letournel F, Bousset L, Honoré A, Rozas N, Pieri L, Madiona K, Dürr A, Melki R, Verny C, Brice A; French Parkinson's Disease Genetics Study Group. G51D α-synuclein mutation causes a novel parkinsonian-pyramidal syndrome. Ann Neurol. 2013 Apr;73(4):459-71. doi: 10.1002/ana.23894. PMID: 23526723.

Lewy, F. Handbuch der Neurologie, Dritter Band, Spezielle Neurologie I. Berlin: Julius Springer; 1912. pp. 920–933.

Li JY, Englund E, Holton JL, Soulet D, Hagell P, Lees AJ, Lashley T, Quinn NP, Rehncrona S, Björklund A, Widner H, Revesz T, Lindvall O, Brundin P. Lewy bodies in grafted neurons in subjects with Parkinson's disease suggest host-to-graft disease propagation. Nat Med. 2008 May;14(5):501-3. doi: 10.1038/nm1746. Epub 2008 Apr 6. PMID: 18391963.

Liao S, Padera TP. Lymphatic function and immune regulation in health and disease. Lymphat Res Biol. 2013 Sep;11(3):136-43. doi: 10.1089/lrb.2013.0012. Epub 2013 Sep 11. PMID: 24024577; PMCID: PMC3780287.

Lim AS, Kowgier M, Yu L, Buchman AS, Bennett DA. Sleep Fragmentation and the Risk of Incident Alzheimer's Disease and Cognitive Decline in Older Persons. Sleep. 2013 Jul 1;36(7):1027-1032. doi: 10.5665/sleep.2802. PMID: 23814339; PMCID: PMC3669060.

Lim KL, Chew KC, Tan JM, Wang C, Chung KK, Zhang Y, Tanaka Y, Smith W, Engelender S, Ross CA, Dawson VL, Dawson TM. Parkin mediates nonclassical, proteasomal-independent ubiquitination of synphilin-1: implications for Lewy body formation. J Neurosci. 2005 Feb 23;25(8):2002-9. doi: 10.1523/JNEUROSCI.4474-04.2005. PMID: 15728840; PMCID: PMC6726069.

Liu, W.J., Ye, L., Huang, W.F. et al. p62 links the autophagy pathway and the ubiqutin–proteasome system upon ubiquitinated protein degradation. Cell Mol Biol Lett 21, 29 (2016). https://doi.org/10.1186/s11658-016-0031-z

Lockhart PJ, Lincoln S, Hulihan M, Kachergus J, Wilkes K, Bisceglio G, Mash DC, Farrer MJ. DJ-1 mutations are a rare cause of recessively inherited early onset parkinsonism mediated by loss of protein function. J Med Genet. 2004 Mar;41(3):e22. doi: 10.1136/jmg.2003.011106. PMID: 14985393; PMCID: PMC1735689.

Lohmann E, Thobois S, Lesage S, Broussolle E, du Montcel ST, Ribeiro MJ, Remy P, Pelissolo A, Dubois B, Mallet L, Pollak P, Agid Y, Brice A; French Parkinson's Disease Genetics Study Group. A multidisciplinary study of patients with early-onset PD with and without parkin mutations. Neurology. 2009 Jan 13;72(2):110-6. doi: 10.1212/01.wnl.0000327098.86861.d4. Epub 2008 Nov 5. PMID: 18987353; PMCID: PMC2677494.

Lu XH, Fleming SM, Meurers B, Ackerson LC, Mortazavi F, Lo V, Hernandez D, Sulzer D, Jackson GR, Maidment NT, Chesselet MF, Yang XW. Bacterial artificial chromosome transgenic mice expressing a truncated mutant parkin exhibit age-dependent hypokinetic motor deficits, dopaminergic neuron degeneration, and accumulation of proteinase K-

resistant alpha-synuclein. J Neurosci. 2009 Feb 18;29(7):1962-76. doi: 10.1523/JNEUROSCI.5351-08.2009. PMID: 19228951; PMCID: PMC2803056.

Lu XH, Fleming SM, Meurers B, Ackerson LC, Mortazavi F, Lo V, Hernandez D, Sulzer D, Jackson GR, Maidment NT, Chesselet MF, Yang XW. Bacterial artificial chromosome transgenic mice expressing a truncated mutant parkin exhibit age-dependent hypokinetic motor deficits, dopaminergic neuron degeneration, and accumulation of proteinase K-resistant alpha-synuclein. J Neurosci. 2009 Feb 18;29(7):1962-76. doi: 10.1523/JNEUROSCI.5351-08.2009. PMID: 19228951; PMCID: PMC2803056.

Lücking CB, Dürr A, Bonifati V, Vaughan J, De Michele G, Gasser T, Harhangi BS, Meco G, Denèfle P, Wood NW, Agid Y, Brice A; French Parkinson's Disease Genetics Study Group; European Consortium on Genetic Susceptibility in Parkinson's Disease. Association between early-onset Parkinson's disease and mutations in the parkin gene. N Engl J Med. 2000 May 25;342(21):1560-7. doi: 10.1056/NEJM200005253422103. PMID: 10824074.

Lücking CB, Dürr A, Bonifati V, Vaughan J, De Michele G, Gasser T, Harhangi BS, Meco G, Denèfle P, Wood NW, Agid Y, Brice A; French Parkinson's Disease Genetics Study Group; European Consortium on Genetic Susceptibility in Parkinson's Disease. Association between early-onset Parkinson's disease and mutations in the parkin gene. N Engl J Med. 2000 May 25;342(21):1560-7. doi: 10.1056/NEJM200005253422103. PMID: 10824074.

Ma Q, Ineichen BV, Detmar M, Proulx ST. Outflow of cerebrospinal fluid is predominantly through lymphatic vessels and is reduced in aged mice. Nat Commun. 2017 Nov 10;8(1):1434. doi: 10.1038/s41467-017-01484-6. PMID: 29127332; PMCID: PMC5681558.

Ma Q, Ries M, Decker Y, Müller A, Riner C, Bücker A, Fassbender K, Detmar M, Proulx ST. Rapid lymphatic efflux limits cerebrospinal fluid flow to the brain. Acta Neuropathol. 2019 Jan;137(1):151-165. doi: 10.1007/s00401-018-1916-x. Epub 2018 Oct 10. PMID: 30306266; PMCID: PMC6338719.

Madsen DA, Schmidt SI, Blaabjerg M, Meyer M. Interaction between Parkin and α-Synuclein in PARK2-Mediated Parkinson's Disease. Cells. 2021 Jan 31;10(2):283. doi: 10.3390/cells10020283. PMID: 33572534; PMCID: PMC7911026.

Mann VM, Cooper JM, Daniel SE, Srai K, Jenner P, Marsden CD, Schapira AH. Complex I, iron, and ferritin in Parkinson's disease substantia nigra. Ann Neurol. 1994 Dec;36(6):876-81. doi: 10.1002/ana.410360612. PMID: 7998774.

Manoj Kumar, Jesús Acevedo-Cintrón, Aanishaa Jhaldiyal, Hu Wang, Shaida A. Andrabi, Stephen Eacker, Senthilkumar S. Karuppagounder, Saurav Brahmachari, Rong Chen, Hyesoo Kim, Han Seok Ko, Valina L. Dawson, Ted M. Dawson. Defects in Mitochondrial Biogenesis Drive Mitochondrial Alterations in PARKIN-Deficient Human Dopamine Neurons, Stem Cell Reports, Volume 15, Issue 3, 2020, Pages 629-645, ISSN 2213-6711, https://doi.org/10.1016/j.stemcr.2020.07.013.

Manzanillo PS, Ayres JS, Watson RO, Collins AC, Souza G, Rae CS, Schneider DS, Nakamura K, Shiloh MU, Cox JS. The ubiquitin ligase parkin mediates resistance to intracellular pathogens. Nature. 2013 Sep 26;501(7468):512-6. doi: 10.1038/nature12566. Epub 2013 Sep 4. PMID: 24005326; PMCID: PMC3886920.

Maor G, Rencus-Lazar S, Filocamo M, Steller H, Segal D, Horowitz M. Unfolded protein response in Gaucher disease: from human to Drosophila. Orphanet J Rare Dis. 2013 Sep 11;8:140. doi: 10.1186/1750-1172-8-140. PMID: 24020503; PMCID: PMC3819655.

Masliah E, Rockenstein E, Veinbergs I, Mallory M, Hashimoto M, Takeda A, Sagara Y, Sisk A, Mucke L. Dopaminergic loss and inclusion body formation in alpha-synuclein mice: implications for neurodegenerative disorders. Science. 2000 Feb 18;287(5456):1265-9. doi: 10.1126/science.287.5456.1265. PMID: 10678833.

McGeer PL, Itagaki S, Akiyama H, McGeer EG. Rate of cell death in parkinsonism indicates active neuropathological process. Ann Neurol. 1988 Oct;24(4):574-6. doi: 10.1002/ana.410240415. PMID: 3239957.

McGonigle P, Ruggeri B. Animal models of human disease: challenges in enabling translation. Biochem Pharmacol. 2014 Jan 1;87(1):162-71. doi: 10.1016/j.bcp.2013.08.006. Epub 2013 Aug 14. PMID: 23954708.

McNaught KS, Jenner P. Proteasomal function is impaired in substantia nigra in Parkinson's disease. Neurosci Lett. 2001 Jan 19;297(3):191-4. doi: 10.1016/s0304-3940(00)01701-8. PMID: 11137760.

Mehanna R, Jankovic J. Young-onset Parkinson's disease: Its unique features and their impact on quality of life. Parkinsonism Relat Disord. 2019 Aug;65:39-48. doi: 10.1016/j.parkreldis.2019.06.001. Epub 2019 Jun 1. PMID: 31176633.

Mestre, Humberto & Mori, Yuki & Nedergaard, Maiken. (2020). The Brain’s Glymphatic System: Current Controversies. Trends in Neurosciences. 43. 10.1016/j.tins.2020.04.003.

Mestre H, Hablitz LM, Xavier AL, Feng W, Zou W, Pu T, Monai H, Murlidharan G, Castellanos Rivera RM, Simon MJ, Pike MM, Plá V, Du T, Kress BT, Wang X, Plog BA, Thrane AS, Lundgaard I, Abe Y, Yasui M, Thomas JH, Xiao M, Hirase H, Asokan A, Iliff JJ, Nedergaard M. Aquaporin-4-dependent glymphatic solute transport in the rodent brain. Elife. 2018 Dec 18;7:e40070. doi: 10.7554/eLife.40070. PMID: 30561329; PMCID: PMC6307855.

Michaud JP, Bellavance MA, Préfontaine P, Rivest S. Real-time in vivo imaging reveals the ability of monocytes to clear vascular amyloid beta. Cell Rep. 2013 Nov 14;5(3):646-53. doi: 10.1016/j.celrep.2013.10.010. Epub 2013 Nov 7. PMID: 24210819.

Miller IN, Cronin-Golomb A. Gender differences in Parkinson's disease: clinical characteristics and cognition. Mov Disord. 2010 Dec 15;25(16):2695-703. doi: 10.1002/mds.23388. PMID: 20925068; PMCID: PMC3003756.

Mollenhauer B, Locascio JJ, Schulz-Schaeffer W, Sixel-Döring F, Trenkwalder C, Schlossmacher MG. α-Synuclein and tau concentrations in cerebrospinal fluid of patients presenting with parkinsonism: a cohort study. Lancet Neurol. 2011 Mar;10(3):230-40. doi: 10.1016/S1474-4422(11)70014-X. Erratum in: Lancet Neurol. 2011 Apr;10(4):297. PMID: 21317042.

Mootaz M Salman, Philip Kitchen, Andrea Halsey, Marie Xun Wang, Susanna Törnroth-Horsefield, Alex C Conner, Jerome Badaut, Jeffrey J Iliff, Roslyn M Bill, Emerging roles for dynamic aquaporin-4 subcellular relocalization in CNS water homeostasis, Brain, Volume 145, Issue 1, January 2022, Pages 64–75, https://doi.org/10.1093/brain/awab311

Morgan JC, Fox SH. Treating the Motor Symptoms of Parkinson Disease. Continuum (Minneap Minn). 2016 Aug;22(4 Movement Disorders):1064-85. doi: 10.1212/CON.0000000000000355. PMID: 27495198.

Mueller JC, Fuchs J, Hofer A, Zimprich A, Lichtner P, Illig T, Berg D, Wüllner U, Meitinger T, Gasser T. Multiple regions of alpha-synuclein are associated with Parkinson's disease. Ann Neurol. 2005 Apr;57(4):535-41. doi: 10.1002/ana.20438. PMID: 15786467.

N. Cummins, J. Gotz. Shedding light on mitophagy in neurons: what is the evidence for PINK1/PARKIN mitophagy in vivo? Cell Mol. Life Sci., 75 (2018), pp. 1151-1162

Narhi L, Wood SJ, Steavenson S, Jiang Y, Wu GM, Anafi D, Kaufman SA, Martin F, Sitney K, Denis P, Louis JC, Wypych J, Biere AL, Citron M. Both familial Parkinson's disease mutations accelerate alpha-synuclein aggregation. J Biol Chem. 1999 Apr 2;274(14):9843-6. doi: 10.1074/jbc.274.14.9843. Erratum in: J Biol Chem 1999 May 7;274(19):13728. PMID: 10092675.

Nielsen S, Nagelhus EA, Amiry-Moghaddam M, Bourque C, Agre P, Ottersen OP. Specialized membrane domains for water transport in glial cells: High-resolution Immunogold Cytochemistry of Aquaporin-4 in rat brain. The Journal of Neuroscience. 1997;17(1):171–180. doi: 10.1523/JNEUROSCI.17-01-00171.1997

Nishitoh H, Kadowaki H, Nagai A, Maruyama T, Yokota T, Fukutomi H, Noguchi T, Matsuzawa A, Takeda K, Ichijo H. ALS-linked mutant SOD1 induces ER stress- and ASK1-dependent motor neuron death by targeting Derlin-1. Genes Dev. 2008 Jun 1;22(11):1451-64. doi: 10.1101/gad.1640108. PMID: 18519638; PMCID: PMC2418582.

Noyce AJ, Bestwick JP, Silveira-Moriyama L, Hawkes CH, Giovannoni G, Lees AJ, Schrag A. Meta-analysis of early nonmotor features and risk factors for Parkinson disease. Ann Neurol. 2012 Dec;72(6):893-901. doi: 10.1002/ana.23687. Epub 2012 Oct 15. PMID: 23071076; PMCID: PMC3556649.

Obergasteiger, J., Frapporti, G., Lamonaca, G. et al. Kinase inhibition of G2019S-LRRK2 enhances autolysosome formation and function to reduce endogenous alpha-synuclein intracellular inclusions. Cell Death Discov. 6, 45 (2020). https://doi.org/10.1038/s41420-020-0279-y

O'Connor RS, Steeds CM, Wiseman RW, Pavlath GK. Phosphocreatine as an energy source for actin cytoskeletal rearrangements during myoblast fusion. J Physiol. 2008 Jun 15;586(12):2841-53. doi: 10.1113/jphysiol.2008.151027. Epub 2008 Apr 17. PMID: 18420707; PMCID: PMC2517193.

O'Connor T, Sadleir KR, Maus E, Velliquette RA, Zhao J, Cole SL, Eimer WA, Hitt B, Bembinster LA, Lammich S, Lichtenthaler SF, Hébert SS, De Strooper B, Haass C, Bennett DA, Vassar R. Phosphorylation of the translation initiation factor eIF2alpha increases BACE1 levels and promotes amyloidogenesis. Neuron. 2008 Dec 26;60(6):988-1009. doi: 10.1016/j.neuron.2008.10.047. PMID: 19109907; PMCID: PMC2667382.

O'Donnell J, Zeppenfeld D, McConnell E, Pena S, Nedergaard M. Norepinephrine: a neuromodulator that boosts the function of multiple cell types to optimize CNS performance. Neurochem Res. 2012 Nov;37(11):2496-512. doi: 10.1007/s11064-012-0818-x. Epub 2012 Jun 21. PMID: 22717696; PMCID: PMC3548657.

Ogen-Shtern N, Ben David T, Lederkremer GZ. Protein aggregation and ER stress. Brain Res. 2016 Oct 1;1648(Pt B):658-666. doi: 10.1016/j.brainres.2016.03.044. Epub 2016 Mar 30. PMID: 27037184.

Oklinski MK, Skowronski MT, Skowronska A, Rützler M, Nørgaard K, Nieland JD, Kwon TH, Nielsen S. Aquaporins in the Spinal Cord. Int J Mol Sci. 2016 Dec 7;17(12):2050. doi: 10.3390/ijms17122050. PMID: 27941618; PMCID: PMC5187850.

Olanow CW, Watts RL, Koller WC. An algorithm (decision tree) for the management of Parkinson's disease (2001): treatment guidelines. Neurology. 2001 Jun;56(11 Suppl 5):S1-S88. doi: 10.1212/wnl.56.suppl_5.s1. PMID: 11402154.

Olzmann JA, Li L, Chudaev MV, Chen J, Perez FA, Palmiter RD, Chin LS. Parkin-mediated K63-linked polyubiquitination targets misfolded DJ-1 to aggresomes via binding to HDAC6. J Cell Biol. 2007 Sep 10;178(6):1025-38. doi: 10.1083/jcb.200611128. PMID: 17846173; PMCID: PMC2064625.

Olzmann JA, Li L, Chudaev MV, Chen J, Perez FA, Palmiter RD, Chin LS. Parkin-mediated K63-linked polyubiquitination targets misfolded DJ-1 to aggresomes via binding to HDAC6. J Cell Biol. 2007;178:1025–1038.

Oresković D, Klarica M. The formation of cerebrospinal fluid: nearly a hundred years of interpretations and misinterpretations. Brain Res Rev. 2010 Sep 24;64(2):241-62. doi: 10.1016/j.brainresrev.2010.04.006. Epub 2010 May 26. PMID: 20435061.

Palacino JJ, Sagi D, Goldberg MS, Krauss S, Motz C, Wacker M, Klose J, Shen J. Mitochondrial dysfunction and oxidative damage in parkin-deficient mice. J Biol Chem. 2004 Apr 30;279(18):18614-22. doi: 10.1074/jbc.M401135200. Epub 2004 Feb 24. PMID: 14985362.

Palacino JJ, Sagi D, Goldberg MS, Krauss S, Motz C, Wacker M, Klose J, Shen J. Mitochondrial dysfunction and oxidative damage in parkin-deficient mice. J Biol Chem. 2004 Apr 30;279(18):18614-22. doi: 10.1074/jbc.M401135200. Epub 2004 Feb 24. PMID: 14985362.

Parkinson J. An essay on the shaking palsy. 1817. J Neuropsychiatry Clin Neurosci. 2002 Spring;14(2):223-36; discussion 222. doi: 10.1176/jnp.14.2.223. PMID: 11983801.

Patel M, Atyani A, Salameh JP, McInnes M, Chakraborty S. Safety of Intrathecal Administration of Gadolinium-based Contrast Agents: A Systematic Review and Meta-Analysis. Radiology. 2020 Oct;297(1):75-83. doi: 10.1148/radiol.2020191373. Epub 2020 Jul 28. PMID: 32720867.

Peng J, Schwartz D, Elias JE, Thoreen CC, Cheng D, Marsischky G, Roelofs J, Finley D, Gygi SP. A proteomics approach to understanding protein ubiquitination. Nat Biotechnol. 2003 Aug;21(8):921-6. doi: 10.1038/nbt849. Epub 2003 Jul 20. PMID: 12872131.

Perez FA, Palmiter RD. Parkin-deficient mice are not a robust model of parkinsonism. Proc Natl Acad Sci U S A. 2005 Feb 8;102(6):2174-9. doi: 10.1073/pnas.0409598102. Epub 2005 Jan 31. PMID: 15684050; PMCID: PMC548311.

Periquet M, Latouche M, Lohmann E, Rawal N, De Michele G, Ricard S, Teive H, Fraix V, Vidailhet M, Nicholl D, Barone P, Wood NW, Raskin S, Deleuze JF, Agid Y, Dürr A, Brice A; French Parkinson's Disease Genetics Study Group; European Consortium on Genetic Susceptibility in Parkinson's Disease. Parkin mutations are frequent in patients with isolated early-onset parkinsonism. Brain. 2003 Jun;126(Pt 6):1271-8. doi: 10.1093/brain/awg136. PMID: 12764050.

Pesah Y, Pham T, Burgess H, Middlebrooks B, Verstreken P, Zhou Y, Harding M, Bellen H, Mardon G. Drosophila parkin mutants have decreased mass and cell size and increased sensitivity to oxygen radical stress. Development. 2004 May;131(9):2183-94. doi: 10.1242/dev.01095. Epub 2004 Apr 8. PMID: 15073152.

Pischedda F, Cirnaru MD, Ponzoni L, Sandre M, Biosa A, Carrion MP, Marin O, Morari M, Pan L, Greggio E, Bandopadhyay R, Sala M, Piccoli G. LRRK2 G2019S kinase activity triggers neurotoxic NSF aggregation. Brain. 2021 Jun 22;144(5):1509-1525. doi: 10.1093/brain/awab073. PMID: 33876242.

Polymeropoulos MH, Lavedan C, Leroy E, Ide SE, Dehejia A, Dutra A, Pike B, Root H, Rubenstein J, Boyer R, Stenroos ES, Chandrasekharappa S, Athanassiadou A, Papapetropoulos T, Johnson WG, Lazzarini AM, Duvoisin RC, Di Iorio G, Golbe LI, Nussbaum RL. Mutation in the alpha-synuclein gene identified in families with Parkinson's disease. Science. 1997 Jun 27;276(5321):2045-7. doi: 10.1126/science.276.5321.2045. PMID: 9197268.

Prell T, Lautenschläger J, Weidemann L, Ruhmer J, Witte OW, Grosskreutz J. Endoplasmic reticulum stress is accompanied by activation of NF-κB in amyotrophic lateral sclerosis. J Neuroimmunol. 2014 May 15;270(1-2):29-36. doi: 10.1016/j.jneuroim.2014.03.005. Epub 2014 Mar 12. PMID: 24666819.

Puschmann A. Monogenic Parkinson's disease and parkinsonism: clinical phenotypes and frequencies of known mutations. Parkinsonism Relat Disord. 2013 Apr;19(4):407-15. doi: 10.1016/j.parkreldis.2013.01.020. Epub 2013 Feb 23. PMID: 23462481.

Rainey-Smith, S.R., Mazzucchelli, G.N., Villemagne, V.L. et al. Genetic variation in Aquaporin-4 moderates the relationship between sleep and brain Aβ-amyloid burden. Transl Psychiatry 8, 47 (2018). https://doi.org/10.1038/s41398-018-0094-x

Regoni M, Zanetti L, Comai S, Mercatelli D, Novello S, Albanese F, Croci L, Consalez GG, Ciammola A, Valtorta F, Morari M, Sassone J. Early Dysfunction of Substantia Nigra Dopamine Neurons in the ParkinQ311X Mouse. Biomedicines. 2021 May 5;9(5):514. doi: 10.3390/biomedicines9050514. PMID: 34063112; PMCID: PMC8148213.

Rennels ML, Blaumanis OR, Grady PA. Rapid solute transport throughout the brain via paravascular fluid pathways. Adv Neurol. 1990;52:431-9. PMID: 2396537.

Rennels ML, Gregory TF, Blaumanis OR, Fujimoto K, Grady PA. Evidence for a 'paravascular' fluid circulation in the mammalian central nervous system, provided by the rapid distribution of tracer protein throughout the brain from the subarachnoid space. Brain Res. 1985 Feb 4;326(1):47-63. doi: 10.1016/0006-8993(85)91383-6. PMID: 3971148.

Rideout HJ, Larsen KE, Sulzer D, Stefanis L. Proteasomal inhibition leads to formation of ubiquitin/alpha-synuclein-immunoreactive inclusions in PC12 cells. J Neurochem. 2001 Aug;78(4):899-908. doi: 10.1046/j.1471-4159.2001.00474.x. PMID: 11520910.

Rietdijk CD, Perez-Pardo P, Garssen J, van Wezel RJ, Kraneveld AD. Exploring Braak's Hypothesis of Parkinson's Disease. Front Neurol. 2017 Feb 13;8:37. doi: 10.3389/fneur.2017.00037. PMID: 28243222; PMCID: PMC5304413.

Ringstad G, Vatnehol SAS, Eide PK. Glymphatic MRI in idiopathic normal pressure hydrocephalus. Brain. 2017 Oct 1;140(10):2691-2705. doi: 10.1093/brain/awx191. PMID: 28969373; PMCID: PMC5841149.

Roher AE, Kuo YM, Esh C, Knebel C, Weiss N, Kalback W, Luehrs DC, Childress JL, Beach TG, Weller RO, Kokjohn TA. Cortical and leptomeningeal cerebrovascular amyloid and white matter pathology in Alzheimer's disease. Mol Med. 2003 Mar-Apr;9(3-4):112-22. PMID: 12865947; PMCID: PMC1430731.

Rossi A, Moritz TJ, Ratelade J, Verkman AS. Super-resolution imaging of aquaporin-4 orthogonal arrays of particles in cell membranes. J Cell Sci. 2012 Sep 15;125(Pt 18):4405-12. doi: 10.1242/jcs.109603. Epub 2012 Jun 20. PMID: 22718347; PMCID: PMC3516444.

Rothfuss O, Fischer H, Hasegawa T, Maisel M, Leitner P, Miesel F, Sharma M, Bornemann A, Berg D, Gasser T, Patenge N. Parkin protects mitochondrial genome integrity and supports mitochondrial DNA repair. Hum Mol Genet. 2009 Oct 15;18(20):3832-50. doi: 10.1093/hmg/ddp327. Epub 2009 Jul 19. PMID: 19617636.

Rüb C, Wilkening A, Voos W. Mitochondrial quality control by the Pink1/Parkin system. Cell Tissue Res. 2017 Jan;367(1):111-123. doi: 10.1007/s00441-016-2485-8. Epub 2016 Sep 2. PMID: 27586587.

Ruffmann, C., Zini, M., Goldwurm, S. et al. Lewy body pathology and typical Parkinson disease in a patient with a heterozygous (R275W) mutation in the Parkin gene (PARK2). Acta Neuropathol 123, 901–903 (2012). https://doi.org/10.1007/s00401-012-0991-7

Sabbatini M, Barili P, Bronzetti E, Zaccheo D, Amenta F. Age-related changes of glial fibrillary acidic protein immunoreactive astrocytes in the rat cerebellar cortex. Mech Ageing Dev. 1999 May 3;108(2):165-72. doi: 10.1016/s0047-6374(99)00008-1. PMID: 10400309.

Saez I, Vilchez D. The Mechanistic Links Between Proteasome Activity, Aging and Age-related Diseases. Curr Genomics. 2014 Feb;15(1):38-51. doi: 10.2174/1389202915011403061133 44. PMID: 24653662; PMCID: PMC3958958.

Samuel F, Flavin WP, Iqbal S, Pacelli C, Sri Renganathan SD, Trudeau LE, Campbell EM, Fraser PE, Tandon A. Effects of Serine 129 Phosphorylation on α-Synuclein Aggregation, Membrane Association, and Internalization. J Biol Chem. 2016 Feb 26;291(9):4374-85. doi: 10.1074/jbc.M115.705095. Epub 2015 Dec 30. PMID: 26719332; PMCID: PMC4813466.

Sang TK, Chang HY, Lawless GM, Ratnaparkhi A, Mee L, Ackerson LC, Maidment NT, Krantz DE, Jackson GR. A Drosophila model of mutant human parkin-induced toxicity demonstrates selective loss of dopaminergic neurons and dependence on cellular dopamine. J Neurosci. 2007 Jan 31;27(5):981-92. doi: 10.1523/JNEUROSCI.4810-06.2007. PMID: 17267552; PMCID: PMC6673194.

Scarpulla RC. Nuclear control of respiratory chain expression by nuclear respiratory factors and PGC-1-related coactivator. Ann N Y Acad Sci. 2008 Dec;1147:321-34. doi: 10.1196/annals.1427.006. PMID: 19076454; PMCID: PMC2853241.

Schaffar G, Breuer P, Boteva R, Behrends C, Tzvetkov N, Strippel N, Sakahira H, Siegers K, Hayer-Hartl M, Hartl FU. Cellular toxicity of polyglutamine expansion proteins: mechanism of transcription factor deactivation. Mol Cell. 2004 Jul 2;15(1):95-105. doi: 10.1016/j.molcel.2004.06.029. PMID: 15225551.

Schapira AH, Cooper JM, Dexter D, Clark JB, Jenner P, Marsden CD. Mitochondrial complex I deficiency in Parkinson's disease. J Neurochem. 1990 Mar;54(3):823-7. doi: 10.1111/j.1471-4159.1990.tb02325.x. PMID: 2154550.

Schenck CH, Boeve BF, Mahowald MW. Delayed emergence of a parkinsonian disorder or dementia in 81% of older men initially diagnosed with idiopathic rapid eye movement sleep behavior disorder: a 16-year update on a previously reported series. Sleep Med. 2013 Aug;14(8):744-8. doi: 10.1016/j.sleep.2012.10.009. Epub 2013 Jan 22. PMID: 23347909.

Schintu N, Frau L, Ibba M, Caboni P, Garau A, Carboni E, Carta AR. PPAR-gamma-mediated neuroprotection in a chronic mouse model of Parkinson's disease. Eur J

Neurosci. 2009 Mar;29(5):954-63. doi: 10.1111/j.1460-9568.2009.06657.x. Epub 2009 Feb 24. PMID: 19245367.

Schröder M, Kaufman RJ. The mammalian unfolded protein response. Annu Rev Biochem. 2005;74:739-89. doi: 10.1146/annurev.biochem.73.011303.074134. PMID: 15952902.

Seirafi M, Kozlov G, Gehring K. Parkin structure and function. FEBS J. 2015 Jun;282(11):2076-88. doi: 10.1111/febs.13249. Epub 2015 Mar 16. PMID: 25712550; PMCID: PMC4672691.

Shaltouki A, Sivapatham R, Pei Y, Gerencser AA, Momčilović O, Rao MS, Zeng X. Mitochondrial alterations by PARKIN in dopaminergic neurons using PARK2 patient-specific and PARK2 knockout isogenic iPSC lines. Stem Cell Reports. 2015 May 12;4(5):847-59. doi: 10.1016/j.stemcr.2015.02.019. Epub 2015 Apr 2. PMID: 25843045; PMCID: PMC4437475.

Sheng ZH, Cai Q. Mitochondrial transport in neurons: impact on synaptic homeostasis and neurodegeneration. Nat Rev Neurosci. 2012 Jan 5;13(2):77-93. doi: 10.1038/nrn3156. PMID: 22218207; PMCID: PMC4962561.

Shin JH, Ko HS, Kang H, Lee Y, Lee YI, Pletinkova O, Troconso JC, Dawson VL, Dawson TM. PARIS (ZNF746) repression of PGC-1α contributes to neurodegeneration in Parkinson's disease. Cell. 2011 Mar 4;144(5):689-702. doi: 10.1016/j.cell.2011.02.010. PMID: 21376232; PMCID: PMC3063894.

Shin JH, Ko HS, Kang H, Lee Y, Lee YI, Pletinkova O, Troconso JC, Dawson VL, Dawson TM. PARIS (ZNF746) repression of PGC-1α contributes to neurodegeneration in Parkinson's disease. Cell. 2011 Mar 4;144(5):689-702. doi: 10.1016/j.cell.2011.02.010. PMID: 21376232; PMCID: PMC3063894.

Si X, Guo T, Wang Z, Fang Y, Gu L, Cao L, Yang W, Gao T, Song Z, Tian J, Yin X, Guan X, Zhou C, Wu J, Bai X, Liu X, Zhao G, Zhang M, Pu J, Zhang B. Neuroimaging evidence of glymphatic system dysfunction in possible REM sleep behavior disorder and Parkinson's disease. NPJ Parkinsons Dis. 2022 Apr 29;8(1):54. doi: 10.1038/s41531-022-00316-9. PMID: 35487930; PMCID: PMC9055043.

Silberstein C, Bouley R, Huang Y, Fang P, Pastor-Soler N, Brown D, Van Hoek AN. Membrane organization and function of M1 and M23 isoforms of aquaporin-4 in epithelial cells. Am J Physiol Renal Physiol. 2004 Sep;287(3):F501-11. doi: 10.1152/ajprenal.00439.2003. Epub 2004 May 18. PMID: 15149973.

Simon DK, Tanner CM, Brundin P. Parkinson Disease Epidemiology, Pathology, Genetics, and Pathophysiology. Clin Geriatr Med. 2020 Feb;36(1):1-12. doi: 10.1016/j.cger.2019.08.002. Epub 2019 Aug 24. PMID: 31733690; PMCID: PMC6905381.

Simon M, Wang MX, Ismail O, Braun M, Schindler AG, Reemmer J, Wang Z, Haveliwala MA, O'Boyle RP, Han WY, Roese N, Grafe M, Woltjer R, Boison D, Iliff JJ. Loss of perivascular aquaporin-4 localization impairs glymphatic exchange and promotes amyloid β plaque formation in mice. Alzheimers Res Ther. 2022 Apr 26;14(1):59. doi: 10.1186/s13195-022-00999-5. PMID: 35473943; PMCID: PMC9040291.

Singleton AB, Farrer M, Johnson J, Singleton A, Hague S, Kachergus J, Hulihan M, Peuralinna T, Dutra A, Nussbaum R, Lincoln S, Crawley A, Hanson M, Maraganore D, Adler C, Cookson MR, Muenter M, Baptista M, Miller D, Blancato J, Hardy J, Gwinn-Hardy K. alpha-Synuclein locus triplication causes Parkinson's disease. Science. 2003 Oct 31;302(5646):841. doi: 10.1126/science.1090278. PMID: 14593171.

Southern, W.M., Nichenko, A.S., Tehrani, K.F. et al. PGC-1α overexpression partially rescues impaired oxidative and contractile pathophysiology following volumetric muscle loss injury. Sci Rep 9, 4079 (2019). https://doi.org/10.1038/s41598-019-40606-6

Spillantini MG, Crowther RA, Jakes R, Hasegawa M, Goedert M. alpha-Synuclein in filamentous inclusions of Lewy bodies from Parkinson's disease and dementia with lewy bodies. Proc Natl Acad Sci U S A. 1998 May 26;95(11):6469-73. doi: 10.1073/pnas.95.11.6469. PMID: 9600990; PMCID: PMC27806.

Sriram SR, Li X, Ko HS, Chung KK, Wong E, Lim KL, Dawson VL, Dawson TM. Familial-associated mutations differentially disrupt the solubility, localization, binding and ubiquitination properties of parkin. Hum Mol Genet. 2005 Sep 1;14(17):2571-86. doi: 10.1093/hmg/ddi292. Epub 2005 Jul 27. PMID: 16049031.

Stevens DA, Lee Y, Kang HC, Lee BD, Lee YI, Bower A, Jiang H, Kang SU, Andrabi SA, Dawson VL, Shin JH, Dawson TM. Parkin loss leads to PARIS-dependent declines in mitochondrial mass and respiration. Proc Natl Acad Sci U S A. 2015 Sep 15;112(37):11696-701. doi: 10.1073/pnas.1500624112. Epub 2015 Aug 31. PMID: 26324925; PMCID: PMC4577198.

Tan JM, Wong ES, Kirkpatrick DS, Pletnikova O, Ko HS, Tay SP, Ho MW, Troncoso J, Gygi SP, Lee MK, Dawson VL, Dawson TM, Lim KL. Lysine 63-linked ubiquitination promotes the formation and autophagic clearance of protein inclusions associated with neurodegenerative diseases. Hum Mol Genet. 2008 Feb 1;17(3):431-9. doi: 10.1093/hmg/ddm320. Epub 2007 Nov 1. PMID: 17981811.

Tang Y, Le W. Differential Roles of M1 and M2 Microglia in Neurodegenerative Diseases. Mol Neurobiol. 2016 Mar;53(2):1181-1194. doi: 10.1007/s12035-014-9070-5. Epub 2015 Jan 20. PMID: 25598354.

Taoka T, Masutani Y, Kawai H, Nakane T, Matsuoka K, Yasuno F, Kishimoto T, Naganawa S. Evaluation of glymphatic system activity with the diffusion MR technique: diffusion tensor image analysis along the perivascular space (DTI-ALPS) in Alzheimer's disease cases. Jpn J Radiol. 2017 Apr;35(4):172-178. doi: 10.1007/s11604-017-0617-z. Epub 2017 Feb 14. PMID: 28197821.

Teng Z, Wang A, Wang P, Wang R, Wang W, Han H. The Effect of Aquaporin-4 Knockout on Interstitial Fluid Flow and the Structure of the Extracellular Space in the Deep Brain. Aging Dis. 2018 Oct 1;9(5):808-816. doi: 10.14336/AD.2017.1115. PMID: 30271658; PMCID: PMC6147590.

Tokarew JM, El-Kodsi DN, Lengacher NA, Fehr TK, Nguyen AP, Shutinoski B, O'Nuallain B, Jin M, Khan JM, Ng ACH, Li J, Jiang Q, Zhang M, Wang L, Sengupta R, Barber KR, Tran A, Im DS, Callaghan S, Park DS, Zandee S, et al. Age-associated insolubility of parkin in human midbrain is linked to redox balance and sequestration of reactive dopamine metabolites. Acta Neuropathol. 2021 May;141(5):725-754. doi: 10.1007/s00401-021-02285-4. Epub 2021 Mar 10. PMID: 33694021; PMCID: PMC8043881.

Trempe JF, Sauvé V, Grenier K, Seirafi M, Tang MY, Ménade M, Al-Abdul-Wahid S, Krett J, Wong K, Kozlov G, Nagar B, Fon EA, Gehring K. Structure of parkin reveals mechanisms for ubiquitin ligase activation. Science. 2013 Jun 21;340(6139):1451-5. doi: 10.1126/science.1237908. Epub 2013 May 9. PMID: 23661642.

Tysnes OB, Storstein A. Epidemiology of Parkinson's disease. J Neural Transm (Vienna). 2017 Aug;124(8):901-905. doi: 10.1007/s00702-017-1686-y. Epub 2017 Feb 1. PMID: 28150045

Valente EM, Abou-Sleiman PM, Caputo V, Muqit MM, Harvey K, Gispert S, Ali Z, Del Turco D, Bentivoglio AR, Healy DG, Albanese A, Nussbaum R, González-Maldonado R, Deller T, Salvi S, Cortelli P, Gilks WP, Latchman DS, Harvey RJ, Dallapiccola B, Auburger G, Wood NW. Hereditary early-onset Parkinson's disease caused by mutations in PINK1. Science. 2004 May 21;304(5674):1158-60. doi: 10.1126/science.1096284. Epub 2004 Apr 15. PMID: 15087508.

van Alphen B, Semenza ER, Yap M, van Swinderen B, Allada R. A deep sleep stage in Drosophila with a functional role in waste clearance. Sci Adv. 2021 Jan 20;7(4):eabc2999. doi: 10.1126/sciadv.abc2999. PMID: 33523916; PMCID: PMC7817094.

van Dijk KD, Bidinosti M, Weiss A, Raijmakers P, Berendse HW, van de Berg WD. Reduced α-synuclein levels in cerebrospinal fluid in Parkinson's disease are unrelated to clinical and imaging measures of disease severity. Eur J Neurol. 2014 Mar;21(3):388-94. doi: 10.1111/ene.12176. Epub 2013 Apr 30. PMID: 23631635.

Van Ham, Tjakko & Thijssen, Karen & Breitling, Rainer & Hofstra, Robert & Plasterk, Ronald & Nollen, Ellen. (2008). C. elegans Model Identifies Genetic Modifiers of ??-Synuclein Inclusion Formation During Aging. PLoS genetics. 4. e1000027. 10.1371/journal.pgen.1000027.

Vandebroek A, Yasui M. Regulation of AQP4 in the Central Nervous System. Int J Mol Sci. 2020 Feb 26;21(5):1603. doi: 10.3390/ijms21051603. PMID: 32111087; PMCID: PMC7084855.

Volles MJ, Lansbury PT Jr. Vesicle permeabilization by protofibrillar alpha-synuclein is sensitive to Parkinson's disease-linked mutations and occurs by a pore-like mechanism. Biochemistry. 2002 Apr 9;41(14):4595-602. doi: 10.1021/bi0121353. PMID: 11926821.

Wahabi K, Perwez A, Rizvi MA. Parkin in Parkinson's Disease and Cancer: a Double-Edged Sword. Mol Neurobiol. 2018 Aug;55(8):6788-6800. doi: 10.1007/s12035-018-0879-1. Epub 2018 Jan 18. PMID: 29349575.

Wakabayashi K, Tanji K, Mori F, Takahashi H. The Lewy body in Parkinson's disease: molecules implicated in the formation and degradation of alpha-synuclein aggregates. Neuropathology. 2007 Oct;27(5):494-506. doi: 10.1111/j.1440-1789.2007.00803.x. PMID: 18018486.

Wang C, Lu R, Ouyang X, Ho MW, Chia W, Yu F, Lim KL. Drosophila overexpressing parkin R275W mutant exhibits dopaminergic neuron degeneration and mitochondrial abnormalities. J Neurosci. 2007 Aug 8;27(32):8563-70. doi: 10.1523/JNEUROSCI.0218-07.2007. PMID: 17687034; PMCID: PMC6672933.

Wang C, Tan JM, Ho MW, Zaiden N, Wong SH, Chew CL, Eng PW, Lim TM, Dawson TM, Lim KL. Alterations in the solubility and intracellular localization of parkin by several familial Parkinson's disease-linked point mutations. J Neurochem. 2005 Apr;93(2):422-31. doi: 10.1111/j.1471-4159.2005.03023.x. PMID: 15816865.

Wang Q, Liu Y, Zhou J. Neuroinflammation in Parkinson's disease and its potential as therapeutic target. Transl Neurodegener. 2015 Oct 12;4:19. doi: 10.1186/s40035-015-0042-0. PMID: 26464797; PMCID: PMC4603346.

Wauer T, Komander D. Structure of the human Parkin ligase domain in an autoinhibited state. EMBO J. 2013 Jul 31;32(15):2099-112. doi: 10.1038/emboj.2013.125. Epub 2013 May 31. PMID: 23727886; PMCID: PMC3730226.

Weller RO, Subash M, Preston SD, Mazanti I, Carare RO. Perivascular drainage of amyloid-beta peptides from the brain and its failure in cerebral amyloid angiopathy and Alzheimer's disease. Brain Pathol. 2008 Apr;18(2):253-66. doi: 10.1111/j.1750-3639.2008.00133.x. PMID: 18363936; PMCID: PMC8095597.

Wenzel DM, Lissounov A, Brzovic PS, Klevit RE. UBCH7 reactivity profile reveals parkin and HHARI to be RING/HECT hybrids. Nature. 2011 Jun 2;474(7349):105-8. doi: 10.1038/nature09966. Epub 2011 May 1. PMID: 21532592; PMCID: PMC3444301.

Winer JR, Mander BA, Helfrich RF, Maass A, Harrison TM, Baker SL, Knight RT, Jagust WJ, Walker MP. Sleep as a Potential Biomarker of Tau and β-Amyloid Burden in the Human Brain. J Neurosci. 2019 Aug 7;39(32):6315-6324. doi: 10.1523/JNEUROSCI.0503-19.2019. Epub 2019 Jun 17. PMID: 31209175; PMCID: PMC6687908.

Xie L, Kang H, Xu Q, Chen MJ, Liao Y, Thiyagarajan M, O'Donnell J, Christensen DJ, Nicholson C, Iliff JJ, Takano T, Deane R, Nedergaard M. Sleep drives metabolite clearance from the adult brain. Science. 2013 Oct 18;342(6156):373-7. doi: 10.1126/science.1241224. PMID: 24136970; PMCID: PMC3880190.

Xu J, Kao SY, Lee FJ, Song W, Jin LW, Yankner BA. Dopamine-dependent neurotoxicity of alpha-synuclein: a mechanism for selective neurodegeneration in Parkinson disease. Nat Med. 2002 Jun;8(6):600-6. doi: 10.1038/nm0602-600. PMID: 12042811.

Yang J, Lunde LK, Nuntagij P, Oguchi T, Camassa LM, Nilsson LN, Lannfelt L, Xu Y, Amiry-Moghaddam M, Ottersen OP, Torp R. Loss of astrocyte polarization in the tg-ArcSwe mouse model of Alzheimer's disease. J Alzheimers Dis. 2011;27(4):711-22. doi: 10.3233/JAD-2011-110725. PMID: 21891870.

Yi W, MacDougall EJ, Tang MY, Krahn AI, Gan-Or Z, Trempe JF, Fon EA. The landscape of Parkin variants reveals pathogenic mechanisms and therapeutic targets in Parkinson's disease. Hum Mol Genet. 2019 Sep 1;28(17):2811-2825. doi: 10.1093/hmg/ddz080. PMID: 30994895; PMCID: PMC6736174.

Yunjong Lee, Daniel A. Stevens, Sung-Ung Kang, Haisong Jiang, Yun-Il Lee, Han Seok Ko, Leslie A. Scarffe, et al. PINK1 Primes Parkin-Mediated Ubiquitination of PARIS in Dopaminergic Neuronal Survival, Cell Reports, Volume 18, Issue 4, 2017, Pages 918-932, ISSN 2211-1247, https://doi.org/10.1016/j.celrep.2016.12.090.

Zanellati MC, Monti V, Barzaghi C, Reale C, Nardocci N, Albanese A, Valente EM, Ghezzi D, Garavaglia B. Mitochondrial dysfunction in Parkinson disease: evidence in mutant PARK2 fibroblasts. Front Genet. 2015 Mar 11;6:78. doi: 10.3389/fgene.2015.00078. PMID: 25815004; PMCID: PMC4356157.

Zarranz JJ, Alegre J, Gómez-Esteban JC, Lezcano E, Ros R, Ampuero I, Vidal L, Hoenicka J, Rodriguez O, Atarés B, Llorens V, Gomez Tortosa E, del Ser T, Muñoz DG, de Yebenes JG. The new mutation, E46K, of alpha-synuclein causes Parkinson and Lewy body dementia. Ann Neurol. 2004 Feb;55(2):164-73. doi: 10.1002/ana.10795. PMID: 14755719.

Zeppenfeld DM, Simon M, Haswell JD, D'Abreo D, Murchison C, Quinn JF, Grafe MR, Woltjer RL, Kaye J, Iliff JJ. Association of Perivascular Localization of Aquaporin-4 With Cognition and Alzheimer Disease in Aging Brains. JAMA Neurol. 2017 Jan 1;74(1):91-99. doi: 10.1001/jamaneurol.2016.4370. PMID: 27893874.

Zhang C, Lin M, Wu R, Wang X, Yang B, Levine AJ, Hu W, Feng Z. Parkin, a p53 target gene, mediates the role of p53 in glucose metabolism and the Warburg effect. Proc Natl Acad Sci U S A. 2011 Sep 27;108(39):16259-64. doi: 10.1073/pnas.1113884108. Epub 2011 Sep 19. PMID: 21930938; PMCID: PMC3182683.

Zhang CW, Hang L, Yao TP, Lim KL. Parkin Regulation and Neurodegenerative Disorders. Front Aging Neurosci. 2016 Jan 12;7:248. doi: 10.3389/fnagi.2015.00248. PMID: 26793099; PMCID: PMC4709595.

Zheng B, Liao Z, Locascio JJ, Lesniak KA, Roderick SS, Watt ML, Eklund AC, Zhang-James Y, Kim PD, Hauser MA, Grünblatt E, et al; Global PD Gene Expression (GPEX) Consortium. PGC-1α, a potential therapeutic target for early intervention in Parkinson's disease. Sci Transl Med. 2010 Oct 6;2(52):52ra73. doi: 10.1126/scitranslmed.3001059. PMID: 20926834; PMCID: PMC3129986.

Zheng L, Bernard-Marissal N, Moullan N, D'Amico D, Auwerx J, Moore DJ, Knott G, Aebischer P, Schneider BL. Parkin functionally interacts with PGC-1α to preserve mitochondria and protect dopaminergic neurons. Hum Mol Genet. 2017 Feb 1;26(3):582-598. doi: 10.1093/hmg/ddw418. PMID: 28053050.

Zittlau KI, Lechado-Terradas A, Nalpas N, Geisler S, Kahle PJ, Macek B. Temporal Analysis of Protein Ubiquitylation and Phosphorylation During Parkin-Dependent Mitophagy. Mol Cell Proteomics. 2022 Feb;21(2):100191. doi: 10.1016/j.mcpro.2021.100191. Epub 2021 Dec 30. PMID: 34974192; PMCID: PMC8808264.

Zou, W., Pu, T., Feng, W. et al. Blocking meningeal lymphatic drainage aggravates Parkinson’s disease-like pathology in mice overexpressing mutated α-synuclein. Transl Neurodegener 8, 7 (2019). https://doi.org/10.1186/s40035-019-0147-y

INDEX OF FIGURES AND TABLES

INDEX OF ABBREVIATIONS

6-OHDA: 6-Hydroxydopamine hydrobromide

AD: Alzheimer's Disease

ALP: autophagy/lysosomal pathway

ALS: Amyotrophic Lateral Sclerosis

AQP1: aquaporin-1

AQP4: aquaporin-4

AQP9: aquaporin-9

AR: antigen retrieval

ATF6: activating transcription factor 6

AVMA: American Veterinary Medical Association

Aβ: amyloid beta/β

BAC: bacterial artificial chromosome

BBB: blood brain barrier

BiP: binding immunoglobulin protein

bp: base pair

BSA: bovine serum albumine

Cas9: CRISPR associated protein 9

CD31: cluster of differentiation 31

cDNA: complementary DNA

CGase: β-glucocerebrosidase

CHOP: C/EBP homologous protein

CNS: central nervous system

CO_2: carbon dioxide

COMT: catechol-o-methyltransferase

COX2: cyclooxygenase 2

CRISPR: Clustered Regularly Interspaced Short Palindromic Repeats

CSA: cross sectional area

CSF: cerebrospinal fluid

DA: dopaminergic

DAB: 3,3′-Diaminobenzidine

DAC: dystrophin-associated complex

DAG1: dystroglycan

DIV: days *in vitro*

DMEM: Dulbecco's Modified Eagle Medium

DMSO: dimethyl sulfoxide

DTI-ALPS: diffusion tensor image analysis along the perivascular space

DTN-A: α-dystrobrevin

EDS: excessive daytime sleep

EDTA: ethylenediaminetetraacetic acid

ER: endoplasmic reticulum

ERAD: endoplasmic reticulum associated degradation

ERQC: endoplasmic reticulum quality control compartment

Ex3Δ40: 40-base pair deletion in exon 3

FBS: fetal bovine serum

GBA: glucosylceramidase beta

GFAP: glial fibrillary protein

GOF: gain of function

Gpe: globus pallidus external

Gpi:globus pallidus internal

HD: Huntington's disease

HPLC: high-performance liquid chromatography

HPRT: hypoxanthine phosphoribosyltransferase

IBR: In Between Ring

IFM: indirect flight muscle

IFN-γ: interferon-gamma

IKK: regulatory kinase IκB

IL-1β: interleukin-1 beta

iNOS: inducible nitric oxide synthase

IRE1: inositol requiring 1

ISF: interstitial fluid

KO: knock-out

LBD: Lewy body dementia

LBs: Lewy bodies

LDclns: ligation of cervical lymphatic vessel

L-DOPA: L-3,4-dihydroxyphenylalanine, Levodopa

LOF: loss of function

LRRK2: leucine-rich repeat kinase2

LVs: lymphatic vessels

MACS: magnetic cell sorting

MAO-B: monoamine oxidase

MCI: mild cognitive impairment

MIM: mitochondrial inner membranes

MOM: mitochondrial outer membrane

MPP+: 4-phenylpyridinium

MPTP: 1-methyl-4-phenyl-1,2,5,6-tetrahydropyridine

MRI: magnetic resonance imaging

MSA: multiple system atrophy

mtDNA: mitochondrial DNA

MW: molecular weight

MYO6: myosin VI

NE: norepinephrine

NEMO: NF-κB essential modulator

NF-κB: pro-survival nuclear factor-kB

NO: nitric oxide

NOR: novel object recognition

nREM: non-rapid-eye movement

Nrf-1: nuclear respiratory factor 1

Nrf-2: nuclear respiratory factor 1

NSF: N-ethylmaleimide sensitive fusion protein

O.C.T.: compound embedding medium for cryostat

OAPs: orthogonal arrays of intramembranous particles

P53: tumour protein 53

P62/SQSTM1: sequestosome 1

PALM: photoactivation localization microscopy

PARIS: Parkin Interacting Substrate

PBS: phosphate-buffered saline

PD: Parkinson’s Disease

PDZ: PSD-95/Discs-large/Zona Occludens-1

PEI: Polyethylenimine

PERK: double-strand RNA-activated protein kinase-like ER kinase

PFA: paraformaldehyde

PGC-1α: peroxisome-activated receptor gamma coactivator 1-alpha

PINK1: PTEN induced kinase 1

pS129 α-syn: α-synuclein phosphorylated on serine 129

PTMs: post translational modifications

PVs: perivascular spaces

qRT-PCR: quantitative real-time PCR

RBD: REM sleep behaviour disorder

RBR: ring between ring

REM: rapid-eye movement

REP: repressor element of Parkin

RING: Really Interesting New Gene

ROS: reactive oxygen species

ROX: residual oxygen consumption

RPL27: ribosomal protein L27

rRNA 18S: 18S ribosomal RNA

RT: room temperature

SEM: standard error mean

SN pc: substantia nigra pars compacta

SNr: substantia nigra pars reticulata

SNTA1: α-syntrophin

SOD1: superoxide dismutase 1

SWA: slow wave of activity

TA: tibialis anterior

TEM: transmitted electron microscopy

TFAM: mitochondrial transcription factor A

TH: tyrosine hydroxylase

TIMM23: translocase of inner mitochondrial membrane 23

TNF-α: tumour necrosis factor-alpha

TOMM: translocase of outer mitochondrial membrane

Tomm20: translocase of outer mitochondrial membrane 20

UBL: ubiquitin-like

UPR: unfolded protein response

UPS: ubiquitin-proteasome system

UTR: untranslated region

WT: wild type

ZNF46: zinc finger protein 46

ACKNOWLEDGEMENTS

To Professor Giovanni Piccoli, who helped me navigate through this project.

To my colleagues, who became my friends.

To Francesco, to my family, and of course to Tayla:

You were my centre when I was spinning away. Thank you for keeping me sane.